Selective permeabilisation of the blood-brain barrier at sites of metastasis

John James Connell

Wolfson College

University of Oxford

2014

Thesis submitted for the degree of Doctor of Philosophy

Scientia nihil aliud est quam veritatis imago.

Dedications

Over the last four years at the University of Oxford, this thesis was completed with help and assistance from scores of people that I have had the pleasure of working with. Primarily, I thank Professors Niki Sibson and Daniel Anthony for all of your guidance, help and support throughout this thesis. Every Monday morning meeting was totally focussed on my work which motivated me to push the project forward.

Labmates were integral to my learning how to be a scientist and a functioning human being. Alastair for your attitude to life, Emma for your kindness, James for your unforgiving nerdiness, Stav for your philosophy, Manuel for your endlessly warm nature, Sébastien for your don't panic efficiency, Kleo for your weekend dedication, Sasha for your Russian jokes, Claire for your constant calm, and Kevin, Greg, Aisling, Clare, Paco, Vas, Matt, Yvonne, Alex, and Helen. Thanks also to Sean, John, Bart, Veerle, Karla and Magda. My colleagues turned into friends and the photographs on the door to the office chart the curiosities of the personalities within, as well as proudly showing the beautiful Gwen, Nozomie and Alexandra.

Lots of thanks must go to my parents for gently guiding me through life, my sister, Anne, my best men James and Clive for looking great in kilts, and to Jamie for showing how easy it is to write a body of work.

Yet above all, my wife, Bec, is my constant source of intrigue, love and happiness that sustains me. Thank you for being in my life and constantly making me a better person.

Table of Contents

Abstract

Over one in five cancer patients will develop brain metastases and prognosis remains poor. Effective chemotherapeutics for primary systemic tumours have limited access to brain metastases owing to the blood-brain barrier (BBB). The aim of this study was to develop a strategy for specifically permeabilising the BBB at sites of cerebral metastases.

Tumour necrosis factor was injected intravenously into mouse models of haematogenously induced brain metastasis. BBB permeability was assessed through histology and *in vivo* MRI and SPECT. Tumour burden and neuroinflammation were assessed after injection of TNF with Caelyx or a novel therapeutic. Mechanism of permeabilisation was investigated through histology and receptor-specific agonist antibodies.

Administration of TNF dose-dependently permeabilised the BBB to exogenous tracers selectively at sites of brain metastasis, with peak effect after six hours. Metastasis-specific uptake of radiolabelled trastuzumab was also demonstrated following systemic cytokine administration. Administration of liposomal doxorubicin formulations in conjunction with TNF reduced tumour burden and mean metastasis size. Localised expression of TNFR1 was evident on the vascular endothelium associated with brain metastases. Human brain metastases displayed a similar TNF receptor profile compared to the mouse model.

These findings describe a new approach to selectively permeabilise the BBB at sites of brain metastases, thereby enabling detection of currently invisible micrometastases and facilitating tumour-specific access of chemotherapeutic agents. We hypothesize that this permeabilisation works primarily though TNFR1 activation and, owing to the similar TNFR1 expression profiles in mouse models and human condition, the strategy has the potential for clinical translation.

Abbreviations

°C	Degrees centrigrade
2B3-101	Glutathione-tagged, PEGylated liposomal doxorubicin
3D	Three dimensional
4T1	Breast cancer cell type
ABC	Avidin biotin complex
AIDS	Acquired immunodeficiency syndrome
AJ	Adherens junction
ALCAM	Activated leukocyte cell adhesion molecule
ALP	Alkalkine phosphatase
ALT	Alanine aminotransferase
ANOVA	Analysis of variance
AST	Aspartate aminotransferase
ATP	Adenosine triphosphate
BALB/c	Bagg albino mouse strain
BBB	Blood-brain barrier
CAM	Cell adhesion molecule
CINC-1	Cytokine-induced neutrophil chemoattractant 1
cm	Centimetre
CNS	Central nervous system
CO_2	Carbon dioxide
CT	Computed tomography
Da	Dalton
DAB	Diaminobenzidine
DMEM	Dulbecco's modified Eagle's medium
DNA	Deoxyribonucleic acid
DPX	Distyrene plasticiser xylene
DTPA	Diethylenetriamine pentaacetic acid
EC	Endothelial cell
EDTA	Ethylenediaminetetraacetic acid
EL4	Lymphoma cell type
EMT	Epithelial-mesenchymal transition
ERBB2	Human epidermal growth factor receptor 2
FBS	Foetal bovine serum
Fe	Iron
g	Gravitational force
G	Gauge (needle)
Gd	Gadolinium
GFP	Green fluorescent protein
GLDH	Glutamate dehydrogenase
GLUT1	Glucose transporter 1

GSH	Glutathione
h	Hour
H_2O_2	Hydrogen peroxide
HCl	Hydrochloric acid
hCMEC/d3	Human cerebrovascular microendothelial cell type
HER2+	Human epidermal growth factor receptor 2
HRP	Horseradish peroxidase
htr-9	TNFR1-selective andibody
Hz	Hertz
i.d.	Internal diameter
Iba1	Ionised-calcium binding adapter 1
IC_{50}	Inhibitory concentration 50%
ICAM-1	Intercellular adhesion molecule 1
IgG	Immunoglobulin G
IgY	Immunoglobulin Y
IL-1β	Interleukin-1β
In	Indium
$InCl_3$	Indium Chloride
IRBE	Inverted research microscope for biology
ITKSnap	Medical image software
JAM	Junctional adhesion molecule
L	Litre
LT	Lymphotoxin
M	Molar
m	milli
m	Metre
MATLAB	Matrix laboratory
Bq	Bequerel
MDA-231-BR-EGFP	MD Anderson brain seeking GFP tagged breast cancer cell type
min	Minute
MRI	Magnetic resonance imaging
MTD	Maximum tolerable dose
MTT	3-(4,5-dimethylthiazol-2-yl)-2,5-diphenyltetrazolium bromide
N_2	Nitrogen
N_2O	Nitrous oxide
NaCl	Sodium chloride
n	Number of subjects
NICE	National institute for Health and Care Excellence
NIfTI	Neuroimaging informatics Technology Initiative

NMR	Nuclear magnetic resonance
o.d.	Outer diameter
O_2	Oxygen
p	pico
P	Probability value
PBS	Phosphate buffered saline
PEG	Polyethylene glycol
PET	Positron emission tomography
pH	Power of hydrogen
P-SCN-BNDTPA	1-(4-isothiocyanatobenzyl)diethylenetriaminepentaacetic acid
RB	Retinoblastoma
RECIST	Response evaluation criteria in solid tumours
RF	Radiofrequency
RMP-7	Cereport
RNA	Ribonucleic acid
ROI	Region of interest
rpm	Revolutions per minute
s	Second
SCID	Severe combined immunodeficiency
SCLC	Small cell lung cancer
SD	Standard deviation
SEM	Standard error of the mea
SPECT	Single photon emission computed tomography
SRS	Stereotactic radiosurgery
T	Tesla
TGFβ	Transforming growth factor beta
TJ	Tight junction
TNB	Tris-NaCl blocking buffer
TNF	Tumour necrosis factor
TNFR1	Tumour necrosis factor receptor 1
TNFR2	Tumour necrosis factor receptor 2
toBBB	Company name
TP53	Tumour protein of 53 kiloDaltons
TSA	Tyramide signal amplification
Tz	Trastuzumab
U87MG	Glioma cell type
U	Unit
µ	Micro
utr-3	TNFR2 selective antibody
v/v	Volume percentage
VCAM-1	Vascular cell adhesion molecule-1

VCAM-MPIO	VCAM-micron sized particles of iron oxide
VE-Cadherin	Vascular endothelial cadherin
VLA4	Very late antigen-4
VWR	Company name
WBRT	Whole brain radiotherapy
ZEN	Zeiss efficient navigation
ZO-1	Zona occludens-1

Chapter 1 – Introduction

1.1 Cancer

The seminal work on cancer is The Hallmarks of Cancer (1), and the updated, over a decade later, The Hallmarks of Cancer: The Next Generation (2). In these reviews, six acquired functional capabilities of cancer are described, further updated with four emerging hallmarks and enabling characteristics. Whilst previously reviewed in depth, a brief outline for understanding of these concepts is important to the premise and hypotheses presented in this thesis.

Arguably the most important trait of cancer cells is their ability to sustain proliferative signalling. Whilst normal cells have carefully controlled cell division, cancer cells can acquire the capability to sustain proliferative signalling through enhanced growth factor production, together with upregulation of growth factor receptor expression, resulting in an autocrine proliferative stimulation (3–5). Elevated levels of growth factor receptor expression can lead to hyper-responsiveness to growth factors, and independence to growth factors for sustained proliferative signalling can be acquired through constitutive activation of downstream components to the receptor signalling pathway.

Cell division describes the process a cell goes through when replicating itself. It is controlled in eukaryotic cells through various cell

cycle checkpoints where the proper functions of cell division are confirmed before continuing into the next phase of the cycle. It is described as four main stages: G1 where the cell is metabolically active and continuously grows; S phase where DNA replication occurs; G2 where the cell continues to grow and generates proteins required for physical division; and M phase where the duplicated DNA splits onto two sides of the cell which then splits into two daughter cells.

Once sustained proliferation is triggered, cancer cells are also able to evade suppression of growth by circumventing negative regulators of cell proliferation. One example of this is the retinoblastoma-associated protein (RB) which determines whether or not a cell should proceed through mitosis (6–8), and loss or inactivation of this gene permits persistent cell proliferation (9). At the same time, resistance to the natural mechanisms that regulate cell proliferation and prevent cancer development, programmed cell death by apoptosis, can be acquired by cancer cells; increasing expression of anti-apoptotic regulators (such as Bcl-2) or the loss of function of TP53 tumour suppressor allows evasion from apoptosis (10).

Under normal conditions, inherent limitations in the number of mitosis cycles a cell can undergo induce senescence and a viable but non-proliferative state, and subsequent crisis of cell death. However, cancer cells are able to acquire replicative immortality by developing functionally significant levels of telomerase that results in extended telomere ends which protect the ends of chromosomes (11,12).

In order to support the enhanced proliferative and survival capacity of cancer cells, as with all tissues, nutrients and oxygen are required and

carbon dioxide and metabolic waste products must be evacuated. When the normal tissue blood supply is insufficient for these metabolically highly active tumours, processes such as hypoxia lead to upregulation of pro-angiogenic vascular endothelial growth factor-A and new blood vessel formation (13–15). This tumour neovasculature is typically aberrant compared to normal physiological angiogenesis, such as in wound healing, and vessels are distorted and enlarged, show haemorrhage and leakiness and have excessive branching (16,17). Nevertheless, these vessels are clearly able to facilitate nutrient delivery to a sufficient extent for maintained tumour growth.

Finally, activation of invasion and metastatic processes is a key component of the late stages of cancer development. The transition of cells from an epithelial to a mesenchymal phenotype arises from the downregulation of E-cadherin by various transcription factors, allowing epithelial cell-cell adhesion complexes to disassemble and tumour cells to disseminate into circulatory systems.

Thus, the hallmarks of cancer are now considered to comprise of: acquisition of sustained proliferative signalling; evasion of growth suppression; resistance to cell proliferation negative regulators; acquisition of replicative immortality; angiogenesis; and crucially for this thesis, activation of invasive and metastatic processes. Further, the emerging hallmarks are deregulation of cellular energetics and avoidance of immune destruction, with enabling characteristics of genome instability and tumour-promoting inflammation describe the characteristics of cancer.

1.2 Metastasis

As discussed above, a key component of cancer development is metastasis, the process of forming a secondary malignant cancerous growth at a site in the body distant from the primary site. An early step in metastatic spread is the detachment of cells from the epithelial basement membrane. Normal cells would, at this point, succumb to a specific type of programmed cell death, anoikis. However, metastatic cells are able to evade anoikis (18,19), through deregulation of TGFβ signalling pathways (20–22). Tumour cells that undergo epithelial-mesenchymal transition (EMT) can travel to distant secondary sites either via the lymphatic system or the blood stream, with differing propensities for secondary organ sites (22–25). The steps involved in extravasation are currently not well understood, but a model similar to leukocyte extravasation is postulated, where luminal endothelial adhesion molecules (26) localise the circulating tumour cell enabling subsequent invasion of malignant cells into the organ parenchyma. A period of dormancy in the perivascular niche has been demonstrated (27,28), with subsequent metastatic outgrowth strongly influenced by endothelial cells.

With regards to metastasis to the brain in particular, much less is currently known than at other organs. However, a number of unique features are becoming clear. The seeding of circulating tumour cells is not fully explained by Ewing's model of circulatory blood flow and mechanical arrest (29), as there is a higher propensity for metastases to seed at the grey/white matter boundary (30,31), and the subtype of tumour cell influences the brain seeding propensity. Small cell lung cancers (SCLC)

form more metastases in the brain than nonSCLC; and lung adenocarcinomas are found in the brain more than squamous lung carcinoma (32). Similarly, certain breast cancers (human epidermal growth factor receptor 2 positive (HER2+)) are more likely to metastasise to the brain than others (33). Clearly, the molecular and genetic make-up of these cells impacts strongly on their metastatic ability, particularly with regard to the secondary organ sites they are able to colonise.

Brain metastasis occurs in 10-40% of all cancer patients (32,34), and there are an estimated 27,000 cases per year in the UK (35). The rates of diagnosis is on the rise, partly owing to increased detection through improved neuro-imaging techniques and their greater availability in hospitals, and partly owing to an increased prevalence in an ageing population with improved treatment of systemic primary and metastatic cancer (36). Consequently, brain metastasis is a significant cause of morbidity and mortality in cancer patients, as well as causing significant cognitive impairment (37,38). Lung and breast tumours account for over half of all brain metastases encountered in the clinic (39), as they present with a high incidence in the general population (40), and the median survival time from diagnosis of brain metastasis is approximately 7 months (41).

Hypoxia promotes the triggering of metastasis, and late-stage metastases themselves and glioblastoma multiforme may become hypoxic (42,43). Hypoxia describes the low oxygen content in the microenvironment of tissues, brought about in tumours by excessive oxygen consumption and insufficient provision of oxygen from the blood

supply leading to necrosis. Often, the triggers of angiogenesis, such as VEGF and FGF, are upregulated at hypoxic tumours, but in an elevated and uncontrolled manner, leading to dysregulated and incomplete growth of new blood vessels. In late stage brain metastases, this presents an incomplete BBB, but requires metastases to be of sufficient size.

1.3 Treatment

Treatment strategies for brain metastases are complex and aim to improve loco-regional control; the most common approaches currently are surgical resection, stereotactic radiosurgery (SRS) and whole brain radiotherapy (WBRT). Recommendations for a single metastasis indicate that a combination of WBRT with surgical resection is better than surgery alone with respect to reduced risk of distant brain metastasis, as well as prolonged survival and functional status (44). SRS and surgical resection can locally control tumours, but are limited by the lesion location and availability of SRS facilities. Further, less cognitive decline is found in patients treated with SRS over WBRT owing to fewer off-target effects.

Clinical guidelines from the National Institute for Health and Care Excellence (NICE) for treatment of patients with lung cancer recommend that dexamethasone should be offered to patients with symptomatic brain metastases to provide relief for symptoms related to increased intracranial pressure (45,46), and that WBRT should be considered for patients with a good performance status. The NICE clinical guidelines for treatment of advanced breast cancer with brain metastasis complications recommend surgery followed by WBRT to patients with a single or small number of potentially resectable brain metastases, a good performance status and no, or well-controlled, other metastatic disease; WBRT when surgery is not appropriate; subsequent rehabilitation and finally specialist palliative care (47).

It is critical to note here that chemotherapy is absent from these guidelines, either as the primary treatment option, as a neoadjuvant therapy (used to shrink the primary tumour so that subsequent local therapy is less destructive or more effective) or as an adjuvant treatment following surgery or radiotherapy. While some patients may already be on a course of chemotherapy for control of the primary tumour, direct application of chemotherapy for treatment of brain metastasis is not used. This omission reflects in large part, the presence of the blood-brain barrier (BBB) which limits entry of most chemotherapeutics into the brain (see Chapter 1.5 for further discussion).

Chemotherapy generally aims to impair cellular mitosis, thereby inducing apoptosis and cell death. As cancer cells divide much more rapidly than normal cells, it is these that are 'targeted'. Chemical compounds that interact with the events of mitosis, such as DNA replication or microtubule formation, are administered during a carefully planned treatment regimen where combinations of different classes of chemotherapeutic agents are used to maximise efficacy, whilst minimising adverse effects. Chemotherapy is a powerful approach to combat the progression of cancer and extensive research has been carried out to test its usefulness in brain metastasis. A number of trials have been performed as a salvage treatment for patients after radiotherapeutic options have been exhausted. Unfortunately, as study methodologies such as patient selection and response criteria have been inconsistent, interpretation of data from these studies is difficult.

As breast cancer accounts for around 17% of brain metastases (48) and systemic therapies of breast cancer improve survival (49), the incidence of brain metastases in these patients is increasing. Treatment with temozolomide (a DNA alkylating agent) has been disappointing with no response in a trial of 19 women (50). Moreover, co-treatment with vinorelbine (semi-synthetic vinca alkaloid agent) with temozolomide only showed a partial response in one patient in a trial of six breast cancer patients with brain metastases (51). However, recent reports describing a phase II trial of Lapatinib (dual tyrosine kinase inhibitor of HER 1 and 2) co-administered with carpecitabine (thimidylate synthase inhibitor, preventing DNA and RNA *de novo* synthesis), showed that 29 of 44 patients with brain metastasis from HER2 positive breast cancer had a partial response of over 50% reduction in the volumetric sum of all assessable lesions (52).

Trials of temozolomide in non-small cell lung cancer patients with brain metastasis have shown mixed responses, with some reporting improvements in progression free survival when used concomitantly with WBRT (53–55), and others reporting no improvement in objective response rate compared to treatment prior to WBRT (56). Reports of the use of gefitinib (a small-molecule tyrosine kinase inhibitor selective for the epidermal growth factor receptor) have suggested efficacy (57,58), but only with very few patients and in pre-treatment regimens with other modalities. Administration of the radiosensitiser motexafin gadolinium (which selectively targets tumour cells and generates reactive oxygen species through oxidation of intracellular metabolites, leading to

radiosensitisation) has been trialled with WBRT, with an delay in the time to neurological progression reported, but no improvement in overall survival (59).

The limited reports on the ineffective use of chemotherapy on brain metastasis may be caused by unwillingness of researchers to publish negative results, or barriers to publishing of clinical trial data by companies considering results commercially sensitive. This phenomenon is clearly demonstrated (60) and may be relevant in the case of negative trials of the use of chemotherapy in patients with brain metastasis.

Counter to these tentatively encouraging results, is the lack of information about the effects on presymptomatic micrometastases or the likelihood of recurrence. As brain metastases must be detected using imaging techniques that require BBB permeability, small lesions or regions of a detectable metastasis where the BBB is still in-tact may still evade treatment. Recurrence at these sites may negate any prior benefits of chemotherapy. The trials described above indicate a gap in the treatment strategies open to oncologists. While chemotherapy may only account for 11% of treatment plans in cancer, with the rest covered by surgery and radiotherapy, this is still a significant population. Effectively delivering chemotherapeutic agents to brain metastases remains an unmet clinical need, and warrants extensive research.

1.4 Diagnosis

As discussed above, the incidence of brain metastasis has appeared to increase in recent years, owing both to better control of symptoms and mortality of the primary disease, and to increased detection of presymptomatic metastases. A study reporting brain metastases in children with solid tumours suggests that the changing incidence of brain metastasis is due to the primary disease being effectively controlled by chemotherapy leading to a prolonged survival, whilst the sanctuary site of the brain permits these metastases to evade treatment and persist (61). The same concept is presented in a review of breast cancer patients, where occurrence of the brain as the first site of relapse was associated with adjuvant systemic therapy of the primary tumour (62). Further, in a retrospective analysis of breast carcinoma, the first site of relapse was the brain in 4.3% of patients receiving adjuvant chemotherapy, whilst for those receiving only surgery, the first site of distant recurrence was never the brain (63). It is evident, therefore, that the strides forward in controlling systemic disease merely buys time for brain metastases to develop into the fatal component of cancer progression.

Diagnosis of cancer has traditionally been triggered by finding a 'lump', or noticing symptoms of organ impairment. In the brain, the skull clearly prevents a palpatable lump, and the typical symptoms of brain metastasis, most frequently headaches, impairment of sensory and motor functions and cognitive impairment (32), may be overlooked or attributed to another cause. Diagnostic imaging such as magnetic resonance imaging (MRI), computerised tomography (CT), or positron emission tomography (PET)

are now most commonly used in the diagnosis and understanding the pathophysiology of brain metastasis.

MRI

MRI dates back to the 1970s, through work by Lautebur and Mansfield (64,65), who developed methods of image formation by nuclear magnetic resonance (NMR). Images in their definition are a "graphical representation of the spatial distribution of one or more properties" (64). This work led to their joint earning of the Nobel Prize in Physiology or Medicine in 2003. It is based on the principle of NMR, developed in the 1930s (66), whereby the spin of a charged particle, or magnetic moment, is measured. Macroscopic density distributions of the nuclear spins within a sample are computed and transformed into an image.

The charged particle most commonly imaged is the proton, found abundantly in the body in water and fats. Under no influence from a magnetic field, the directions about which protons spin in are randomly distributed. When placed within a static magnetic field, however, the spins align about direction of the magnetic field (Z direction), with a slight propensity for the lower energy state of spin up (parallel to the magnetic field) rather than spin down (antiparallel). The precession about their axis in this alignment leads to an overall sample magnetisation vector in the direction of the magnetic field.

When an electromagnetic pulse (within radiofrequency ranges, determined by the Larmor equation) is applied, the spin up and spin down distribution is perturbed, and the phase of the spins becomes aligned

giving magnetisation vector in the plane perpendicular to the magnetic field (XY). This excited state relaxes in two forms, T_1 longitudinal relaxation, where the overall magnetisation vector is restored to the Z direction, and T_2 transverse relaxation where the spins dephase from each other within the XY plane, reducing this magnetisation vector. The two forms of magnetisation relaxation occur simultaneously and independently, and can be measured by the induction of currents in receiver coils surrounding the sample. The rates at which these excited states decay back to equilibrium are influenced by the magnetic field strength and the local environment of the nuclei. It is the macroscopic distributions of these environments that give rise to the changing signal intensities of voxels within a sample, leading to detection of anatomical structures. In pathology, this normal environment and tissue structure is disturbed and a trained radiographer can identify unusual regions of contrast and interpret these as disease. MRI provides fantastic precision in spatial localisation and interpretation of pathological phenotype.

Large brain metastases can be detected through the gross abnormalities observed on T_2-weighted images. Additionally, contrast at sites of pathology can be generated by administration of gadolinium-containing compounds (such as gadodiamide) that can pass through a damaged blood-brain barrier (BBB) and accumulate at sites of metastases larger than 0.5 - 1 cm in diameter (67). This then alters the T_1 relaxation rate and generates a hyperintense signal. Both contrast mechanisms generate significant changes at the site of tumours and are routinely used in the diagnosis of brain metastasis.

However, after the diagnosis of a solitary or multiple metastases, follow-up imaging at a later time point often identifies further sites of metastasis that were not identified previously. These previously undetected metastases may be because they were at an early stage and the BBB here was still impermeable to contrast agent, or through further seeding of new metastases. Achieving 'early' detection of new brain metastases is recommended by frequent follow-up evaluations (68). However, detection through this method, where the BBB is already damaged, indicates the development of the pathology at a late stage and not at the early micrometastatic stage.

Research into enhancing the stage at which brain metastases can be detected through medical imaging would offer oncologists the information of current and likely progression of the metastatic burden and may therefore change the course of treatment. Confirmation of identification of a solitary, or a few metastases could prompt the surgical resection treatment option; identification of more but still treatable number could change treatment plans to WBRT; and identification of a substantial metastasis burden may alter the treatment plan of the primary and secondary tumours to palliative care and maintenance of the quality of life years for as long as possible. The ability to diagnose brain metastatic burden could make substantial changes to the treatment and subsequent outcome and experience of the patient.

1.5 Blood-brain barrier

The (BBB) is a critical and intriguing component of brain homeostasis physiology, evolved to ensure a sanctuary site for the brain away from blood-borne pathogens and dietary toxins that would elicit devastating effects on the host organism. With the brain controlling myriad aspects of the body's functions and being metabolically highly active and homeostatically finely balanced, any pathogenic infection can potentially be lethal. In contrast, other distant organs such as the liver and skin have scope for temporary diminished function while the pathogen is removed and pathogenic effects resolved. Consequently, the central nervous system has evolved to invest heavily in metabolically costly processes to evade this threat.

At its core, the BBB is located on the blood vessels that are densely embedded within the brain with individual neurons seldom more than 8 – 20 μm from a brain capillary (69). It can be considered to be made of up cells, specialised inter-cellular junction complexes, extracellular protein matrices and protein complexes to facilitate selective transport across the BBB.

Cellular basis of the BBB

The cellular components of the BBB are outlined in schematic form in Figure 1.1. Between the blood and brain tissues lies a dense collection of four cell types: endothelial cells, pericytes, smooth muscle cells and astrocytes.

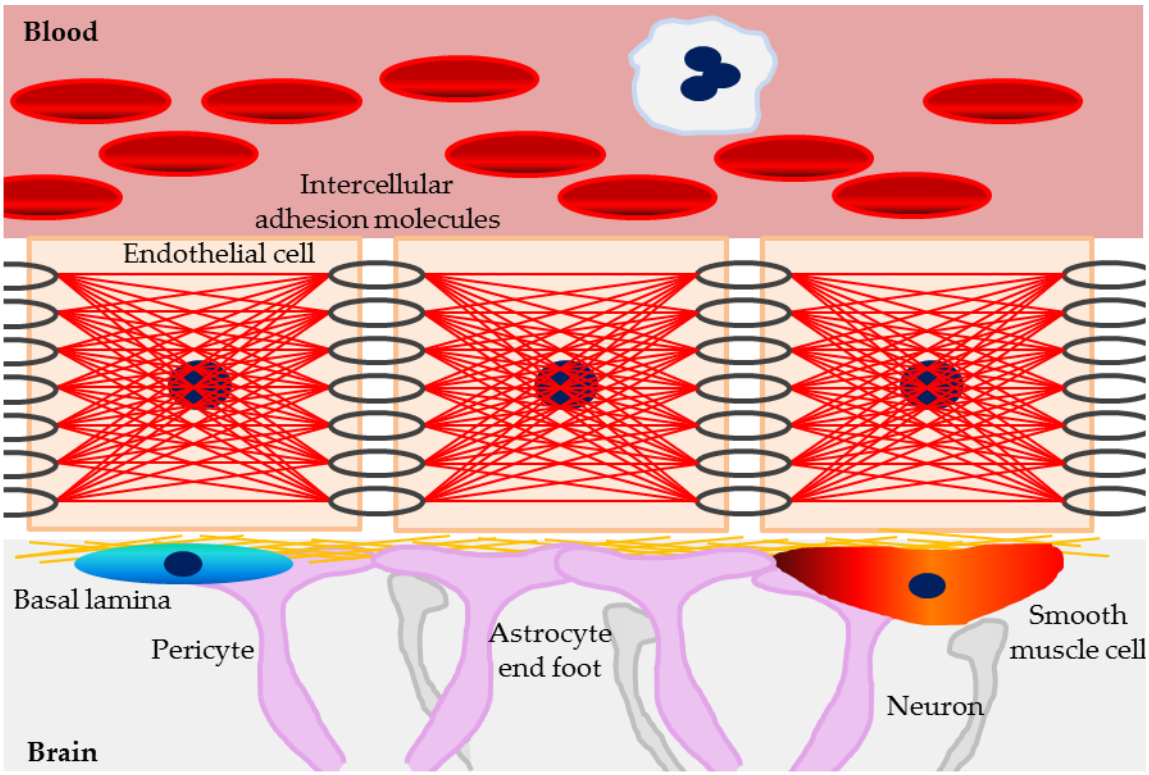

Figure 1.1: Schematic of the blood-brain barrier. Endothelial cells form the barrier between blood and brain, linked tightly together via their cytoskeleton by intercellular adhesion molecules and surrounded on the brain compartment by pericytes, astrocytic endfeet, smooth muscle cells and basal lamina.

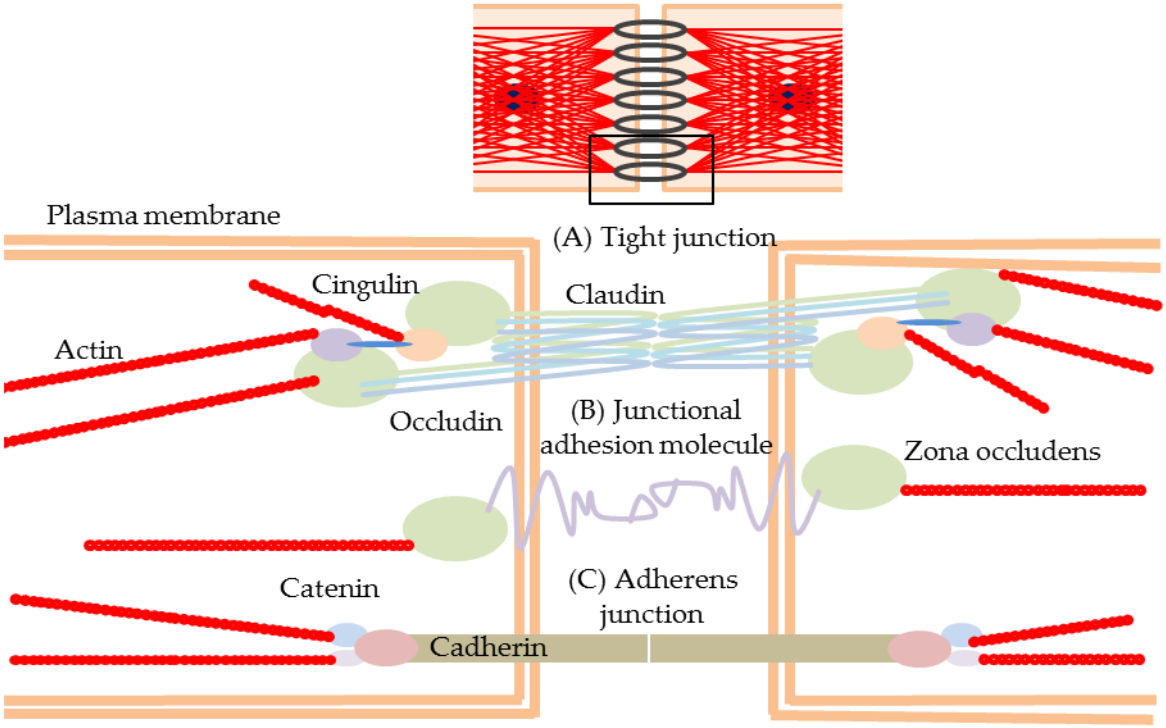

Figure 1.2: Schematic of inter-endothelial adhesion molecules. (A) Tight junctions are composed of homophilic paracellular associations of the 4 transmembrane domain claudin and occludin linked to the actin cytoskeleton by zona occludens scaffolding proteins. (B) Junctional adhesion molecules form further cell-cell adhesion and regulate paracellular monocyte transmigration. (C) Adherens junctions are complexes of homophilic associations of cadherins, linked to actin cytoskeleton by catenin subunits.

Endothelial cells line the entire circulatory system, forming a tubular structure, and are linked tightly together with various junctional complexes. The endothelium is versatile and multifunctional, influencing the coagulation process, angio- and vasculogenesis, vascular tone and blood flow and the immune and inflammatory responses (70,71). Procoagulant factors such as von Willebrand Factor and platelet activating factor, can be expressed by endothelial cells, whilst vasoconstriction influences haemostasis by expression of vasoactive agents by endothelial cells activating smooth muscle cells. Resolution of the coagulation process is further influenced by the endothelium through expression of tissue type plasminogen activator and expression of heparin like glycosaminoglycan receptors which inactivate thrombin. Angiogenesis, the formation of new blood vessels and a particularly important feature of the tumour microenvironment, is controlled by signalling cascades in endothelial cells largely influenced by fibroblast growth factor and vascular endothelial growth factor (71). Vascular tone is the contractile activity of vascular smooth muscle cells in the walls of small arteries and arterioles (72), and plays an important role in distribution of blood flow in tissues of the body. The regulation of this activity is a result of the complex interplay between vasodilator and vasoconstrictor stimuli, some of which are derived from the endothelial cells. Finally, the influence of endothelial cells on the immune response includes attraction of circulating leukocytes by luminal expression of cell adhesion molecules (73) and dynamic cytoskeletal rearrangement to facilitate diapedesis. Nevertheless, despite all of the above functions, the endothelium is first and foremost a physical barrier component of the BBB, limiting the transcellular diffusion of blood-borne

compounds. Endothelial cells are held tightly together by various junctional complexes, described below.

The other cellular components of the BBB have more subtle roles in the BBB. Pericytes (74), astrocytic endfeet and smooth muscle cells influence capillary blood flow, crucial for efficient energy delivery to active sites of the brain, but also function as a further physical barrier and communicate with the endothelium (75) to influence permeability. Glycocaelyx is a negatively charged layer of fibrous chains that are found on the luminal surface of endothelial cells (76) and contribute to restriction of passage of macromolecules across the BBB based on their charge. Additionally, the endothelium is ensheathed in a basement membrane of a matrix of collagenous proteins forming an anchor between cells giving structural integrity to the system, and a further physical barrier.

Inter-endothelial junctions

There are two main groups of proteins complexes that form the tight seal between the plasma membranes of adjacent endothelial cells (see Figure 1.2): tight junctions (TJ) and adherens junctions (AJ). Further, the junctional components can be defined in three categories: structural proteins necessary for initiation of the junctions, plaque proteins associated with the cytoskeleton and signalling proteins.

TJ describe the homophilic binding of multi-protein complexes between the plasma membrane of adjacent endothelial cells (Figure 1.2 A). The cell-cell adhesion complexes form strong junctions by linking to the

rigid yet dynamic actin cytoskeleton. The transmembrane components found between cells at tight junctions are IgG-like junctional adhesion molecules (JAMs, Figure 1.2 B) and the 4-transmembrane domain claudin and occludin families. The cytoplasmic tail of claudins and occludins are linked to actin through scaffolding proteins such as the zona occludens family and vinculin. Charge-selective passive diffusion of ions between cells are thought to be permitted by extracellular loops of claudins forming paracellular pores (77,78); and the apical/basolateral diffusion of lipids is regulated between membranes of endothelial cells (79). TJ are sensitive to physiological requirements and acutely communicate with the cell through signalling cascades (reviewed in depth (80)) to regulate junction assembly and to modulate gene expression and cell behaviour (81).

Adherens junctions also describe the homophilic binding of multi-protein complexes between the plasma membrane of adjacent endothelial cells (Figure 1.2 C). In these structures, the nectin-afadin and cadherin-catenin complexes facilitate linking of the cytoskeletons of adjacent endothelial cells. Similarly to TJ, endothelial cell-cell junction integrity is regulated by AJ, along with leukocyte transmigration and angiogenesis (82,83). They are distinct in that AJ initiate and maintain cell-cell contacts, while TJ regulate the paracellular permeability (84).

These junctional proteins are localised at the plasma membrane between adjacent endothelial cells of the whole circulatory system, and are particularly abundant at the blood brain barrier. Critically, these junctions can be regulated and are dynamic (85): phosphorylation of key components, endocytosis and proteolytic cleavage can regulate

formation/degradation; transcriptional regulation by endothelial cells can change the expression of the various components; and cytoskeletal rearrangements can alter the dynamic maintenance of adherens junctions and cell shape. Further, during diapedesis, VE-cadherin remains on the plasma membrane, but redistributes to the luminal endothelial surface (86) again highlighting the dynamic nature of the junctions. These structures allow selective passage of blood-borne compounds into the brain (Figure 1.3).

Interendothelial junctions have been shown to be disrupted in cerebral malaria. This is a serious consequence of Plasmodium falciparum infection, and BBB breakdown was observed in children, where staining for ZO-1, occludin and vinculin was reduced (87) and upregulated levels of proinflammatory cytokines TNF and IL-1β were found (88). The BBB is also affected in multiple sclerosis, often as one of the earliest cerebrovascular abnormalities (89), again with disrupted interendothelial junctions. Indeed, even neuroinflammation and subsequent leukocyte recruitment itself is sufficient to trigger junctional disorganisation and BBB

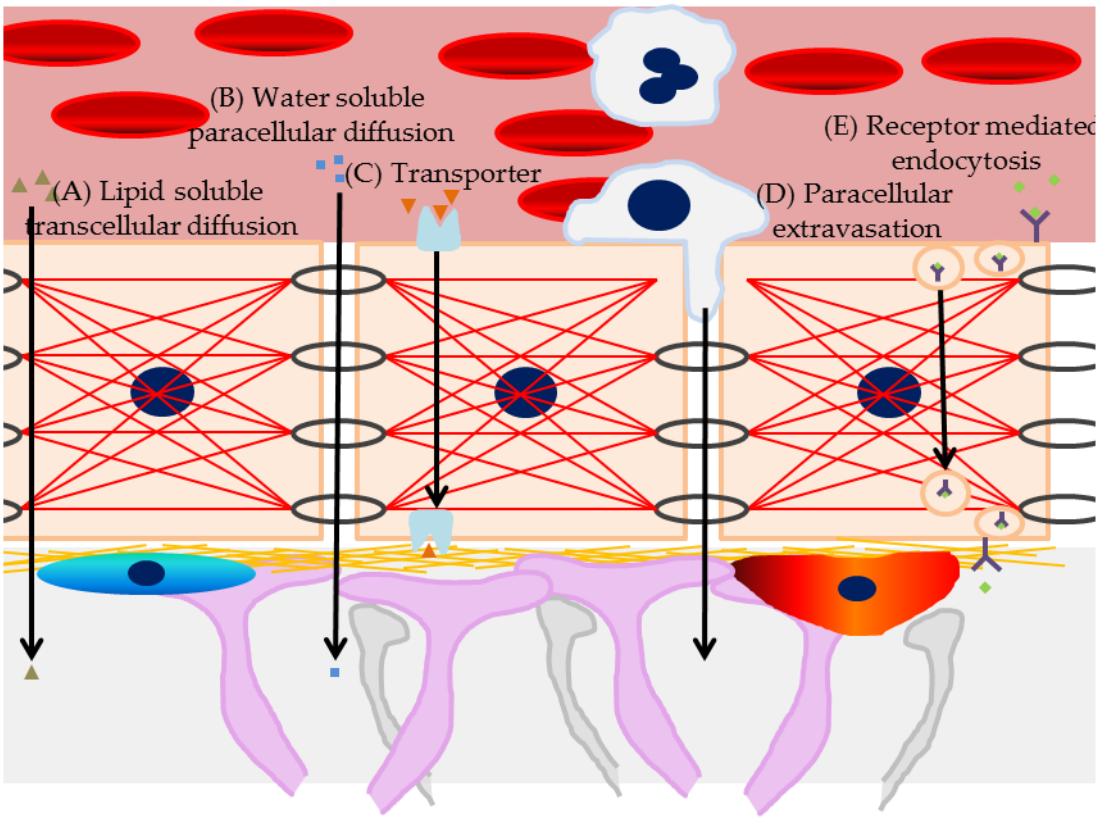

Figure 1.3: Schematic showing pathways across the blood-brain barrier. (A) Small lipophilic molecules can diffuse passively across endothelial cells. (B) Small hydrophilic molecules can diffuse passively between endothelial cells. (C) Small hydrophilic essential molecules use specific transporters to shuttle across endothelial cells. (D) Infiltration of systemic immune cells occur by adhesion to the endothelium, reorganisation of inter-endothelial adhesion junctions and paracellular extravasation. (E) Larger hydrophilic essential molecules use specific receptors to facilitate transcytosis into the brain.

breakdown (90). Thus, interendothelial junctions are physiologically dynamic, as well as in response to pathology. BBB breakdown in late stage brain metastasis is a consequence of tumour angiogenesis forming chaotic and leaky vessels where a BBB is not truly formed. Early stage metastases are co-optive with parenchymal vessels that display an intact BBB (91).

Efflux proteins

The function of the BBB is further enhanced by the expression of drug efflux transporters. These proteins use ATP hydrolysis to transport a variety of structurally unrelated compounds across the EC irrespective of the concentration gradient. P-glycoprotein (92), breast cancer resistant protein (88) and the multidrug resistance-associated protein family (93) all function to expel molecules that have diffused into the brain back into the blood providing an additional barrier to bioavailabilty of potential therapeutics at sites of brain tumours and metastases. The *in vitro* transport rate of novel drugs by these proteins indicates the brain penetration of drug candidates (94), giving important information when developing novel CNS treatments.

1.6 Strategies to circumvent the BBB

This highly complex and active physiology ensures successful neuronal function, but also causes a negative impact on modern medical attempts to use exogenous chemical compounds to modulate CNS disease. Many compounds developed for use as drugs are unable to cross from the blood to the brain in sufficient concentrations, if at all, to allow a therapeutic effect. A range of approaches to in some way circumvent the BBB have been investigated, with varying degrees of success and safety. Generating new drugs to cross the BBB must be of low molecular weight (<400 Da) and fewer than 8 hydrogen bonds as polar compounds are excluded (95).

A wafer polymer containing chemotherapeutic drugs can be implanted into the brain, often at the close of surgery (96,97). This strategy facilitates a local diffusion of drugs for an extended period of time around the site of implant, but diffusion decreases with distance meaning precise mapping and placement is required. An improvement in overall survival in a trial with malignant glioma was seen following implantation of a biodegradable carmustine (a mustard gas related DNA alkylating agent) wafer with few added adverse effects (97). Alternatively, a catheter can be inserted into the brain and drugs actively pumped into the tumours site over time, with delivery up to 2 cm from insertion point (98), depending on drug molecular weight, polarity and infusion rates. However, some brain regions are difficult to reach safely.

Methods aimed to actively damage the blood-brain barrier are also under investigation with a view to increase drug delivery in the same way as the enhanced permeability and retention effect is observed in the field of drug delivery to tumours with leaky neovasculature (99). It is observed, in this effect, that molecules with a larger hydrodynamic radius have a lower diffusion coefficient and thus effectively diffuse less from the vasculature to tumour cells (100). One approach involves an intracarotid infusion of a hyperosmotic agent such as mannitol which results in the osmotic shrinkage of endothelial cells and physical disruption of tight junctions (101). Intravenously injected dyes which bind albumin proteins were shown to permeate into the brain, indicating a large size threshold to facilitated entry. This approach has been trialled in patients, with some positive results (102), including an increase in survival to 23 months (103) and 17 months (104) in patients with high grade glioma, where a typical survival of 14 months is reported (105). However, the short working window of 40 minutes is a serious limitation to potential therapeutic efficacy (106) and the lack of specificity for tumour sites is a major confound with regards to risking adverse effects to healthy brain tissue, such as stroke like syndromes, temporal seizures and new tumour-nodule formation (107).

A novel approach uses the focussed ultrasound-mediated bursting of intravenously injected microbubbles of gas to actively damage the endothelial cells. Cavitation of microbubbles excited by ultrasound physically interacts with the surroundings and has been shown to enhance the delivery of Herceptin in a mouse model (108,109). However, this

approach requires prior knowledge of the tumour site and use of MRI guidance.

The most promising approach to date has involved the development of an analogue of the ligand for the bradykinin B2 receptor, (cereport or RMP-7). Injection of this compound initiated an opening of tight junctions through a calcium-mediated mechanism (110,111). This promising approach however, only generated a short (5 – 10 min) window of permeabilisation, and was halted in trials after a dose limiting side effect of hypotension (112). It has been demonstrated that the permeabilisation induced by cereport is through alteration of the integrity of endothelial tight junctions (113), mediated by TNF (114).

Limitations to the strategies described above such as the minor improvement in patient outcome, safety issues, non-targeting of early or undetected metastases and the requirement for prior knowledge of position of the tumour site, all indicate further research into this field is required. Further, knowing the precise size threshold of macromolecules to cross the BBB is difficult to quantify, although use of known dextran beads is a possibility(115). A safe and effective strategy that targets early metastases as well as the infiltrative edge, where the BBB is in-tact, may confer a significant benefit in the treatment of patients with brain metastases.

1.7 Aims of this thesis

Based on previous work in the literature as described above, and recognising the unmet clinical needs in the treatment of brain metastasis, the primary aims of this thesis were to:

1. Develop an *in vivo* strategy for permeabilising the BBB specifically at the sites of brain metastases.
2. Determine the effectiveness of this permeabilisation strategy in enhancing the efficacy of chemotherapy in brain metastasis.
3. Assess the potential for translation of this permeabilisation strategy into the human condition.

Chapter 2 - Methods

The *in vivo* models used in this work were broadly similar, employing an intracardially-induced burden of metastatic breast cancer cells in the brain, various time points of intravenous injections, *in vivo* imaging and end points determined by organ dissection. Specific experimental procedures will be detailed in relevant results chapters.

All experiments carried out at room temperature (21°C) unless otherwise stated. Experiments were performed at the University of Oxford at the Experimental Neuroimaging Group, Radiobiology Research Institute and at the Experimental Neuropathology Lab, Department of Pharmacology.

P-values are used throughout with a significant result accepted if $P<0.05$.

2.1 In vitro procedures

2.1.1 General cell culture

All cell culture was performed in sterile conditions in a BioMAT2 class II microbiological safety cabinet. Mycoplasma testing was performed monthly on all cell lines using a kit (Lonza). Cell line authentication was not performed. Large frozen stocks of cells were generated at the start of the project, and similar passage cell lines were always used. Misidentification could influence cell behaviour growth of cells and response to treatment.4T1-GFP (murine mammary carcinoma (116) and

MDA-231-Br-eGFP (human mammary carcinoma (24)) cells were grown in Dulbecco's modified Eagle's medium (DMEM, Invitrogen) supplemented with 10% (v/v) heat-inactivated foetal bovine serum (FBS) (Biosera) and 1% (v/v) 200 mM L-glutamine (GE Healthcare). 4T1.2 parental and 4T1.2-erbB2 cells were grown in Roswell Park Memorial Institute medium (RPMI1640) (Invitrogen) supplemented with 10% (v/v) FBS, 1% (v/v) 200 mM L-glutamine and 1% (v/v) penicillin/streptomycin mix for a final concentration of 10000 U/mL penicillin and 10 mg/mL streptomycin (GE Healthcare). 4T1.2-erbB2 cells were previously transfected with a plasmid carrying the *ERBB2* gene (kind gift from Professor Michael Kershaw, University of Melbourne). hCMEC/d3 (human cerebromicrovascular endothelial cells) were grown in endothelial basal medium-2 (Lonza) with added 5% (v/v) FBS, 1% (v/v) penicillin-streptomycin, 1.4 μM hydrocortisone (Sigma Aldrich), 28.4 μM ascorbic acid, chemically defined lipid concentrate (1:100 (Life Technologies)), 10 mM HEPES (Life Technologies), 57 pM bFGF (Life Technologies). Cells were a kind gift from Dr Couraud, INSERM, Paris. hCMEC/d3 cells were grown on 60 mm plates or 25 cm^2 flasks precoated for 4 h with 10 $\mu g/cm^2$ rat collagen in water (Sigma Aldrich).

All other cells were grown in tissue culture flasks of 75 cm^2 in 13 mL of complete medium. These were grown in a Hera2 incubator (Heraeus) with a humidified atmosphere at 37°C with 5% CO_2. The cells were grown up to a maximum of 90% confluency and periodically tested for mycoplasma infection (Lonza). Cells were passaged and treated in the same manner to minimise variability in separate experiments.

Cells were detached for further use with 5 min incubation in 3 mL 0.05% trypsin-EDTA (ethylenediaminetetraacetic acid, Sigma Aldrich) at 37°C and resuspended in 7 mL complete medium. Cells were collected by centrifugation (250 g, 4°C), resuspended in 1 mL phosphate buffered saline (PBS) and counted using Nucleocounter system (Sartorius Stedim).

For long term storage, 10^6 cells were resuspended in 1 mL of incomplete medium supplemented with 20% FBS (v/v) and 10% dimethyl sulphoxide (DMSO) (v/v) (Sigma), frozen in Mr Freezy boxes at -80°C and transferred to liquid nitrogen storage. For thawing, cells were rapidly warmed in 37°C water bath and resuspended in 9 mL complete medium, centrifuged into a pellet (5 min at 1200 rpm) and resuspended in 13 mL complete medium.

2.1.2 Assay for cell proliferation

At 90% confluency, cells were detached and counted as above. Cells were diluted in complete medium to and 150 μL of cell suspension containing 5000 cells was added to each well of a 96-well plate, with wells containing only complete medium as control. Cells were then incubated in the humidified CO_2 incubator at 37°C overnight to allow seeding. Medium was aspirated and replaced with complete medium containing a range of concentrations of compounds: (doxorubicin (Sigma Aldrich) 0 – 10^5 ng/mL; trastuzumab (Genentech, USA) 0 - 100 μg/mL; 2B3-101 (toBBB, Netherlands) 0 – 10^5 ng/mL; Caelyx (Janssen, UK) 0 – 10^5 ng/mL; recombinant mouse tumour necrosis factor (rmTNF, Peprotech) 0 – 200

ng/mL). Cells were incubated at 37°C for 24 - 72 h. 50 μL of MTT (3-(4,5-dimethylthiazol-2-yl)-2,5-diphenyltetrazolium bromide; Sigma Aldrich; 5 mg/mL in water) was added to each well, and incubated in the dark at 37°C for 4 h as defined from pilot data. Medium was then aspirated and the water-insoluble purple formazan dye produced by living cells was resuspended in 200 μL DMSO (Sigma Aldrich). After agitation, the absorbance of each well at 570 nm was measured in a photometric microplate reader (Infinite200, Tecan) with 25 averages per well, within 30 min of resuspension to prevent degradation of reaction product. Mean value of cell-free wells was subtracted from all wells and cell proliferation relative to control conditions is calculated.

2.1.3 Cell preparation for *in vivo* injections

At 90% confluency, cells were washed with PBS and detached from the culture flask, collected by centrifugation, counted and diluted in PBS to either $1x10^4$ or $1x10^5$ cell/mL for intracardiac injection (below), or $1x10^7$ cells/mL for intracerebral injection (below) and stored on ice. Cells were then injected within two hours and counted again to verify viability (mean cell concentration 2 hours after injection 84.6% (Figure 2.4).

2.1.4 VCAM-MPIO contrast agent conjugation

Tosylactivated MyOne Dynabeads (micron sized particles of iron oxide; 100 mg beads/mL; Invitrogen) were conjugated to rat anti-mouse vascular cell adhesion molecule-1 antibody (VCAM-1, Cambridge

Biosciences) using 0.1 M sodium borate buffer pH 9.5 and 3 M ammonium sulphate for 24 h at 37°C in a 1000 rpm orbital mixer (Thermomixer). The solution was separated with a magnet, aspirated and replaced with PBS + 0.5% (w/v) bovine serum albumin (BSA, Sigma) + 0.05% (v/v) Tween 20 and incubated overnight at 37°C at 1000 rpm. The solution was again separated, washed three times with PBS + 0.1% BSA + 0.05% Tween 20. The solution was separated and contrast agent was stored in PBS + 0.1% NaN_3 + 0.1% BSA (w/v) at 4°C in a 1000 rpm mixer at a final concentration of 25 mg beads/ml (6.5 mg Fe/mL).

2.2 *In vivo* procedures

All experiments were carried out in accordance with the UK Animals (Scientific Procedures) Act 1986 and with local ethical committee approval under Home Office project licence number 30/2620 and personal licence number 30/9223. Welfare was monitored before and after procedures by named animal care and welfare officers.

Female BALB/c or SCID mice (Charles River, UK) at age 6-8 weeks (19.1 g ±1.6 g) were used in all experiments, housed in cages of up to 6 with *ad libitum* access to food and water, temperature maintained at 19-21°C, humidity maintained at 50% ±15%, on a 12 h light/dark cycle; with bedding, dark tube and running wheel stimulation and weekly nuts and sweets treats. Mice were allowed to acclimatise to their new environment for three days after arrival in the facility prior to any experiments. All mice were inspected daily for natural behaviour and, when under an experimental protocol, weighed and scored for natural and provoked behaviour every two days. A weight loss of more than 20% from starting weight indicated illness. This occurred in less than 2% of mice.

2.2.1 Anaesthesia

All animals undergoing tail vein cannulation, MRI, intracardiac injection, intracerebral injection or SPECT imaging were anaesthetised using inhaled isoflurane (IsoFlo®, Abbott Laboratories, UK). 3% isoflurane was used for induction in bottled gas (BOC, UK) and 1.5-2.0% was used for maintenance with respiration and/or visual monitoring with a target minimum

respiration rate of 60 breaths per minute. The carrier gas for intracardiac injections was 100% O_2 at a flow rate of 1 L/min; for cannulation and MRI, 70:30 N_2:O_2 was used at a flow rate of 1 L/min; for intracerebral injections 70:30 N_2O:O_2 was used at a flow rate of 1 L/min; for SPECT imaging, pumped air was used at a flow rate of 1 L/min. A Fluovac scavenging system was used to remove excess anaesthetic agent (International Market Supply, UK).

Prior to transcardial perfusion, mice were injected intraperitoneally with 200 μL of pentobarbitone mix. Before any invasive procedure, anaesthesia was confirmed by absence of reflex reaction to a toe pinch of an extended hind limb.

2.2.2 Intracardiac injections

A single cell suspension was prepared as described and stored on ice. A stereotaxic frame was prepared consisting of needle holder, heated mouse platform and ultrasound probe holder. A Vevo 770b (Visualsonics, Canada) ultrasound probe was positioned and aligned with a dummy needle. Mice were anaesthetised as described and secured in a supine position with surgical tape on a 37°C heated plate. Heart rate and pedal reflex was monitored to assess the depth of anaesthesia. Hair was removed from the left chest with depilatory cream (Veet, UK) and a live sagittal image of the left ventricle of the heart was acquired through ultrasound gel (Aquasonics, USA). Cells were gently triturated using a 25 G needle and 100 μL was injected into the left ventricle over 10 s using a 27 G needle. A successful injection was determined by the presence of blooming contrast

on the ultrasound image at the point at which cells were injected and also by the return of pulsed blood back up the needle after the injection (117). Mice were recovered from anaesthesia in a heated recovery cage and weighed and monitored as described. Typical procedure time was 10 min per animal.

2.2.3 Intravenous

All intravenous injections were performed on conscious animals. Tails were immobilised by use of an injection box. Tails were swabbed using 70% v/v industrial methylated spirits in water and warmed using a heat lamp and gently rubbed for 10 s to promote peripheral circulation prior to injection. 100 μL of well mixed injection solution was injected over 3 s into a lateral tail vein. Liposome formulations were injected over 6 s. Blood was swabbed dry and tail inspected for good blood flow.

Tail vein cannulae were applied to mice to facilitate intravenous injection when restrained within the MRI magnet bore. Mice were anaesthetised on a heating pad, tail prepared as described, and a custom cannula (needle tip from 30 G insulin syringe glued to polythene tubing 0.4/0.8 mm i.d/o.d, (VWR, USA) 1 m long with dead volume ≈ 100 μL) was inserted and secured in place with surgical tape. For contrast agent injection, the saline dead volume was injected followed by the dose of contrast agent. After imaging, cannulae were removed, then mice were recovered and monitored as described.

2.2.4 Intrastriatal

Mice were anaesthetised as described and a small patch of hair was clipped off the top of the head prior to surgery. Mice were introduced to a sterile environment and mounted on a stereotaxic frame (Kopf, USA) using ear bars, nose clamp and tooth bar. The scalp was swabbed with 5% v/v Hibiscrub in water prior to making a 5 mm long posterior-anterior incision 1 mm left of the midline. Bregma was identified and a burr hole was made using a dental drill 0.5 mm anterior and 2 mm left of bregma. 0.5 μL of cell solution, chemokine or saline was injected over the course of five minutes through a pulled glass microcapillary at a depth of 2.5 mm from the dorsal surface of the brain. Capillary for cell injection: Clark Electromedical Instruments GC100F-15 capillary pulled at power level 76.7 and trimmed to 75 μm o.d. under a light microscope; capillary for chemokine injection: Sigma Aldrich P0549 capillary pulled at power level 72.8 and trimmed (Capillary heater PP-830, Narishige, Japan). At the end of the injection the microcapillary was slowly removed, the scalp was sutured and the animal was recovered and monitored as described. Typical procedure time was 20 min per animal.

2.2.5 MRI

Mice were anaesthetised and a tail vein cannula was applied as described. Mice were positioned in a quadrature birdcage 26 mm RF coil within a 7 T horizontal bore Varian Inova spectrometer (Varian, UK). The head was fixed to a custom cradle within the RF coil with a tooth bar, screw tightened cheek bars and surgical tape to prevent respiration induced

motion artefacts. Respiration was monitored with a breathing pad and BioPac datalogger and software, temperature monitored with a rectal thermometer and maintained at 37°C with a heating blanket; lubricating eye drops were applied and an isoflurane scavenging system was used. Isoflurane concentrations were adjusted to maintain a breathing rate of approximately 60 breaths per minute.

Once the mouse was mounted correctly, confirmed by a short scout imaging sequence identifying the brain at RF centre, the RF coil was tuned and matched by adjusting variable capacitors and the magnetic field homogeneity was adjusted by shimming to a typical linewidth of ≈ 200 Hz across the whole field of view, and gain and power settings were optimised.

BBB assessment

Before, and 2 h after, a 3 μg intravenous injection of TNF or LT or 4 h after intrastriatal injection of CINC-1, a set of 10 serial T_1-weighted images were acquired using a spin-echo sequence both prior to and 5 min after intravenous injection of 1.2 mg/kg gadolinium-diethylenetriaminepentaacetic acid (Gd-DTPA; Omniscan, GE Healthcare, Little Chalfont, UK) to assess BBB permeability. Regions of interest (ROIs) containing metastases (confirmed histologically) and contralateral same-slice non-tumour ROIs were segmented using VnmrJ (Varian) on post-Gd images. The mean signal intensity values of the ROIs were quantitated before and after LT or TNF administration.

Neuroinflammation assessment

1 h prior to imaging, mice were injected via a tail vein with 4 mg Fe/kg VCAM-MPIO (see above for synthesis). T_2*-weighted 3D gradient echo datasets were acquired to detect contrast agent binding to indicate neuroinflammation. Data were analysed with a voxel-wise hypointensity detection method (see below).

MRI sequences

Shim

Single pulse 1D; mean line width = 217 Hz.

T_1-weighted

Spin echo multi slice; TR 500 ms; TE 20 ms; 2 averages; data matrix 256x256; field of view 25x25 mm; 10 slices 1 mm thick. 98 μm^2 resolution; scan time ≈ 5 min.

Spin echo multi slice with inversion recovery; TR 1200ms; TE 16.4 ms; Ti 1040ms; 4 average; data matrix 256x256; field of view 25x25 mm; 1 slice 1 mm thick. 98 μm^2 resolution; scan time ≈ 20 min.

T_2-weighted

Fast spin echo multi slice; TR 1000 ms; effective TE 40 ms; 8 averages; data matrix 256x256; field of view 25x25 mm; 10 slices 1 mm thick; 98 μm^2 resolution; scan time ≈ 4 min.

T_2-weighed*

Gradient echo 3D; TR 65 ms; TE 7.5 ms; flip angle 27°; 1 average; 256 dummy scans; data matrix 256x192x192; field of view 22.5x22.5x22.5 mm; post-processing zero filling to isotropic resolution of 88 μm^3; scan time ≈ 40 min.

MRI analysis

T_2*-weighted MR images sets were zerofilled in VnmrJ software and processed by masking the volume of interest using Turtleseg software producing a binary mesh map. The raw data and masked brain volume NIfTI files were loaded into MATLAB software, normalised and analysed using automated hypointensity detection software (manuscript in preparation). Briefly, data were run through a script to identify voxelwise regions of hypointensity based on neighbourhood comparison. A voxel was defined as hypointense if it was at or below 65% of the signal intensity of the mean of the surrounding neighbourhood voxels. Regions of greater than 1 but fewer than 20 adjacent voxels calculated to be hypointense were quantified and compared between treatment groups. See appendix for MATLAB script. False positive and false negative identifications were altered subjectively by an observer blind to treatment group using ITKSnap software.

Pre-gadolinium T_1-weighted MR image sets were subtracted from post-gadolinium T_1-weighted MR image sets. Areas of unilateral high signal intensity indicating BBB breakdown were identified and quantified compared to same-slice contralateral region signal intensity.

T_2-weighted MR image sets were viewed for gross changes to brain anatomy.

2.2.6 SPECT/CT

Purified isolated trastuzumab (Tz) (Herceptin, Genentech, USA) was conjugated to para-isothiocyanyl-benzyl-diethylenetriaminepentaacetic acid (p-SCN-BnDTPA) (Macrocyclics, Texas, USA) to allow ^{111}In labelling (118). Excess BnDTPA was removed by size exclusion chromatography using a Sephadex G50 mini-column (Sigma, ON, Canada). Radiolabeling was performed by adding 2 MBq [^{111}In]$InCl_3$ per microgram of antibody (MDS Nordion, BC, Canada) to the BnDTPA-Tz immunoconjugate. The radiochemical yield was 97%, determined by instant thin layer chromatography run in 0.1 M sodium citrate (pH 5.0). Mice injected intracardially with 4T1-GFP cells 13 days prior (n=3 per group) were injected intravenously with 100 μL saline containing 3 μg TNF or LT or no cytokine together with 0.185 mg/kg ^{111}In-BnDTPA-Tz, 2 h prior to single photon emission computed tomography (SPECT) under anaesthesia. SPECT/CT was performed using a nanoSPECT/CT scanner (Bioscan, Washington, USA). Anaesthesia was induced as described above.

Imaging parameters

CT: 45 kV; 180 projections at 45 ms/projection; FOV 35.2x35.2x16.8 mm; data matrix, 176x176x84; voxel size 0.008 mm^3. SPECT: ^{111}In energy window; 4-head tungsten insert with 9x1 mm apertures; 24 projections at

100 s/projection; FOV 35.2x35.2x16.8 mm; data matrix, 124x124x56; voxel size 0.027 mm^3; acquisition time ≈ 1 h. Data were reconstructed using InVivoScope software (Bioscan) with an ordered subset expectation maximisation algorithm with 9 iterations, and analysed using Inveon Research Viewer (Siemens). Hotspots of interest, as indicated from subsequent histological analysis, were normalised against a muscle ROI to compensate for intersubject variability in radioactivity dose.

2.2.7 Blood collection

Mice were terminally anaesthetised. The thoracic cavity was exposed and an incision was made into the left ventricle. Blood was collected using heparin-coated 1 ml syringes and transferred into EDTA-coated vacutainers and stored at 4°C. Cells were separated by centrifugation within 4 h (1100 g, 10 min, 4°C). Frozen plasma fractions were sent to Sequani Ltd. for enzyme and protein assays.

2.2.8 Perfusion

Mice were terminally anaesthetised and the chest cavity exposed to reveal the heart. Mice were transcardially perfused at a rate of 6-8 mL/min with cold 0.9% (w/v) saline with 12,500 U/L heparin followed by fixative (PLP_{light} or Karnovsky's fixative, see below for formulation). Following complete fixation, organs were dissected out and post-fixed for 4 h at 4°C before being transferred to a 30% (w/v) sucrose solution in water at 4°C for 24 h for cryoprotection.

Fixative Recipe

PLP_{light} fixative: Water containing 13.7 g/L lysine-HCl, 1.8 g/L disodium hydrogen orthophosphate dihydrate, 20 g/L paraformaldehyde, 2.14 g/L sodium metaperiodate (VWR), 0.025% (v/v) glutaraldehyde (Sigma), pH 7.2.

Karnovsky's fixative: Phosphate buffer containing 4% (v/v) paraformaldehyde, 2.5% glutaraldehyde, pH 7.2

2.3 Ex vivo procedures

2.3.1 Immunohistochemistry

Cryoprotected brain tissue samples were removed from sucrose solution and frozen in TissueTek (Sakura, UK) using dry ice cooled isopentane and stored at -20°C. Samples were mounted in a cryostat and cut into coronal sections 20 μm thick and mounted on positively charged glass slides (SuperFrost Plus, Menzel Glazer). Slides were air dried overnight and then frozen at -20°C for mid-term and -80°C for long term storage. Slides were dried in a 37°C oven for 5 min prior to immunohistochemical staining using the following protocol, with minor changes for optimal conditions for each target antigen (Table x).

Slides were transferred to metal slide racks and washed in 500 mL containers in 300 mL PBS on a shaker for 5 min. An optional additional antigen retrieval step was performed prior to quenching by heating slides to 80°C in 10 mM sodium citrate in water with 0.05% Tween20 pH 6, and leaving to cool to room temperature for 30 min. Slides were quenched with 1% (w/v) hydrogen peroxide (30% w/v H_2O_2, Sigma) in methanol for 20 min. Slides were washed three times (5 min each) in PBS. Slides were transferred to individual Sequenza slide cassettes and incubated with 130 μL of a blocking solution in PBS for 1 h. Slides were then incubated in 130 μL of primary antibody solution in PBS overnight at 4°C. Slides were washed with PBS three times and then incubated in 130 μL of biotinylated secondary antibody solution (VectorLabs, UK) for 45 min at room temperature. Avidin biotin complex solution (ABC kit, VectorLabs) was prepared 45 min prior to use for substrate development as specified in

product sheet. Slides were then incubated in 130 μL of ABC kit for 45 min. Slides were transferred to metal racks and washed three times in 0.1 M phosphate buffer and exposed to 2.3 mM 3'-3'-diaminobenzidine (DAB) chromagen with $1.5x10^{-4}$ v/v 30% H_2O_2 until maximum antigen staining with minimal background staining (10 s – 8 min). Slides were washed three times in 0.1 M phosphate buffer and incubated in 13 μM acetic acid in water for 3 min, counterstained in 1% cresyl violet acetate solution (Sigma) in water for 1 minute, dipped in water, dehydrated sequentially in 70/80/95% w/v ethanol in water, incubated twice for 5 min in 100% ethanol, incubated three times for 5 min in xylene and coverslips added with distyrene plasticizer and xylene (DPX, VWR) mounting medium.

Human brain tissue sections (4 μm formalin fixed paraffin-embedded; provided by pathology departments of John Radcliffe Hospital, Prof. Olaf Ansorge; and The Walton Centre, Mr Rasheed Zakaria) were dewaxed in xylene and rehydrated in decreasing concentrations of ethanol in water before staining and processing as above.

2.3.2 Immunofluorescent staining

Other tissue sections were quenched with 1% v/v of 30% w/v H_2O_2 in PBS, streptavidin and biotin blocked (SP-2002, Vector Laboratories) and incubated with Tris-NaCl blocking buffer (TNB, PerkinElmer). Sections were subsequently incubated for 16 h at 4 °C with the primary antibodies, rinsed with PBS and incubated with the appropriate biotinylated secondary antibody in TNB for 30 min. Sections were washed with PBS, incubated

with streptavidin-HRP (PerkinElmer; 1:200) in TNB for 30 min, washed and incubated for 8 min in the dark with TSA-biotin (PerkinElmer; 1:100) in amplification buffer (PerkinElmer). Slides were washed and incubated with a streptavidin-Cy3 fluorophore (Invitrogen, 1:300) and AMCA-conjugated secondary antibody (1:150) for 2 h. Slides were coverslipped using Vectashield mounting medium (VectorLaboratories). Images were acquired using a Leica DM IRBE epifluorescent microscope (Leica, Germany) attached to a camera (Hamamatsu, Japan) and analysed using ImageJ. Other images were acquired using a Zeiss confocal microscope using ZEN acquisition software. One-dimensional lines of interest were drawn on images and signal intensity over distance plots were generated.

Fluorescence	DAB	Antigen retrieval	Secondary	Primary	Block	Antigen
x	x	Citrate buffer	Biotinylated horse anti-goat IgG	Goat anti-mouse TNFR1 IgG	10% normal horse serum	TNFR1
x	x	Citrate buffer	Biotinylated horse anti-goat IgG	Goat anti-mouse TNFR2 IgG	10% normal horse serum	TNFR2
x	x	-	Biotinylated rabbit anti-chicken IgY	Chicken anti-GFP IgG	10% normal rabbit serum	GFP
-	x	-	Biotinylated goat anti-rabbit IgG	Rabbit anti-active caspase-3 IgG	10% normal goat serum	Active caspase-3
x	-	-	Biotinylated horse anti-goat IgG	Goat anti-mouse Glut-1 IgG	10% normal horse serum	Glut-1
x	-	-	Biotinylated horse anti-goat IgG	Goat anti-IBA-1 IgG	10% normal horse serum	IBA-1

2.3.3 Hanker-Yates histology

To identify areas of BBB permeability, mice were injected via a tail vein with 100 μL type II horseradish peroxidise (300 units; SigmaAldrich, Dorset, UK) and transcardially perfused 30 minutes later under terminal anaesthesia with 50 mL 0.9% heparinised saline followed by 50 mL Karnovsky's fixative. Brains were post-fixed, cryoprotected, embedded in Tissue-Tek and frozen as described. Free-floating 20 μm thick coronal brain sections were collected in 0.1 M phosphate buffer and stained using a modified Hanker-Yates method (see below). Slides were imaged as described below. The histological tracer horseradish peroxidase (HRP) is a 44 kDa glycoprotein that is excluded from the neuropil by the BBB based on its molecular size, and is only detected in the brain at sites of incomplete BBB such as the median eminence. Each metastasis was described as either positive or negative for brown staining indicating BBB permeabilisation, giving a percentage of positive metastases for each group.

Hanker-Yates method

Hanker-Yates solution was prepared fresh for each experiment (0.2 M sodium cacodylate (pH 5.2) + 0.2% w/w *p*-phenylenediamine + 0.4% w/w catechol. Metal solution was prepared using 48 mL of 1% cobalt (ii) chloride solution in water, 32 mL of 1% ammonium nickel sulphate solution in water and 40 mL Hanker-Yates solution. Developing solution was prepared using 120 mL Hanker-Yates solution with 1.25% v/v H_2O_2.

Free-floating sections were washed in 0.1 M phosphate buffer and transferred using a fine paintbrush into metal solution for 10 min, washed twice in 0.1 M phosphate buffer, exposed to developing solution for 10 min

and washed twice in 0.1 M phosphate buffer. Tissue sections were then transferred to glass slides using glycerin albumin solution and allowed to dry in air overnight. Slides were counterstained in cresyl violet solution, mounted and imaged.

2.3.4 Haematoxylin and eosin histology

Frozen brain sections were air dried and rehydrated in PBS. Slides were incubated in Mayer's haematoxylin solution for 5 min and rinsed in running tap water for 10 min. Slides were sequentially dipped in differentiating solution, water and Scott's tap water solution. Slides were incubated in 95% alcohol in water for 1 min, and dipped in eosin solution (10% v/v in water) for 10 s. Slides were then dehydrated in increasing concentrations of alcohol and xylene and mounted using DPX mounting medium as above.

2.3.5 Immunohistochemistry analysis

Slides were digitally scanned using ScanScope CS slide scanner (Aperio, Vista, CA, USA) and analysed using ImageScope (Aperio). Area of tumour (defined as positive GFP staining with typical cresyl violet counterstain pattern) and total area of tissue was determined using ImageScope software and manual segmentation. Ratio of sum of tumour area and sum of total brain area analysed was calculated. The relative frequency of metastases in increasing bin sizes was calculated for each treatment group. A measure of circularity was calculated for each

treatment group as the ratio between the perimeter length of each metastasis and the perimeter length of a perfect circle of the same area.

Chapter 3 – Permeabilisation of the blood-brain barrier at sites of metastasis: proof-of-principle.

3.1 Introduction

Brain metastases pose a significant challenge for chemotherapeutic treatment owing to the impermeable nature of the blood-brain barrier (BBB), which limits access of drugs and, thus, prevents accumulation of clinically effective doses at tumour sites. It is now known that brain metastases, once extravasated from the blood system, spend some time of growth behind an intact BBB (119) in the perivascular niche. By the time the BBB becomes naturally compromised, the metastases are large, highly aggressive, symptomatic and hard to treat. At the same time, the impermeable BBB also prevents early diagnosis of small brain metastases by the current clinical gold-standard method of gadolinium-enhanced magnetic resonance imaging (MRI). This diagnostic approach enables detection of large cerebral metastases and primary brain tumours, but only once gross structural abnormalities have developed.

Paradoxically, substances with good penetration of the BBB have limited activity against breast cancer, one of the most common cancers metastasising to the brain, whilst the most active therapeutics for breast cancer (including doxorubicin and trastuzumab) appear not to reach the CNS (120) owing to their hydrophilic nature. Moreover, while BBB compromise may allow limited access of drugs to the tumour, this BBB permeability is frequently inhomogenous and generally poor around the

tumour margin (121). Thus, the late stage of BBB disruption and inhomogeneity across the tumour mean treatment is largely ineffective. Smaller metastases possessing an intact BBB evade both detection and treatment, and will inevitably develop into symptomatic tumours.

A number of approaches to transiently circumvent the BBB have been investigated for the delivery of chemotherapeutics to brain tumours (for a review see (122)). Bradykinin B2 receptor activation by cereport (RPM-7) was the first pharmacological treatment to be shown to transiently modify the BBB in a receptor-mediated manner (110,111) and to increase drug transport into rat and human gliomas. This approach, however, did not improve the efficacy of Carboplatin in a phase II trial in glioma patients at the dose used, owing to the dose-limiting side effect of hypotension induced by cereport (112). The efficacy of cereport in brain metastases has not been investigated. Alternatively, intravenous infusion of the hyperosmotic agent, mannitol, has been shown to globally induce endothelial cell shrinkage and tight junction separation, and has been proposed as a means of transiently providing access to cerebral tumours (101). This approach has been performed in humans and has been shown to cause BBB disruption. However, the lack of specificity for tumour sites is a serious confound with regard to healthy brain tissue, whilst the short working window limits therapeutic efficacy (106). Alternatively, ultrasound-mediated focused BBB disruption is a promising technique, but relies on prior knowledge of metastatic sites (123) which currently limits application to late-stage metastases in which the BBB is at least partially compromised. Thus, further work in this area is critical if brain metastases are to be detected and treated earlier, and, hence, more effectively.

Preclinical studies aimed at increasing drug delivery to systemic tumours have demonstrated the ability of an intravenous bolus dose of recombinant human tumour necrosis factor (TNF), a pro-inflammatory cytokine, to disrupt endothelial tight junctions in the tumour vasculature through the RhoA/Rho kinase pathway (124). This approach was shown to enhance the permeability of tumour vasculature and to facilitate virus particle delivery to a solid subcutaneous xenograft EL4 lymphoma model in mice. Additionally, induction of transendothelial permeability by TNF has been shown to be mediated by tissue factor (125), regulatory G-proteins (126) and protein kinase C-α (127), which suggests a complex multifactorial mechanism. TNF has two endogenous receptors (TNFR1 and TNFR2) which mediate endothelial cytoskeletal reorganisation and destabilisation of inter-endothelial adhesion complexes (128). Whilst their activation is generally associated with pathophysiological processes, the effect of TNF receptor activation in controlled low dose administration may be beneficial. However, the normal adult brain microvasculature, unlike peripheral blood vessels, is known to be resistant to the permeabilising effects of cytokines (129). This resistance can be modified by a number of factors and previous work in the group has shown that microinjection of TNF into the rat brain can cause focal, but delayed, disruption of the BBB in association with a focal inflammatory response (130). More recent work in the group has shown that the early phases of metastasis development in the brain are associated with a strong inflammatory response and activation of the cerebral endothelium (91,131). Based on the above findings, it was hypothesised that cerebral metastases may provide a unique environment for TNF receptor activation on the associated vasculature and that this

might yield a target for specific and local opening of the tumour-associated BBB.

3.2 Hypotheses

The primary hypothesis to be tested in this chapter, therefore, are:

1. Intravenous administration of TNF, or its endogenous analogue, lymphotoxin (LT), can permeabilise the BBB specifically at sites of cerebral metastasis throughout the brain.
2. This permeabilisation will allow entry of (a) diagnostic imaging agents for early detection of metastases and (b) a clinically relevant anticancer therapeutic agent.

3.3 Methods

In this chapter, a mouse model of brain metastasis was used with a similar experimental schedule for all experiments (see below). See Chapter 2 for further detail of all experimental techniques.

3.3.1 Histological detection of BBB permeability

Female BALB/c mice (n=3 per group) were injected intracardially with 10,000 4T1-GFP cells and monitored for natural and provoked behaviour and weight for 13 days (see Chapter 2.2.2, Figure 2.1). Mice were then injected intravenously with 100 μL saline containing 1-5 μg of either recombinant mouse TNF (TNF, Peprotec) or recombinant mouse lymphotoxin (LT, R&D Systems) or no cytokine as control. After 1.5 h, 3.5 h, 5.5 h, 23.5 h or 71.5 h, mice were injected intravenously with 100 μL saline containing 300 units type II horseradish peroxidase (HRP, Sigma Aldrich); 30 min later, mice were terminally anaesthetised, transcardially perfusion-fixed and brains removed. Brains were histologically analysed using a modified Hanker-Yates method (see Chapter 2.3.3).

In parallel experiments, female SCID mice (n=3/5 per group) were injected intracardially with 10,000 MDA-231-Br-eGFP cells and monitored for 21 days as above. Mice were then injected intravenously with 100 μL saline containing 3 μg TNF or no cytokine as control; 90 min later, mice were processed as above.

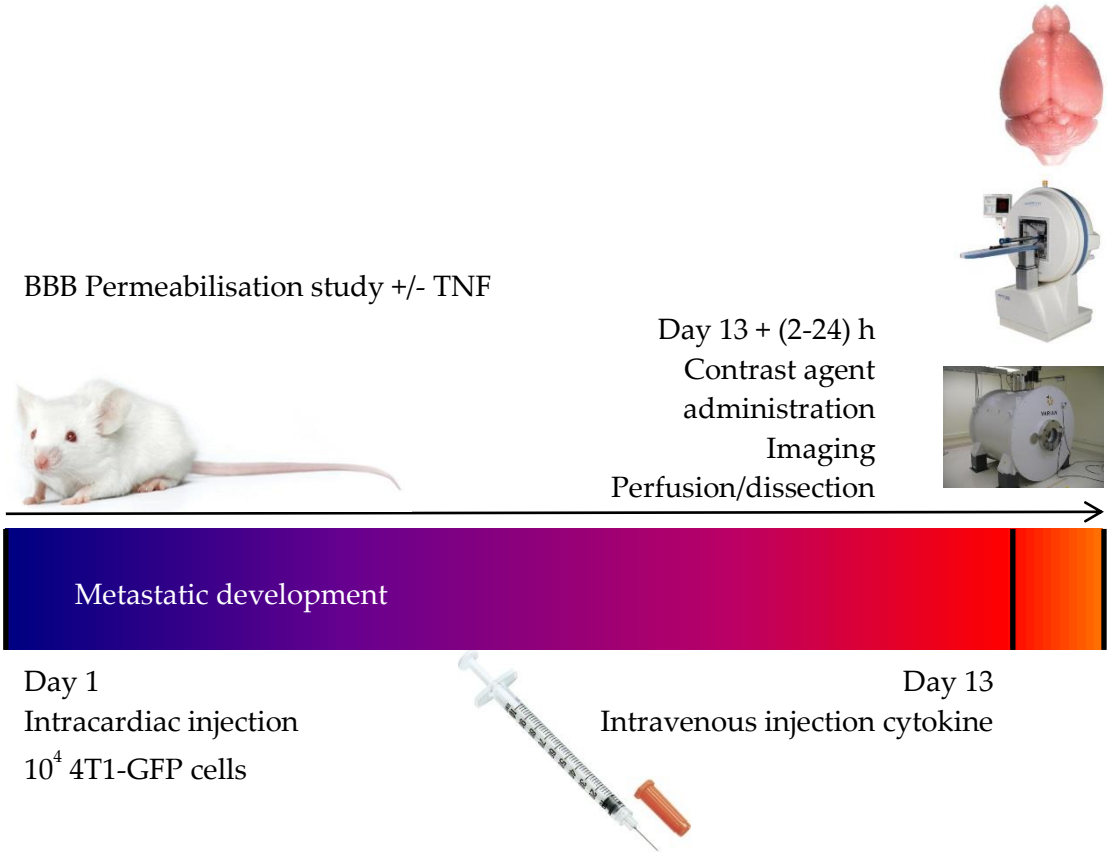

Figure 2.1. Experimental schedule used in Chapter 3. Mice are injected intracardially with 10^4 4T1-GFP cells. Thirteen days later, mice are injected intravenously with cytokine. 2 h later, mice are injected with contrast agent (HRP, Gd-DTPA or ^{111}In-Trastuzumab). Mice are imaged using MRI or SPECT/CT, perfusion fixed and brains are dissected.

3.3.2 *In vivo* MRI detection of BBB permeability

Mice (n=3 per group) were injected intracardially with 10,000 4T1-GFP cells and monitored for 13 days as above. At day 13, mice were then anaesthetised and imaged using MRI (see Chapter 2.2.5). Sets of T_1-weighted data sets were acquired before and 5 min after injection of 1.2 mg/kg Gd-DTPA contrast agent both before and 2 h after injection of 3 μg of rmTNF or rmLT. Mice were recovered and were treated as above for histological detection of BBB permeability directly afterwards.

3.3.3 *In vivo* detection of radiolabeled anti-cancer drug

Mice (n=3 per group) were injected intracardially with 10,000 4T1-GFP cells and monitored for 13 days as above. At day 13, mice were then injected intravenously with 100 μL saline containing 3.7 μg ^{111}In-BnDTPA-Trastuzumab together with 3 μg of either rmTNF or rmLT or no cytokine as control. Mice were anaesthetised and a 3D dataset of SPECT images were acquired (see Chapter 2.2.6). Mice were terminally anaesthetised and brains processed for histological detection of brain metastases as above. Filled syringes were counted using a gamma counter immediately prior to injection and a dose of 9.7 MBq ± of ^{111}In (Figure 3.4 E) was administered to each mouse. This dose and timepoint was selected to match the lowest dose and at the earliest time-point that elicited a significant difference as detected through histology to minimise potential side effects of TNF injection and to maximise radioactive signal from the injected indium.

3.3.4 Analysis of model of frank BBB breakdown

Mice (n=2) were injected intracerebrally with 0.5 μL of 1 mg/mL CINC-1 via a fine-pulled glass capillary under anaesthesia. After 4 h, mice were anaesthetised and imaged using MRI, as described above, after intravenous injection of 1.2 mg/kg Gd-DPTA. Mice were then recovered, intravenously injected with 300 units of HRP, perfusion fixed and brain tissue was stained using the Hanker-Yates method.

3.4 Results

Observations of mice injected with TNF or LT suggested transient and mild sickness behaviour with a hunched appearance, piloerection and reduction in natural, but not provoked exploratory behaviour. In this model of intracardially-induced brain metastasis, no neurological symptoms were observed at the stages used here.

3.4.1 Histological detection of BBB permeabilisation

Following intravenous injection of horseradish peroxidase (HRP), BBB permeabilisation was defined as brown HRP staining within Hanker-Yates treated tissue sections at metastases larger than ≈ 1000 μm^2 in area to ensure correct identification of metastatic colonies. 1,102 separate metastatic colonies, identified by microscopy of cresyl violet counterstained sections, were analysed blind to treatment group to determine their status with respect to BBB integrity as either positive or negative for brown HRP staining. No BBB breakdown was observed in 4T1-GFP injected mice at non-metastatic sites before or after cytokine injection (Figure 3.1 A and D). TNF (B and E) or LT (C and F) induced HRP staining that was largely restricted to the metastatic colony, whilst some displayed minor spread to the surrounding tissue. Frequency with which BBB

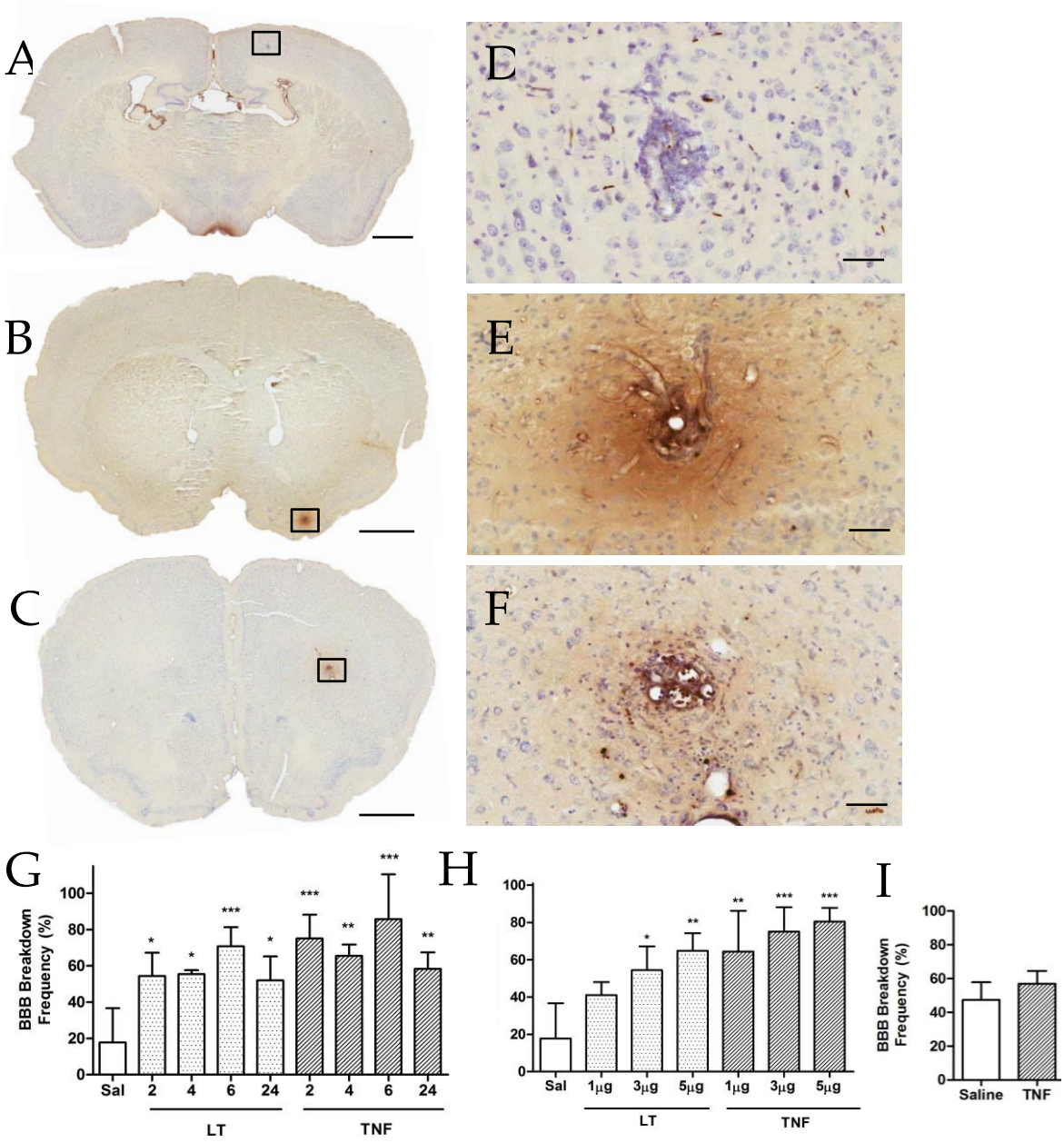

Figure 3.1: Histological detection of brain metastases and cytokine-induced BBB breakdown. Brain metastases from mice injected systemically with HRP and saline (A, D), 3 μg TNF (B, E) or 3 μg LT (C, F). Hanker-Yates histology for HRP detection (brown) reveals areas of BBB breakdown. Cresyl violet counterstain. Scale bars (A - C) 1 mm, (D - F) 50 μm. (G) Graph showing temporal analysis of BBB breakdown 2, 4, 6 or 24 h after systemic administration of 3 μg LT or TNF. (H) Graph showing dose-response of BBB breakdown at metastatic sites 2 h after systemic administration of 1, 3 or 5 μg of LT or TNF. Statistical analyses: 1 way ANOVA with Dunnet's post-hoc test *vs*. saline group (**P*< 0.05, ***P*< 0.01, ****P*< 0.005; Mean ± SD, n=3 per group). (I) Incidence of BBB breakdown at sites of metastasis 72 hours after intravenous TNF or saline administration (n=3 per group). No significant difference *P*=0.2740; unpaired t-test.

breakdown was observed in metastases after intravenous cytokine treatment was significantly higher than in non-cytokine treated controls (Figure 3.1 G; 1-way ANOVA followed by Dunnett's post-hoc test *vs* saline ***P<0.001, **P<0.01, *P<0.05). The frequency of BBB breakdown after intravenous administration of either LT or TNF (3 μg) appeared to peak at 6 h (Figure 3.1 G). Breakdown was still evident at 24 h, but appeared to be decreasing in both TNF and LT groups, although this decrease did not reach significance (1-way ANOVA). The frequency of BBB breakdown in metastases appeared to escalate with dose (1, 3 or 5 μg of LT or TNF), but this did not reach significance (1-way ANOVA). To further investigate the window of BBB permeabilisation, an additional group of animals were injected intravenously with either 3 μg TNF or saline as control 13 days after metastasis induction. After 72 h, no significant differences were found in the incidence of breakdown between TNF and control groups (Figure 3.1 I; unpaired t-test P=0.274).

The above histological experiment was repeated in SCID mice bearing intracardially injected human breast carcinoma cells (MDA-231-Br-eGFP). In this model, TNF was injected intravenously at a later time point (21 days post-induction), owing to the slower growth rate of the human tumour cell line. The frequency with which BBB breakdown was observed at sites of metastasis was significantly higher in mice injected intravenously with TNF than saline (Figure 3.2; n=5 each group; *P<0.05; unpaired t-test).

3.4.2 *In vivo* MRI detection of BBB permeabilisation

Next, the hypothesis was tested that the cytokine-enhanced permeabilisation would enable early detection of micrometastases by gadolinium-enhanced MRI. Subtracting pre-Gd-DTPA T_1-weighted image sets from post-Gd-DTPA image sets reveals the presence of BBB breakdown as hyperintense areas in pre-cytokine (Figure 3.3 A) and post-cytokine (Figure 3.3 B) administration. In histologically confirmed sites of metastasis (Figure 3.3 C), regions of interest were drawn around difference images and mean signal intensity values were calculated. The ratio of signal intensity at sites shown to contain metastases *vs*. non-metastasis containing equivalent regions in the contralateral hemisphere was significantly greater 2 h after administration of 3 μg of LT (n=6, P=0.0313) or TNF (n=8, P=0.0078) than those regions before cytokine administration (Figure 3.3 D; two-tailed Wilcoxon signed rank test). T_1-weighted

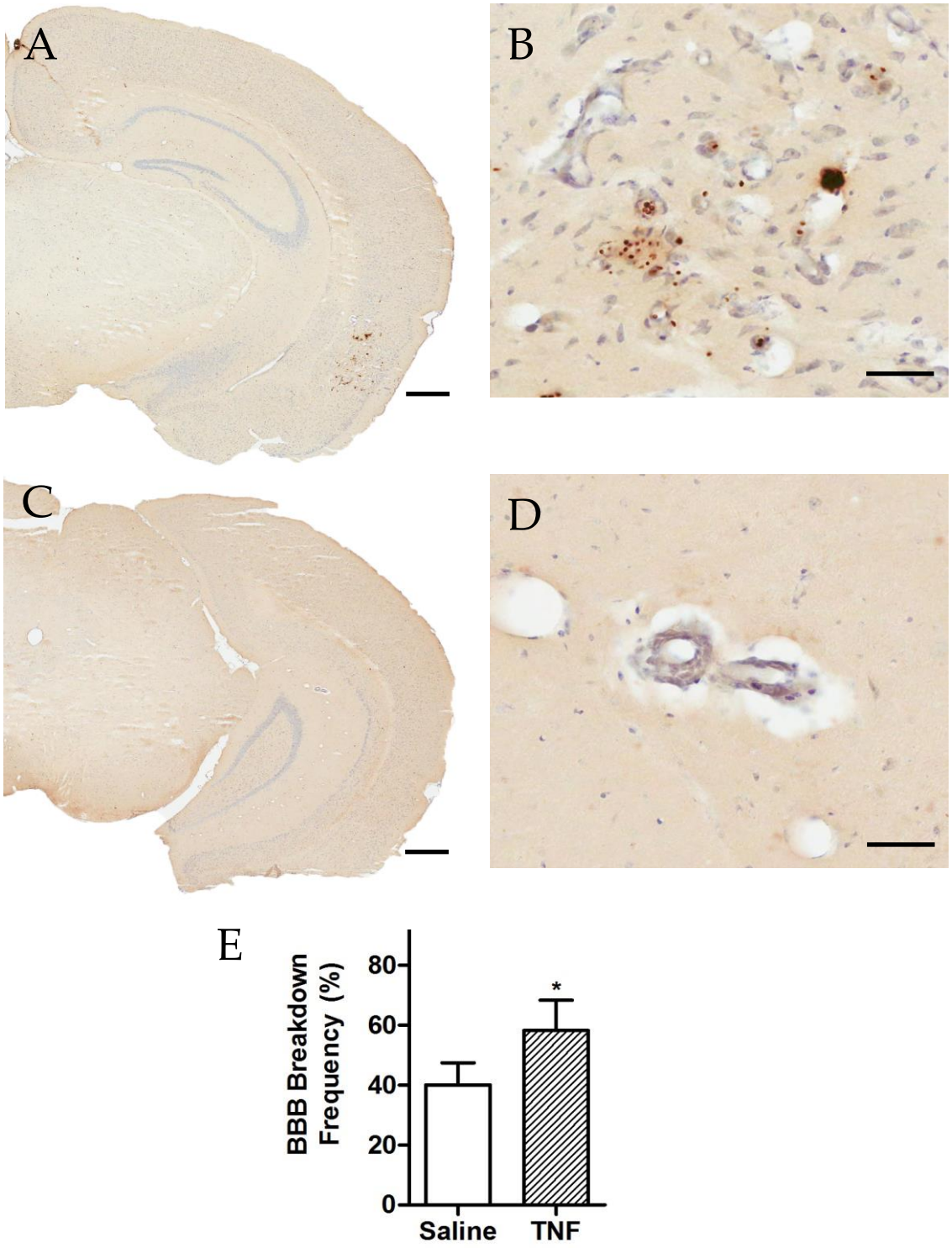

Figure 3.2: Incidence of BBB breakdown in SCID mice 21 days after intracardiac injection of MDA-231-Br-eGFP cells. Mice injected intravenously with TNF (A and B; n=3) showed significantly higher incidence of metastases with a permeable BBB than mice injected intravenously with saline (C and D; n=5). (E) Graph representing frequency of BBB at sites of metastasis. *P<0.05 unpaired t-test. Scale bars (A and C = 500 μm; B and D = 50 μm).

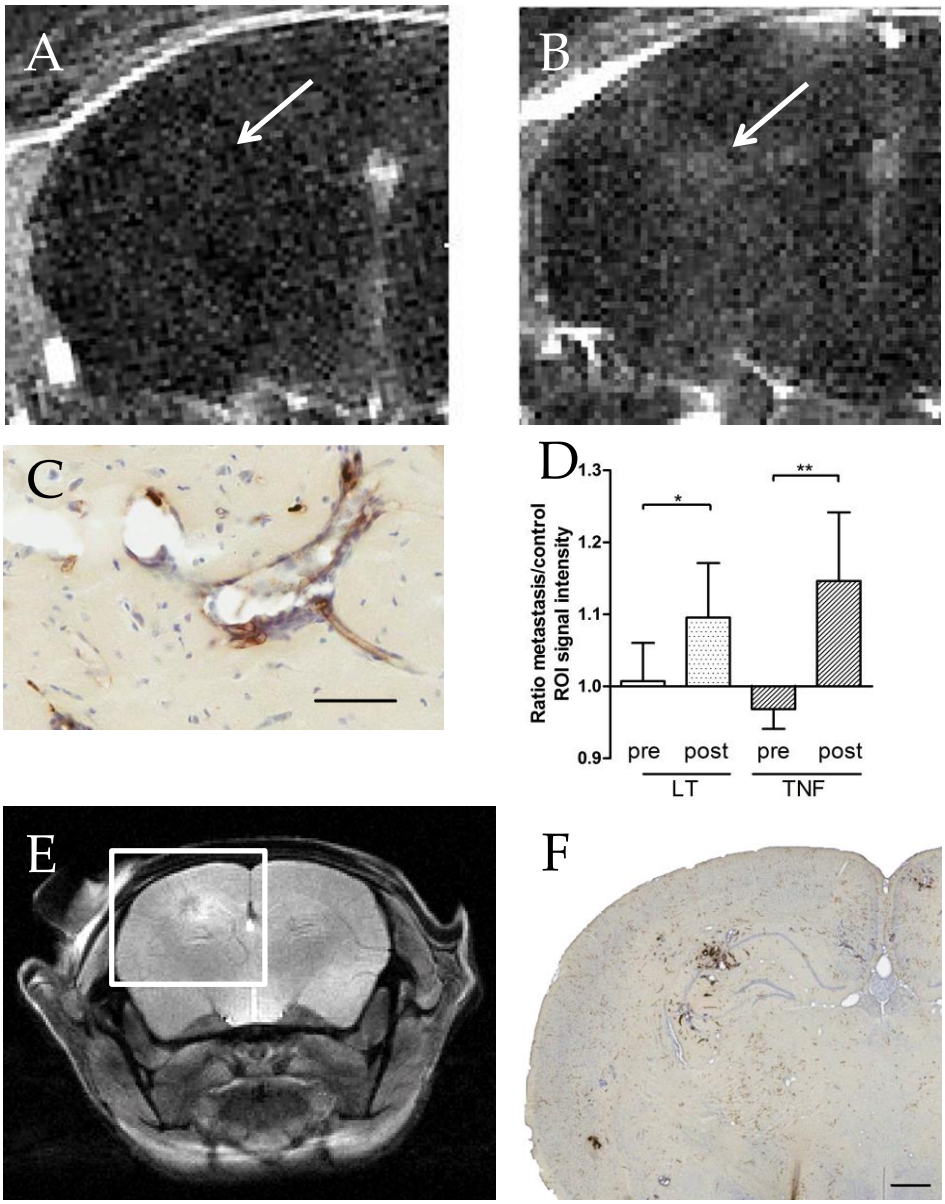

Figure 3.3: MRI detection of cytokine-induced BBB breakdown at sites of metastasis. Representative example of difference of T_1-weighted post-gadolinium images minus pre-gadolinium images (A) before and (B) 2 h after intravenous injection of 3 μg TNF. Areas of high signal intensity (white) infer areas of BBB breakdown and Gd-DTPA entry. Regions of signal enhancement were histologically shown to be sites of metastasis (arrows; C). Region of interest (ROI, n=14) signal intensities, correlating to histologically verified metastatic sites, in LT and TNF treated brains were significantly higher than equivalent control ROIs. Signal intensity of metastasis ROI divided by signal intensity of equal ROI on contralateral hemisphere; ratio of 1.0 represents no breakdown. Mean ±SD. Wilcoxon signed rank test (two tailed) LT (n=6, **P*=0.0313), TNF (n=8, ***P*=0.0078). (E) Heavily T_1-weighted inversion recovery image from metastasis-bearing mouse injected intravenously with 3 μg of TNF, brain 5 minutes after Gd-DTPA injection. (F) Photomicrograph of Hanker-Yates stained tumour colony from brain slice corresponding to white box. Scale bars = (C) 50 μm; (F) 500 μm.

images with high resolution reveal the close correlation of Gd-DTPA entry and accumulation (Figure 3.3 E) to HRP entry and accumulation (Figure 3.3 F).

3.4.3 *In vivo* detection of radiolabelled trastuzumab

Having demonstrated enhanced permeabilisation both *ex vivo* by histology and *in vivo* by MRI, it was next considered whether delivery of a relevant chemotherapeutic agent could be facilitated.

^{111}In-BnDTPA-Tz was administered intravenously in combination with TNF, LT or saline as control, to determine whether cytokine-mediated permeability changes facilitated trastuzumab delivery to metastases. Antibody was excluded from the brain at sites of metastasis in mice injected intravenously with saline (Figure 3.4 A), as well as at non-tumour sites in the brain. In contrast, following systemic injection of ^{111}In-BnDTPA-Tz in combination with either LT (Figure 3.4 B) or TNF (Figure 3.4 C) isolated regions of increased SPECT signal were evident within the brain, which correlated histologically with sites of metastases (Figure 3.4 a-c). Quantification of intracerebral radioactivity revealed significantly greater

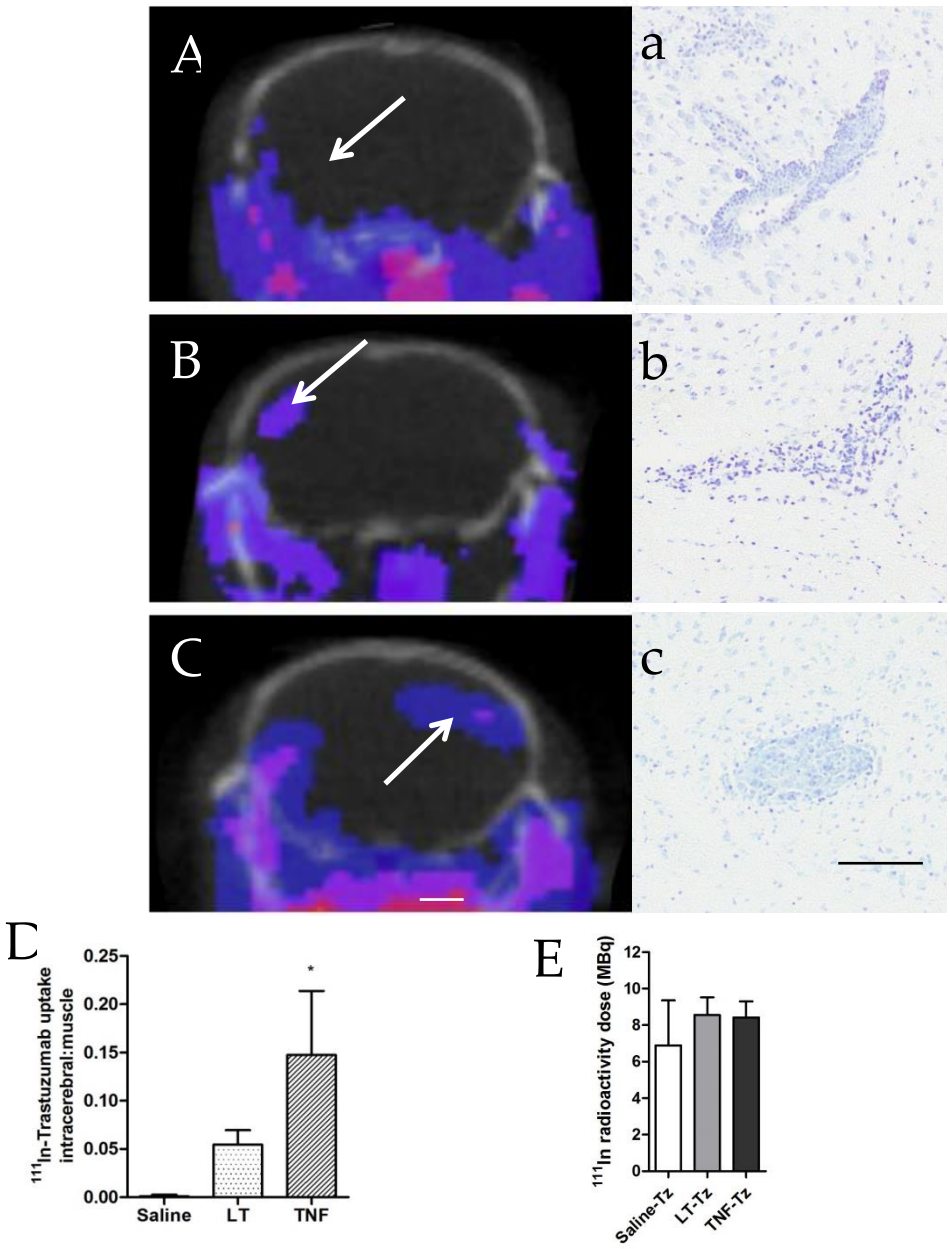

Figure 3.4: Detection of ^{111}In-BnDTPA-Tz using SPECT/CT. Single slice SPECT/CT images showing localisation of radiolabelled antibody (heat map) in mice treated with saline (A), 3 μg LT (B) or 3 μg TNF (C). Intracerebral SPECT signal reveals accumulation of antibody at sites of BBB breakdown. Regions showing SPECT signal enhancement (arrows) were later confirmed to be sites of metastasis with cresyl violet histology (a - c). Note site of metastasis shown in (a) was not detected with SPECT in mouse injected systemically with ^{111}In-BnDTPA-Tz and saline (A; arrow). Scale bars: (A - C) 2 mm, (a - c) 100 μm. (D) Ratio of radioactivity count from sum of intracerebral ROIs compared to muscle ROI (n=3 per group). Statistical analysis: Kruskal-Wallis with Dunn's multiple comparison test (*P< 0.05). (E) Injected doses of radioactivity were not significantly different between groups.

signal in the brains of metastasis bearing mice treated with TNF than controls (Figure 3.4 D; *P<0.05; Kruskal-Wallis with Dunn's multiple comparison test).

3.4.4 Demonstration of frank BBB breakdown

Having demonstrated minor breakdown of the BBB, it was considered important to show detection of frank BBB breakdown in a different model to demonstrate safety as strategies to elicit BBB breakdown post the hazard of haemorrhage. Haemorrhage was not seen in normal brain or associated with brain metastasis 72 h after intravenous injection of TNF (Figure 3.5 A – B) or after injection of saline (Figure 3.5 C). In a rat model of late-stage brain metastasis (Figure 3.5 D image kindly provided by Dr Sébastien Serres), extravascular erythrocytes are clearly visible within and surrounding the metastatic lesion. Further, in mice injected intracerebrally with 0.5 μL the chemokine CINC-1, extensive spread of BBB breakdown is seen both with gadolinium-enhanced MRI (Figure 3.5 E) and with Hanker-Yates histological staining of intravenous HRP.

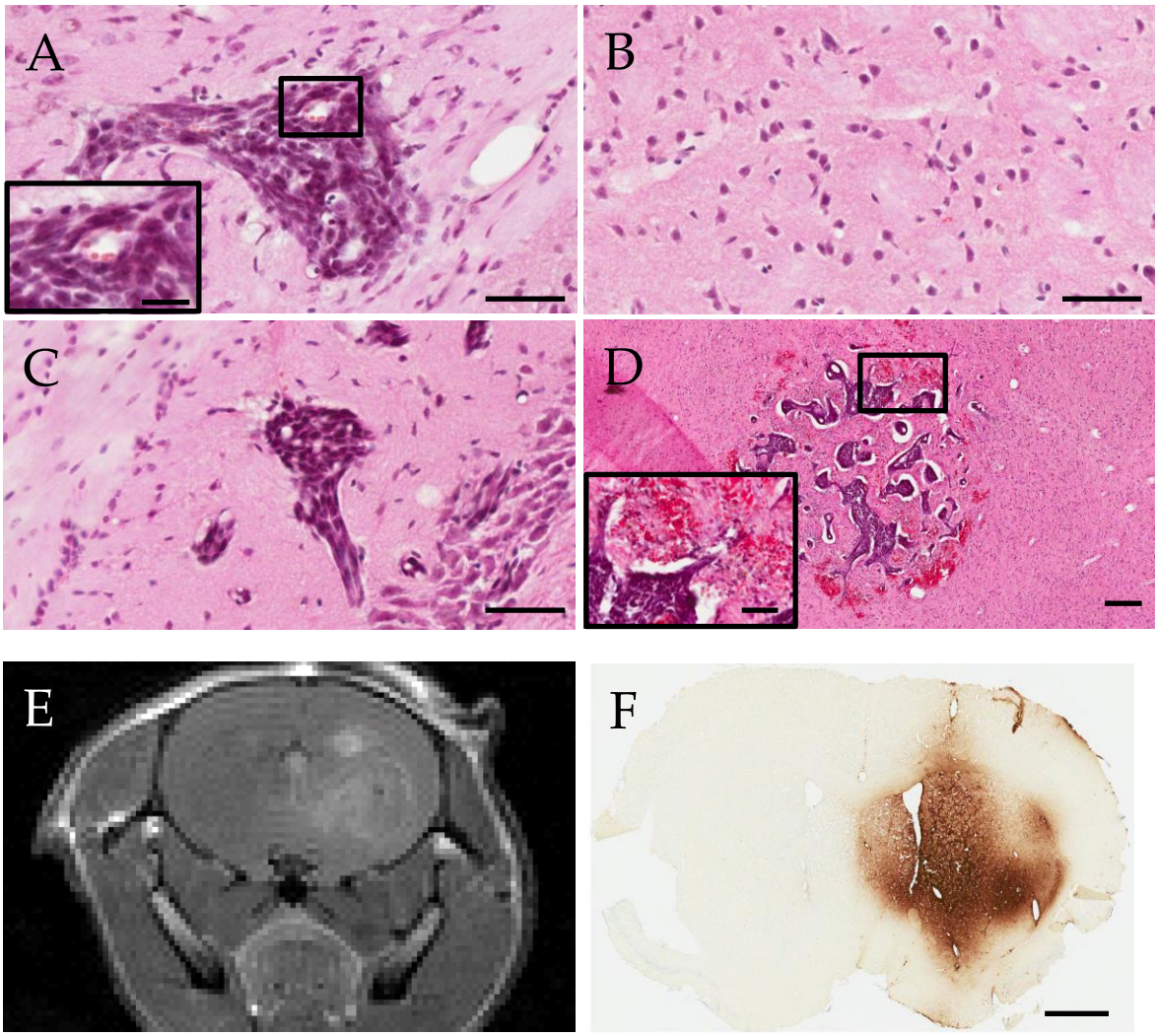

Figure 3.5: (A - D) Representative photomicrographs showing haematoxylin and eosin staining of brain tissue from mice injected intracardially with 4T1-GFP cells, 72 h after either 3 μg TNF (A - B) or saline (C) intravenous injection. No extravascular erythrocyte accumulation was evident either at sites of metastasis (A, C) or in normal parenchymal brain tissue (B). Insets in (A and D) show higher magnification of boxed region. (D) Photomicrograph showing positive control of frank haemorrhage in a later stage intracerebrally injected brain metastasis in the rat (kindly provided by Dr Sébastien Serres). Scale bars = (A - D) 50 μm; (A and D insets) 20 μm. Frank BBB breakdown 4 h after intracerebral injection of 0.5 μg CINC-1 shown by (E) gadolinium-enhanced T_1-weighted MRI and (F) Hanker-Yates detection of intravenous HRP. Scale bar = (F) 1 mm.

3.5 Discussion

This study has described a new approach to permeabilise the vasculature of brain metastases that is based specifically on the stromal vascular phenotype of these tumours, with a view to enhancing detection and improving the delivery of chemotherapeutic agents. A mouse model of brain metastasis was used that generates micrometastases in the brain, which, at the timepoint used here, rarely present with a permeable BBB. Systemic administration of the cytokines LT or TNF induced permeabilisation of the BBB specifically at the sites of brain metastases, as revealed both *ex vivo* through histology and *in vivo* through contrast-enhanced MRI. Moreover with this method trastuzumab was successfully delivered selectively to metastatic colonies in the brain as revealed by SPECT/CT imaging.

3.5.1 Permeabilisation of the BBB: *Ex vivo*

Following treatment with 1, 3 or 5 μg of either cytokine, the intravenous tracer HRP was found within metastases in the brain, indicating compromise of the BBB. The increasing dose gave rise to an increase in frequency of metastases exhibiting a permeable BBB but no significant differences were found between doses. The counterstaining of HRP may introduce bias in identifying metastases, but care was taken to scan all of the section, and include metastases negative for HRP staining. Breakdown of the BBB was highly specific and local to the sites of brain metastases, and no other permeabilisation of the BBB was observed in

normal brain tissue. This effect was maintained for all of the time points studied here; the greatest number of HRP-positive metastases was evident at 6 h, whilst an apparent decrease in the number of HRP-positive metastases at 24 h suggests that this is an extended, but transient opening of the BBB. In accord with this, no significant difference in the frequency of metastases with a permeable BBB was found 72 h after systemic injection of either TNF or saline as control. Whilst the percentage of HRP-positive metastases at 72 h was similar to the 24 h time point, the control animals also displayed a permeable BBB at 45% of analysed sites of metastasis. The control animals were at this point 16 days post-metastasis induction, and this reflects the natural time course of metastasis permeabilisation in this mode. This finding highlights a limitation of this model which was a highly aggressive metastatic cell line and the rapid progression of these tumours to natural BBB permeability. Nevertheless, the appropriate tumour burden and low permeability frequency at day 13 provided a good model for the study described here.

No significant differences were found between LT and TNF effects in either the dosing and time range used here. Given that both LT and TNF elicited a permeabilisation effect and have activity at shared receptors, these findings may suggest that the mechanism is mediated by one of the TNF receptors. This concept will be investigated further in Chapter 3.

3.5.2 Permeabilisation of the BBB: *in vivo*

Numerous local hyperintensities were evident in brains of metastasis-bearing mice on post-Gd-DTPA T_1-weighted images following systemic treatment with LT or TNF. Whilst all of these regions correlated with sites of metastasis detected histologically, some sites of histologically evident metastasis were not detectable with MRI. This apparent lack of permeability in some metastases may be due to the limited resolution of the *in vivo* scans (*ca.* 160 μm), giving a higher size detection threshold than the histological method (*ca.* 1 μm). Nevertheless, even metastases of around 50 μm diameter showed sensitivity to cytokine-induced permeabilisation, which is considerably smaller than those currently detectable clinically (0.5 – 1.0 cm diameter) owing to natural BBB permeability (67,132).

These findings suggest that this method could be applicable to enhancing diagnosis of early stage metastasis through MRI by selectively facilitating localisation of contrast agent to lesion sites.

3.5.3 Delivery of trastuzumab to brain metastases

Trastuzumab is a monoclonal antibody that is active against *HER2*-overexpressing breast cancer, leading to reduced breast tumour burden and increased patient survival (133). Extravasation of circulating antibodies and binding to the Her2 receptor leads to a number of anti-tumour actions (for review see (134)). However, trastuzumab is ineffective in treating brain metastases, largely due to restricted access to the Her2 receptor once the metastatic tumour cells are sequestered on the brain side of the BBB, since

it does not effectively cross the BBB (120,135,136). Similarly, in the 4T1-GFP model used here, trastuzumab was excluded both from normal brain (distant from a metastasis) and from sites of brain metastasis in saline-treated controls. However, in mice treated systemically with LT or TNF, the antibody was found to permeate the BBB and accumulate within the brain to a level detectable by SPECT imaging. Metastases were present at all sites of intracerebral SPECT signal, but were much smaller than the volume of signal presenting on the SPECT/CT image. Thus, whilst accurately displaying the amount of radioactivity, the partial volume effect and potential spread of antibody from point of delivery may over-represent the metastasis size. As with the MRI studies, some metastases were present in the brain that did not appear to accumulate radiolabelled antibody. Again, this may reflect the low spatial resolution of SPECT detection (0.027 mm^3) precluding detection of small micrometastases. Once again, the metastases that were detected, and thus exposed to the therapeutic compound, were well below the detection threshold currently possible clinically (67,132). These micrometastases would not otherwise be accessible to the therapeutic and, thus, this approach could confer a significant advantage for treatment of early brain metastases, when therapeutic efficacy may be greatly enhanced.

It is important to state that the 4T1-GFP cells used here are not HER2 overexpressing cells (121)(as tested in subsequent chapter Figure 4.1), so the detection of SPECT signal can only allow the interpretation of an accumulation of the antibody at the site of interest, as opposed to the typical binding of antibody to its target antigen, which is required for

efficacy of the antibody as a therapy. Repetition of these experiments involving a HER2 overexpressing cell line and a suitable dosing scheme would allow any increased efficacy to be detected as a consequence of TNF-enhanced trastuzumab delivery.

The detection of permeabilisation presented here appears very local to the site of metastasis and the normal brain is spared. In another, more advanced rat model of brain metastasis, haemorrhage is apparent around the whole site of metastasis, and in a model of frank BBB breakdown, contrast agent extravasation has spread from the 0.5 μL injection site to the whole hemisphere, only contained within the striatum by the corpus callosum. This indicates that the permeabilisation at sites of metastasis is local and spares normal brain tissue.

Additionally, work was attempted to increase the spatial resolution f these results by performing *ex vivo* autoradiography on the brains that were scanned using SPECT. Unfortunately, technical issues prevented completion of this result, owing to overly rapid freezing of the brains in an effort to minimise exposure to radiation. The brains disintegrated upon sectioning as suitable cryoprotection such as 24 h incubation in 30% sucrose was not performed.

Previous work using bradykinin analogues to enhance permeabilisation in glioma models demonstrated a peak of increased drug delivery after 15 minutes of cereport infusion (137), a size limitation for access to the brain of 1 kDa sized molecules (138) and dose-limiting side-effects. Interestingly, it has been suggested that a possible mechanism of action of bradykinin involves the accelerated release of TNF (114). The

approach described here of a direct systemic administration of TNF, or its endogenous analogue LT, may have three significant advantages over the use of bradykinin. Firstly, the 'window' of permeability is substantially extended, evident from 2 h, although earlier time points have not yet been investigated. Subsequently, permeabilisation appeared to peak 6 h after cytokine administration and to be maintained to at least 24 h. This extended window of permeability would increase the opportunity for intravenous drugs to bind to their targets. It is of interest to note that the downstream effects of TNF persist to well beyond the point of which TNF is detectable in plasma. Secondly, entry of a range of molecules was facilitated with this approach, from gadolinium-DTPA (938 Da) to HRP (44 kDa) and up to the therapeutic monoclonal antibody, trastuzumab (148 kDa), suggesting that drug size may not be prohibitive. Although using an experimental approach of testing a range of sizes of fluorescently labelled dextran beads to quantify precise permeability size would be of great benefit in a similar manner to previously reported (115). Finally, while conscious of the potential concerns over TNF toxicity such as cardiac toxicity that correlates with dose (139), the human equivalent of the range of doses used in the mouse model here should elicit the desired response within the maximum tolerable dose (MTD 150 $\mu g/m^2$ (140)). Use of a dosing schedule with several repeated smaller doses, calculated through knowledge of the plasma half-life of TNF in the blood (141) may allow for a therapeutic action while also avoiding off target effects. With the permeabilisation response only detected in blood vessels at sites of metastasis, and knowledge that TNF elicits its response through specific receptors that can be found on endothelial cells (142), differential

expression of TNF receptors may be behind the selective aspect of the permeabilisation response. This will be further investigated in chapter 5.

3.6 Conclusion

The work presented here shows a novel approach to facilitating the delivery of therapeutic and diagnostic agents to cerebral metastases. Critically, even small metastases (*ca.* 200-fold smaller than those currently detectable in the clinic) are targeted with this approach. This work has demonstrated that cytokine-enhanced drug delivery to brain metastases is possible, and that this strategy may be critically important for the detection and treatment of brain metastases clinically.

With the proof-of principle of this approach now demonstrated, it is important to extend the approach to effectively reduce tumour burden. There is a range of approaches to combat cancer that employ injected chemical agents. Radiotherapy is currently one of the top therapy options in brain metastasis, however, it only confers a minimal advantage in patients (44). Therefore, enhanced delivery of radiosensitisers to sites of brain metastasis may significantly enhance effectiveness and particularly when metastases are small and less aggressive. Indeed, enhanced delivery of chemotherapeutics would enhance reduction in tumour burden and could confer a significant improvement in treatment of this pathology. Going forward, the key questions are whether this approach can elicit a reduction in tumour burden through enhancing delivery of active chemotherapeutics at sites of metastasis.

Chapter 4 – Enhanced delivery of chemotherapy to sites of brain metastasis.

4.1 Introduction

In the previous chapter it was demonstrated that it is possible to permeabilise the blood-brain barrier specifically at sites of metastasis through systemic administration of TNF and lymphotoxin. Also demonstrated was the effective delivery of Trastuzumab (Herceptin), a monoclonal antibody directed against the erbB2 receptor (Her2), which is commonly used therapeutically in Her2 positive breast cancer patients (143).

Delivery of trastuzumab to micrometastases in the brain indicates the potential of this therapy enhancement approach and trastuzumab was used as it is a relatively large molecule, thus highly likely to be excluded from the brain by an intact BBB (136). The study was designed to demonstrate enhanced delivery rather than therapeutic effects of a widely used therapeutic agent. However, for this approach to be of value, it must facilitate drug delivery to such an extent that a reduction in tumour burden is achieved.

The murine mammary carcinoma cell line used in this model does not over-express erbB2 receptor, which is a requirement for the action of trastuzumab. Therefore, to assess whether the permeabilisation strategy would confer enhanced therapeutic effect, another commonly used breast cancer therapeutic was used. Liposomal doxorubicin is known to be

largely excluded from normal brain (144,145) but if it would be delivered to brain metastases then it might be expected to have significant therapeutic value, given its profile in peripheral tumours.

Doxorubicin (or Adriamycin) is an anthracycline antibiotic and has been used as a chemotherapeutic agent since the 1970s. The precise mechanism of action is unknown, but it is thought to intercalate DNA, resulting in DNA synthesis inhibition due to template disordering and steric obstruction (146). As doxorubicin elicits cell death by interrupting mitosis, it can be considered to 'target' tumour cells that are rapidly dividing, as compared to normal cells in the body (such as endothelial cells) that divide less rapidly. Accordingly, typical side effects of doxorubicin include hair loss and nausea due to effects on rapidly dividing hair follicles and cells in the digestive tract. The current therapeutic formulation is a PEGylated (polyethylene glycol) liposomal compound marketed as Caelyx (also named Doxil/Myocet; $402 million sales worldwide in 2011 (147)). This formulation is approved for AIDS related Kaposi's sarcoma and recurrent ovarian carcinoma (148,149). The liposomes can deliver their payload to tumours by extravasating through the permeable tumour vasculature, through convection and diffusion processes, and gradually release the drug into the extracellular fluid compartment. The cellular uptake of the drug is in the non-liposomal form. This formulation has a significantly improved pharmacokinetic profile compared to free doxorubicin (60-fold increase in area under the plasma concentration-time curve (150)) which is critical in allowing repeated passages through the tumour microvascular bed to facilitate the slow extravasation process.

Thus, the first aim of the experiments described in this chapter is to determine whether Caelyx can induce a reduction in tumour burden in the intracardially-induced 4T1-GFP model of brain metastasis, and whether this effect can be enhanced by TNF co-treatment.

The novel compound 2B3-101 (glutathione-PEG liposomal doxorubicin) has been developed by the company toBBB (Leiden, The Netherlands), to facilitate delivery of doxorubicin across the in tact BBB through use of the glutathione transporter (151,152). The success of this approach is thought to reflect a localisation of the glutathione-linked liposome to the cerebral endothelium owing to luminal expression of the glutathione transporter. This interaction of the liposome with the endothelium is believed to enhance subsequent endocytosis of the liposome into endothelial cells or paracellular extravasation. The doxorubicin cargo can then be released from the endothelial cell abluminally, and thus target tumours that may reside behind an intact or partially intact BBB, such as small metastases or primary tumours. 2B3-101 is currently in an open-label, phase I/IIa, multi-centre dose escalating study in patients with solid tumours and brain metastases, or recurrent malignant glioma (153). As this drug was being trialled for brain metastases, we wished to use it to enhance its efficacy.

Efficacy of 2B3-101 has been demonstrated in an intracerebral glioblastoma mouse model, with reduction in tumour growth as measured by change in bioluminescence of luciferase-tagged U87MG cells (154). In addition, reduction in tumour growth in a breast carcinoma xenograft

subcutaneous model has also been shown. In both cases, treatment with 2B3-101 was shown to be more effective than Caelyx treatment. However, an intact BBB was not seen in either of these models.

Thus, the second aim of this chapter was to determine whether 2B3-101 accumulates in micrometastases across an intact BBB and reduce tumour burden, and whether TNF co-treatment could further enhance this effect.

Previous work in our group has demonstrated the early detection of brain metastasis using contrast-enhanced MRI (131,155,156). A signature of brain metastasis is the local expression of inflammatory proteins and, in particular, endothelial VCAM-1 expression on vessels associated with metastasis (157). It has been shown that micron-sized particles of iron oxide conjugated to monoclonal antibodies directed against VCAM-1 selectively bind to the luminal surface of the endothelium in the region of metastases and can be detected by T_2*-weighted MRI. On these MR images, negative contrast is generated by the dephasing effects of iron on the proton relaxation rates. That study demonstrated both early detection of micrometastases with an intact BBB, and an increase in metastatic burden over time, which was corroborated histologically (131).

Thus, the final aim of this chapter, therefore, was to determine whether VCAM-MPIO can act as a surrogate marker for drug efficacy tumour burden change.

In summary, the overall goal of this chapter is to extend the proof of principle studies presented in chapter 3 to determine whether the permeabilisation strategy facilitates delivery of therapeutically active

compounds to sites of micrometastasis at a therapeutically effective concentration.

4.2 Hypotheses

The specific hypotheses to be tested in this study are:

1. TNF permeabilisation of metastasis-associated vasculature facilitates enhanced therapeutic efficacy of Caelyx.
2. 2B3-101 effectively accumulates in micrometastases across an intact BBB and reduces tumour burden.
3. TNF permeabilisation strategy enhances effects of 2B3-101.
4. VCAM-1 targeted MRI can be used as a surrogate marker of therapeutic effect and of a decrease in metastatic burden.

4.3 Methods

In vitro assay for cytotoxicity of doxorubicin

To demonstrate cytotoxic effect of the therapeutic compounds used in this chapter, 4T1-GFP cells were seeded on a 96-well plated and exposed for 36 h to a range of concentrations of doxorubicin, Caelyx or 2B3-101 (10^{-7} – 10^{-4} M). Cell metabolism as a marker for viability was measured through the photometric MTT assay (described in full in Chapter 2.1.2). Cells were also exposed for 36 h to a range of concentrations of TNF (10^{-7} – 10^{-4} M).

Histological detection of tumour burden after systemic administration of Caelyx ±TNF

Experimental protocol is illustrated in Figure 2.1. Mice (n=19) were intracardially injected with 100,000 4T1-GFP cells (see Chapter 2.2.2, Figure 2.2) and monitored for 13 days. Mice were then injected intravenously with 10 mg/kg Caelyx (n=5); 0.15 mg/kg TNF (n=3); 10 mg/kg Caelyx with 0.15 mg/kg TNF (n=4); or saline as control (n=7). After 24 hours, identical repeat injections were made. Four days later, mice were transcardially perfusion-fixed and dissected. Brains were processed histochemically for GFP immunoreactivity (see Chapter 2.3.1). n-numbers were chosen based on pilot data of previous studies involving this compound (154). Funding and time scale limitations prevented repetition of a better powered study.

Histological detection of tumour burden by systemic administration of 2B3-101 ±TNF

Experimental protocol is described in Figure 2.2. Mice (n=18 per group) were intracardially injected with 100,000 4T1-GFP cells (see Chapter 2.2.2, Figure 2.3) and monitored for 7 days. Mice were then injected intravenously with 10 mg/kg 2B3-101 (n=5); 0.15 mg/kg TNF; 10 mg/kg 2B3-101 with 0.15 mg/kg TNF (n=5); or saline as control (n=7). Seven days later mice were transcardially perfusion-fixed dissected. Brains were processed histochemically for GFP immunoreactivity.

Analysis of BBB patency and tumour burden by MRI with VCAM-MPIO contrast agent

Mice were injected intravenously with VCAM-MPIO contrast agent, and a 3D T_2*-weighted MRI dataset was acquired. A T_1-weighted image data set was acquired before and 5 minutes after an intravenous injection of gadolinium (see Chapter 2.2.5).

Quantification of tumour burden

Analysis was performed blind to all treatment groups. Starting from the olfactory bulbs, every twentieth 20 μm thick coronal tissue section was sampled until cerebellum, stained and analysed. Every metastasis area within the analysed sections was circumscribed and summed to give a total tumour area. The quotient of the tumour area and brain area analysed

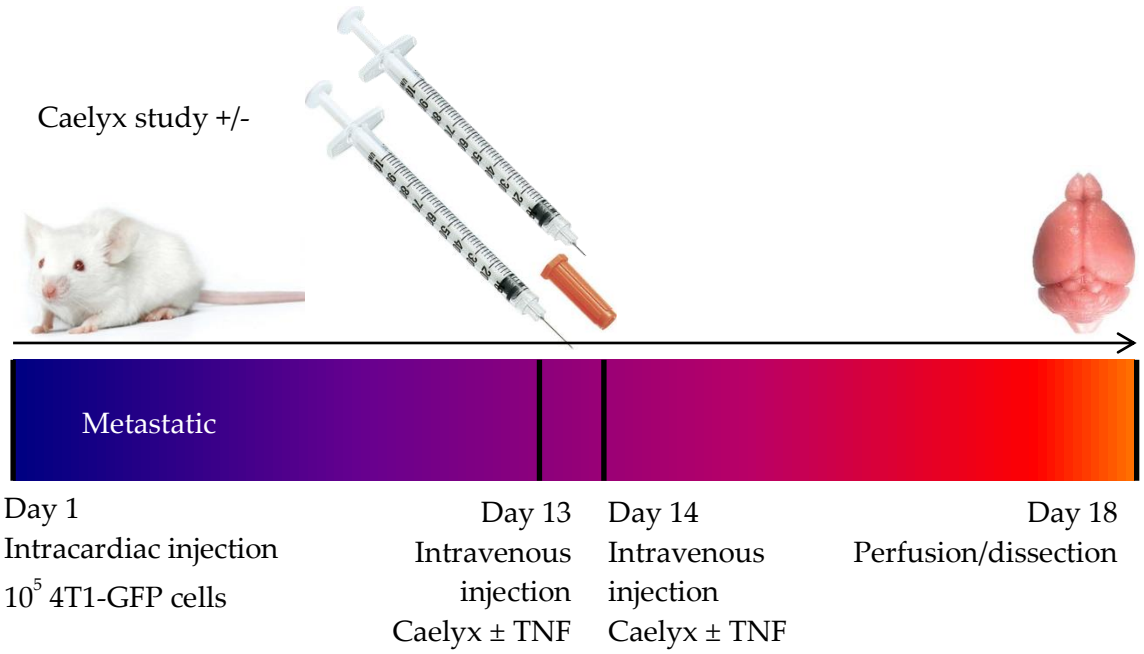

Figure 2.2. Experimental schedule used in Chapter 3. Mice are injected intracardially with 10^5 4T1-GFP cells. 13 days later, mice are injected intravenously with Caelyx ± TNF. 1 day later, mice are injected again with Caelyx ± TNF. 4 days later, mice are perfusion fixed and brains are dissected.

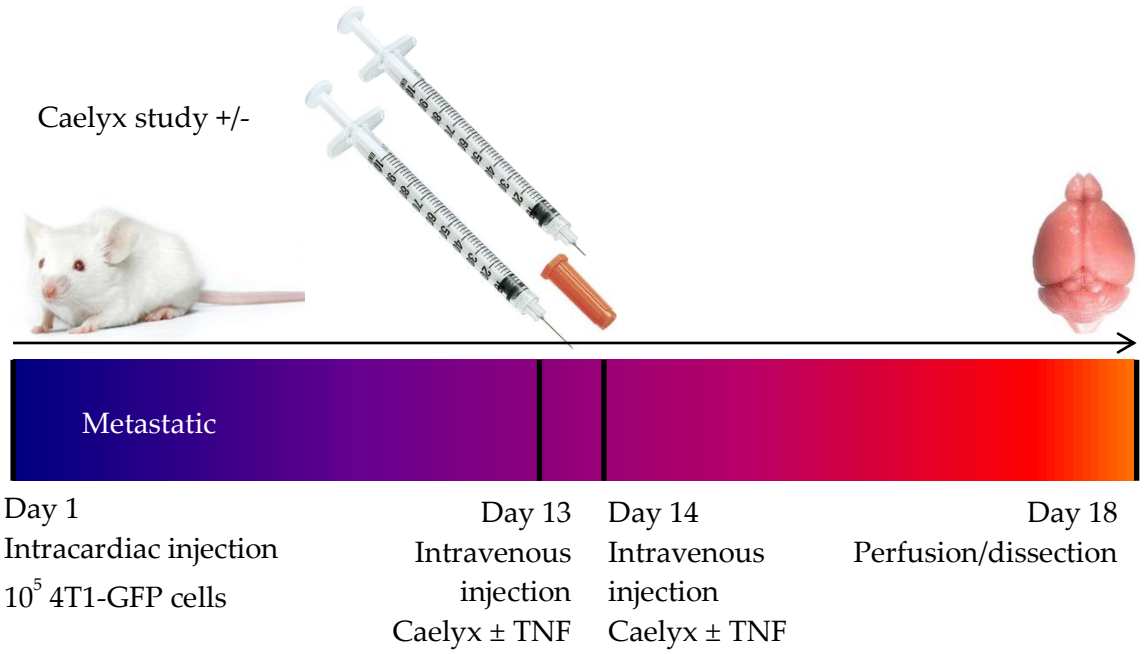

Figure 2.2. Experimental schedule used in Chapter 3. Mice are injected intracardially with 10^5 4T1-GFP cells. 13 days later, mice are injected intravenously with Caelyx ± TNF. 1 day later, mice are injected again with Caelyx ± TNF. 4 days later, mice are perfusion fixed and brains are dissected.

yielded tumour burden per mm^2 of brain analysed and mean metastasis size was also calculated. The circularity of each metastasis was determined, as defined by factor of change in perimeter to that of a perfect circle of the same area.

Histological detection of apoptosis

Brain tissue sections were also stained immunohistochemically for active-caspase-3, a marker for apoptosis (see 2.3.1). From mice injected with 2B3-101+TNF or saline, 70 metastases were analysed blind to treatment group, by two separate observers for number of active-caspase-3 positive cells per area of tumour.

4.4 Results

4.4.1 Cytotoxicity of doxorubicin, Caelyx, 2B3-101 and TNF

In order to demonstrate therapeutic potential of Caelyx and 2B3-101, tumour cells were seeded onto 96-well plates and exposed to a range of concentrations of Trastuzumab, doxorubicin, Caelyx, 2B3-101 or TNF (10^{-7} - 10^{-4} M). Quantitative analysis demonstrated that proliferation of 4T1-GFP cells is reduced after incubation for 36 h with doxorubicin (IC_{50} 6.96 $x10^{-7}$ M). Additionally, a reduction in cell proliferation was observed after incubation for 36 h with either Caelyx (IC_{50} 1.95 $x10^{-6}$ M) or 2B3-101 (IC_{50} 2.37 $x10^{-6}$ M) (Figure 4.1). TNF did not produce a well-fitting dose response curve, but did seem to reduce cell proliferation at the highest concentration tested (Figure 4.1) Trastuzumab did not significantly reduce cell metabolism.

4.4.2 Histological appearance of brain metastases

At day 18 after intracardiac 4T1-GFP cell injection, mice presented with metastases (Figure 4.2) in all regions of the brain. 86,643 metastases were analysed in total, with a mean area of 2157 μm^2, displaying immunoreactivity to GFP and hypercellularity as shown by cresyl violet

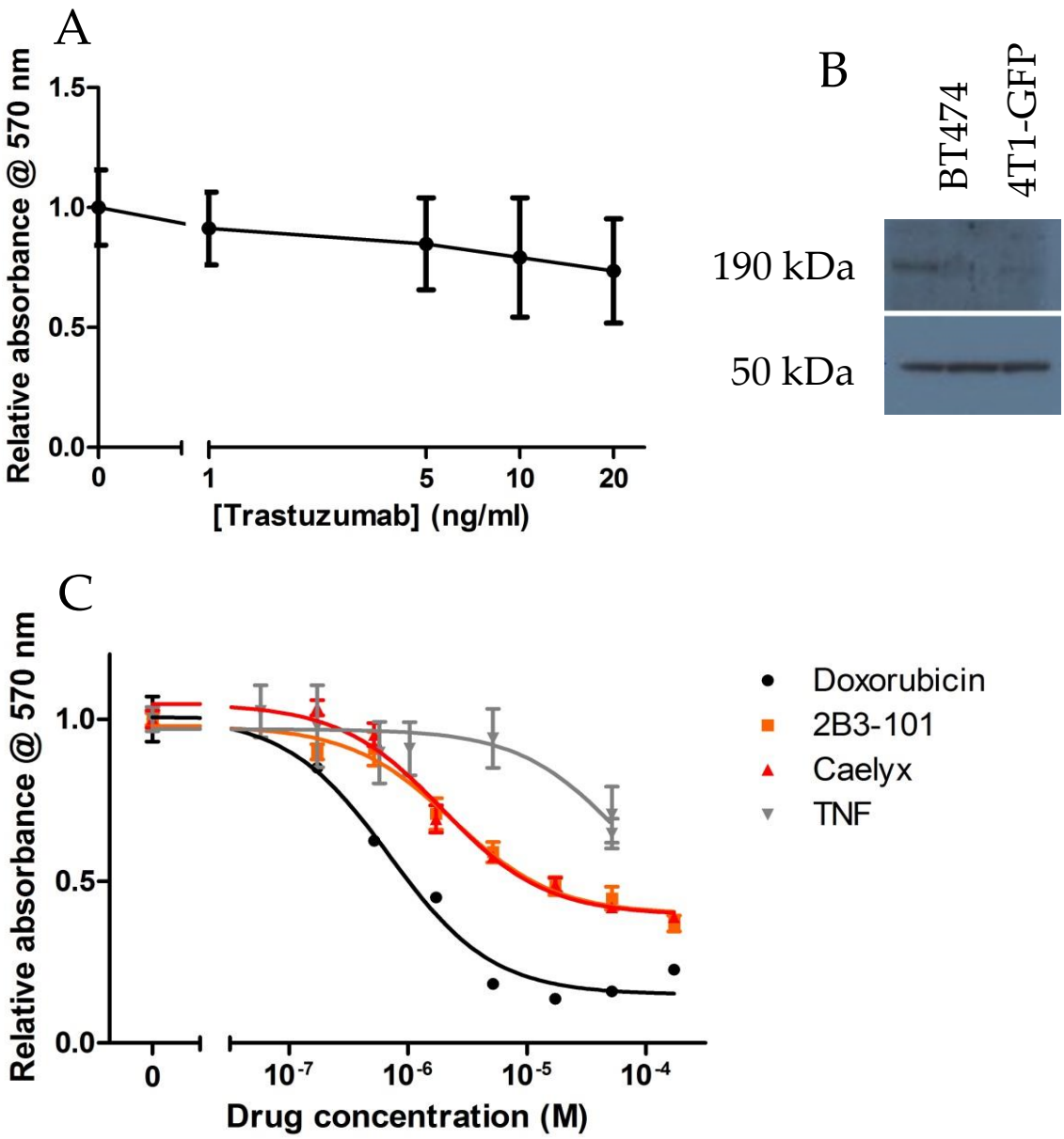

D

	IC_{50} (M)	95% CI (M)	R^2
Doxorubicin	6.96×10^{-7}	5.15×10^{-6} to 9.41×10^{-7}	0.95
Caelyx	1.95×10^{-6}	1.34×10^{-6} to 2.81×10^{-6}	0.94
2B3-101	2.37×10^{-6}	1.43×10^{-6} to 3.90×10^{-6}	0.89
TNF	-	-	0.33

Figure 4.1: (A) Proliferation of 4T1-GFP cells after incubation with trastuzumab for 72 h. (B) Western blot using antibodies against tubulin (50 kDa band) and HER2 (190 kDa band) with known HER2 expressing cell line (BT474) and 4T1-GFP cells. (C) Proliferation of 4T1-GFP cells after incubation with Caelyx, Doxorubicin, 2B3-101 or TNF for 36 h, calculated as relative absorbance at 570 nm compared to untreated cells. (D) 50% Inhibitory concentration value (IC_{50}), 95% confidence intervals (CI) and goodness of fit value of nonlinear fitted curves.

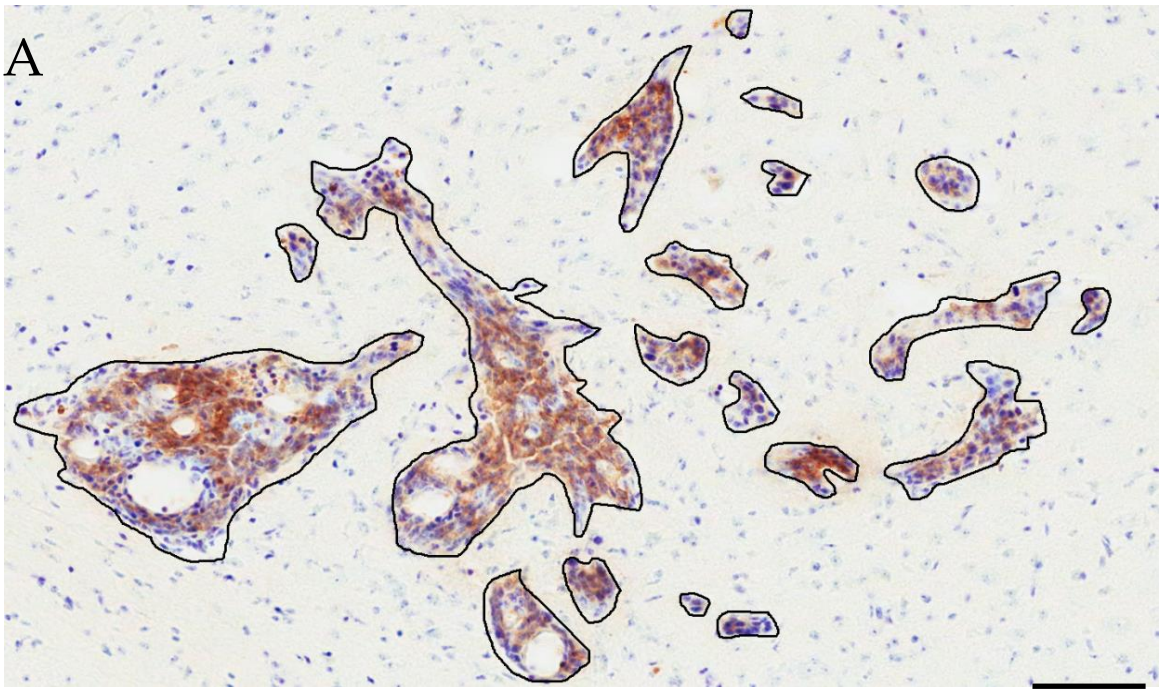

Figure 4.2: (A) Example metastasis image. Brown DAB staining identifies GFP-expressing tumour cells with cresyl violet counterstain. Black circumscribing lines indicate area measurements. Scale bar 100 μm.

staining. Histological sections of metastases displayed a mean perimeter:area ratio 1.3 times greater than a circle, indicating a diffuse and infiltrative phenotype rather than a single spherical mass.

In general, tumour colonies appeared to be still largely perivascular at day 18, however, some evidence of expansion into parenchymal tissue was evident in larger tumour colonies.

4.4.3 Effect of Caelyx treatment on brain metastasis burden

To determine a measure of tumour burden, a histological analysis of brain metastasis area per area of brain analysed was calculated. Mice were treated at days 13 and 14 after tumour cell injection and tumour burden was assessed at day 18. Mice presented with no weight loss or neurological symptoms up to 18 days after intracardiac injection with 10^5 4T1-GFP cells. However, in 2 of 21 cases, mice presented with hind-limb paralysis at day 17 after tumour cell injection and were omitted from the study. This may bias results and would prompt one to plan a more well powered experiment in the future. No adverse effects were observed after injection of Caelyx, whilst mild and transient sickness behaviour (hunched posture and piloerection) was observed after injection of TNF.

At 18 days after metastasis induction, despite a 66% reduction in tumour burden in the Caelyx-treated group, no significant change in tumour burden was evident after treatment with Caelyx, TNF or both combined compared to control (P=0.2185; 1-Way ANOVA) (Figure 4.3 A). The high variability in tumour burden in the control group (n=7) may preclude a statistical significance from being calculated. However, a

significant reduction in the mean metastasis area was found following treatment with Caelyx, TNF or both combined compared to control (Figure 4.3 B; 1-way ANOVA $P<0.05$; Dunnett's multiple comparison test *vs.* saline group). No significant difference was found between mean metastasis area in mice treated with Caelyx or Caelyx with TNF (unpaired *t* test $P=0.6273$).

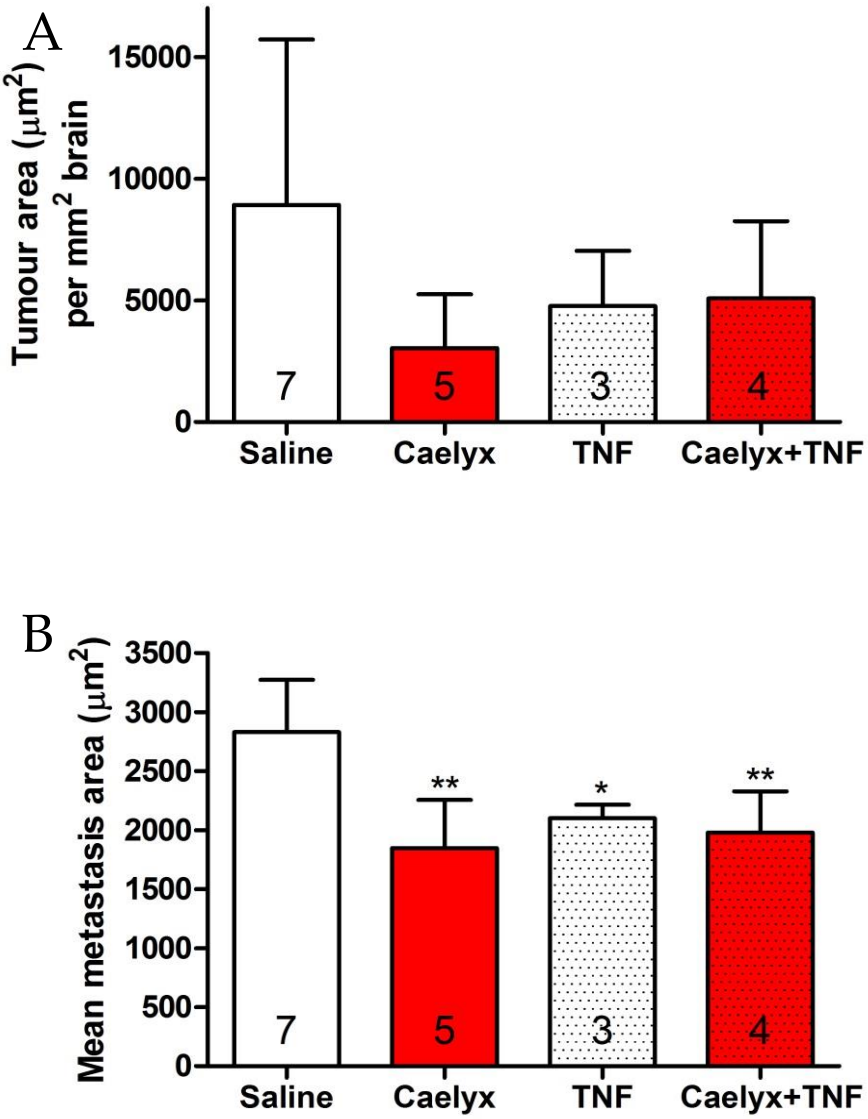

Figure 4.3: Histological analysis of brain metastases in Caelyx ± TNF treated mouse brains at day 18 Mice were injected intracardially with 10^5 4T1-GFP cells and with (i) saline as control (ii) 10 mg/kg Caelyx, (iii) 0.15 mg/kg TNF, or (iv) both TNF and Caelyx on both days 13 and 14 after tumour cell injection. (A) Tumour burden quantification. A representative sample of 18 coronal 20-μm thick tissue sections per mouse brain were circumscribed along with all metastases within these sections. Data shown as mean ±SD; number in bars represent number of mice per group; 1-way ANOVA *P*=0.2185. (B) Mean area of all metastases in the sample. Data shown as mean ±SD; number in bars represent number of mice per group; 1-way ANOVA (*P*=0.0022) with Dunnett's multiple comparison test *vs.* saline group.

4.4.4 Effect of 2B3-101 treatment on brain metastasis burden

To determine a measure of tumour burden, a histological analysis of brain metastasis area per area of brain analysed was calculated. Mice were treated at days 7 after tumour cell injection and tumour burden was assessed at day 14. Mice presented with no weight loss or neurological symptoms up to 14 days after intracardiac injection with 10^5 4T1-GFP cells. No adverse effects were observed after injection of 2B3-101, whilst mild and transient sickness behaviour (hunched posture and piloerection) was observed after injection of TNF.

At 14 days after metastasis induction, a significant reduction in tumour burden was found in mice treated with 2B3-101, TNF or both combined compared to control animals (1-way ANOVA; P=0.0013; Dunnett's multiple comparison test *vs.* saline group; Figure 4.4 A). However, in comparison to the Caelyx study, no significant differences in mean metastasis area were found between the groups (Figure 4.4 B; 1-way ANOVA P=0.5655).

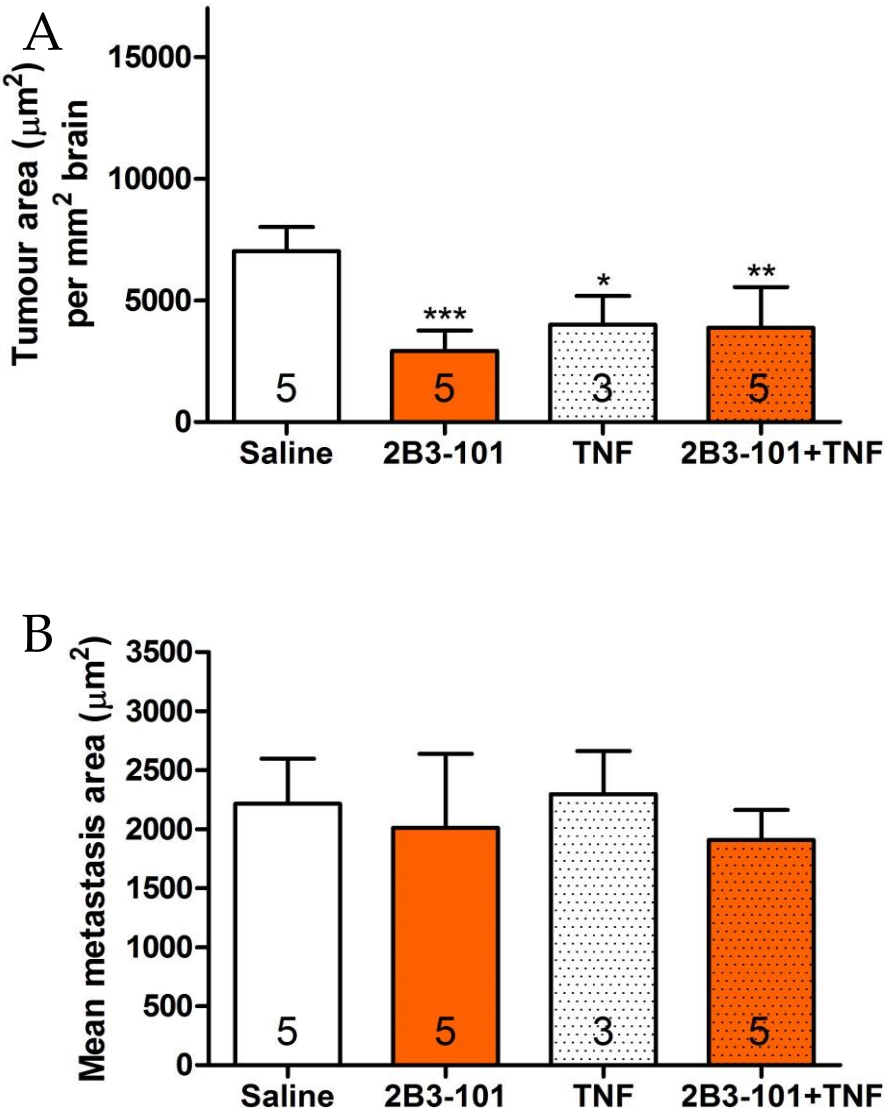

Figure 4.4: Histological analysis of brain metastases in 2B3-101 ± TNF treated mouse brains at day 14. Mice were injected intracardially with 10^5 4T1-GFP cells and with (i) saline, (ii) 10 mg/kg 2B3-101, (iii) 0.15 mg/kg TNF, or (iv) both TNF and 2B3-101 on day 7 after tumour cell injection. (A) Tumour burden quantification. A representative sample of 18 coronal 20 μm thick tissue sections per mouse brain were circumscribed along with all metastases within these sections. Data are shown as mean ±SD; number in bars represent number of mice per group; 1-way ANOVA (*P*=0.0013) with Dunnett's multiple comparison test. (B) Mean area of all metastases in the sample. Data are shown as mean ±SD; number in bars represent number of mice per group; 1-way ANOVA (*P*=0.5655) with Dunnett's multiple comparison test.

4.4.5 MRI assessment of BBB patency and endothelial activation in 2B3-101 study

As 2B3-101 is purported to cross the BBB mice were imaged using gadolinium-enhanced T_1-weighted MRI to confirm BBB patency, a known aetiology of this model. No BBB breakdown was observed in any of the treatment groups at day 14 after tumour cell injection (Figure 4.5).

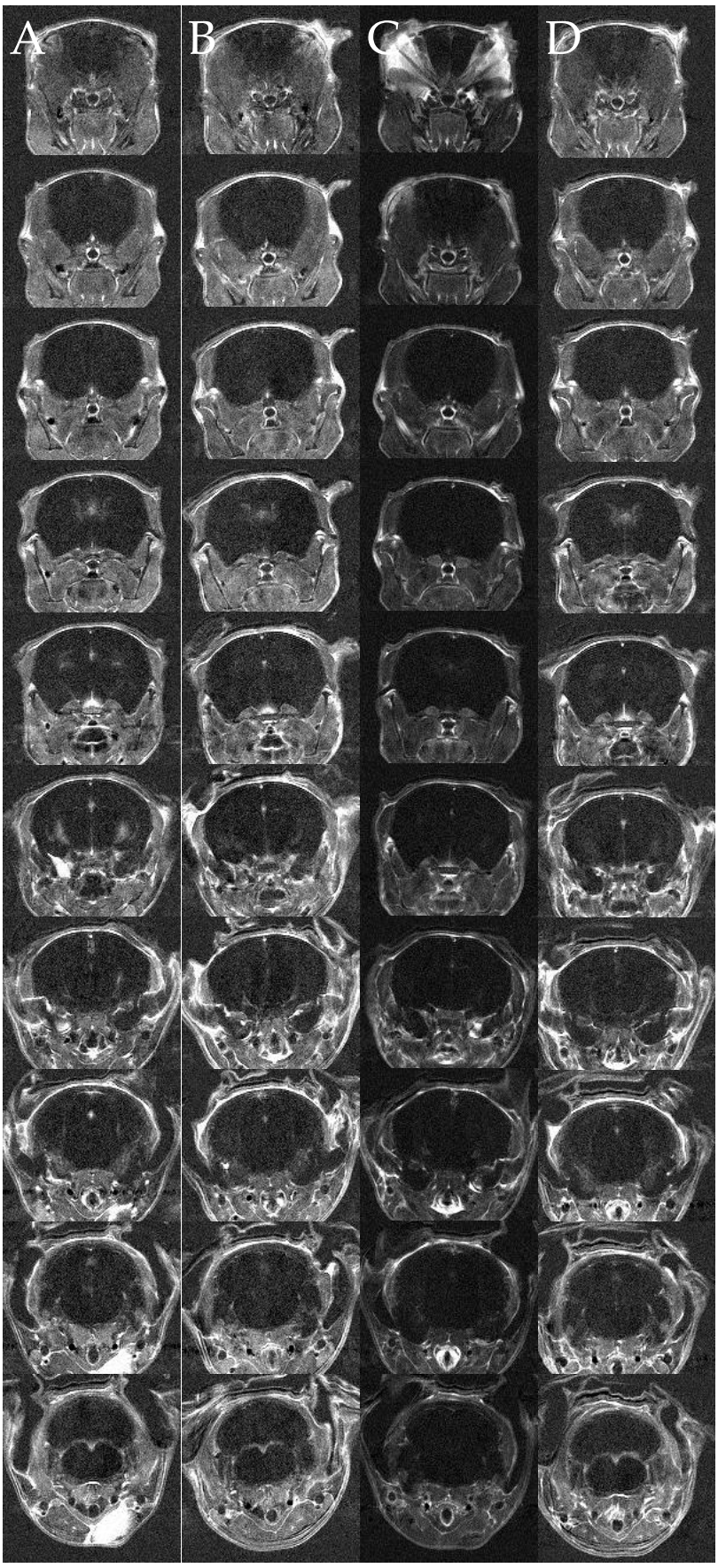

Figure 4.5: Subtraction image from T_1-weighted images of mouse brains at day 14 post injection of tumour cells (post- minus pre-gadolinium images), seven days after injection of (A) saline, (B) 2B3-101, (C) TNF, (D) 2B3-101 + TNF. White regions within the brain correspond to ventricles and the median eminence where contrast agent is expected to accumulate and generate hyperintense regions. No additional regions of BBB permeability were detected.

To determine whether VCAM-MPIO can act as a surrogate marker of drug efficacy, T_2*-weighted MR images were acquired prior to histological analysis of tumour burden in 2B3-101 treated mice. It has previously been shown that VCAM-1 expression is correlated with tumour burden (131). Assessing this through MRI would allow a useful longitudinal measure of tumour burden.

Minimal hypointense areas were detected on T_2*-weighted images in the brains of naïve mice following intravenous injection of the VCAM-MPIO contrast agent. These hypointense areas indicate either a low level of non-specific contrast agent accumulation within the brain and brain structures with an inherently fast T_2*relaxation rate, such as the ventricles. Assessment of these areas enabled masking of brains for analysis of true VCAM-MPIO induced hypointensities in metastasis bearing mice, and exclusion of non-specific effects

Mice injected with VCAM-MPIO presented with additional regions of hypointense signal (Figure 4.6 A) 14 days after injection of tumour cells. These regions correlated histologically with sites of brain metastasis (Figure 4.6 B). A volume of hypointense voxels was calculated for each brain, indicating tumour burden as a surrogate marker represented visually (Figure 4.6 C). No significant difference in VCAM-MPIO induced hypointensities was found between mice treated with 2B3-101 or saline (Figure 4.6 D; unpaired t-test P=0.2167).

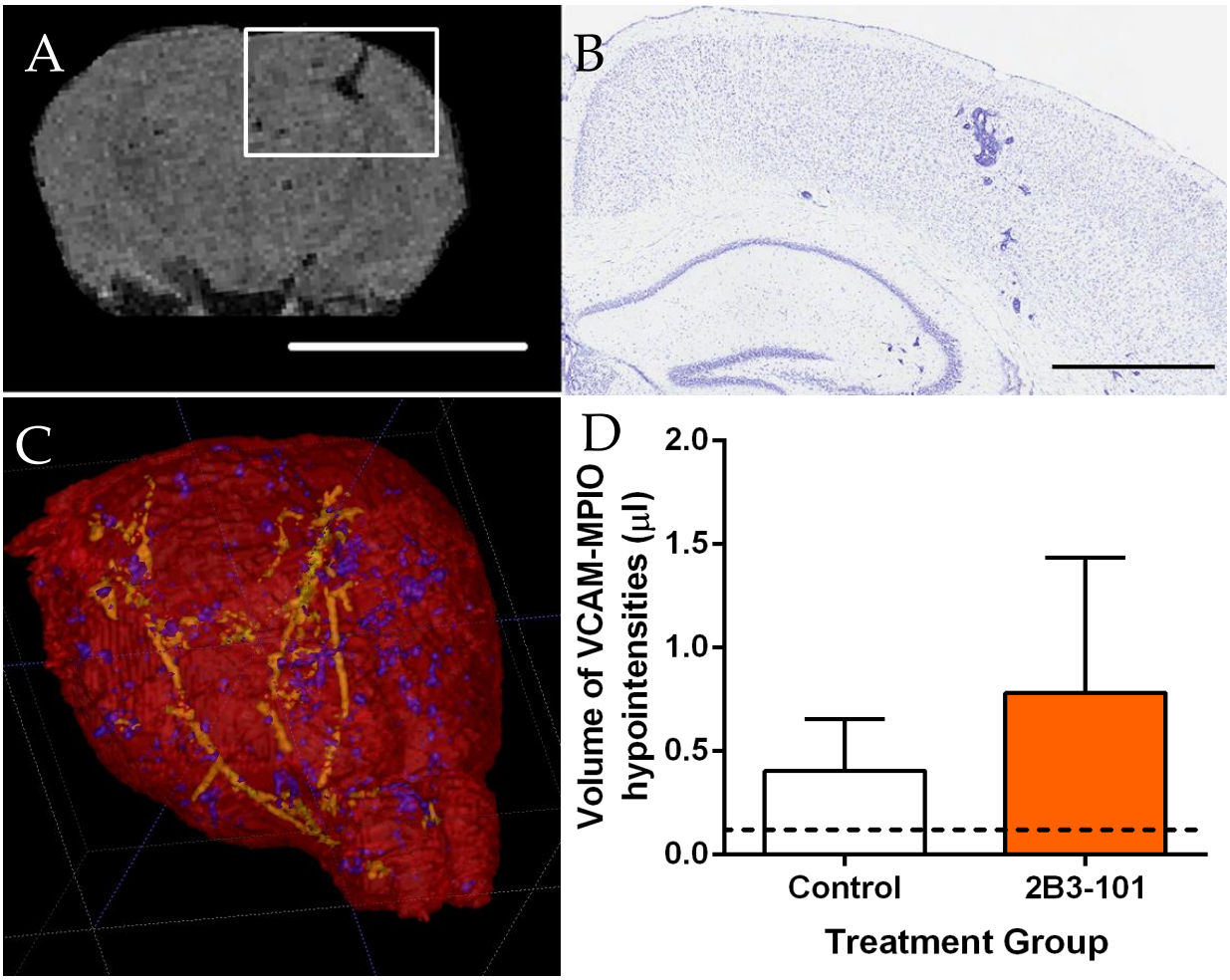

Figure 4.6: (A) Example image from T_2*-weighted dataset acquired from mouse brain containing metastases and injected intravenously with VCAM-MPIO. Scale bar 500µm. (B) Corresponding cresyl-violet stained histological section showing metastasis colocalising to area of signal reduction in (A). Scale bar 100µm. (C) 3D reconstruction mask of mouse brain (red) with regions highlighted in yellow indicating ventricles, or blue indicating VCAM-MPIO induced hypointensities. (D) Graph showing volume of VCAM-MPIO induced hypointense regions on T_2*-weighted images on control and 2B3-101 treated mice (n=6 each group). Unpaired t-test shows no significant difference between groups (*P*=0.2167),dotted line indicates mean endogenous hypointensities from naïve controls.

4.4.6 Histological detection of marker of apoptosis

As a reduction in tumour burden after injection of a cytotoxic agent suggests the induction of apoptosis, tissue sections adjacent to those used for tumour burden quantification was immunohistochemically stained for a marker of apoptosis. Caspase-3 is an intracellular protein that is activated during apoptosis and, thus, enables assessment of the degree of apoptosis. Eight tissue sections from the whole forebrain were examined by two blinded observers for expression of active-caspase-3 (Figure 4.7 A). A significantly greater number of caspase-3 positive tumour cells were seen in mice treated with 2B3-101 compared to the control, saline treated, group (Figure 4.7 B; Mann-Whitney U-test $P<0.0001$).

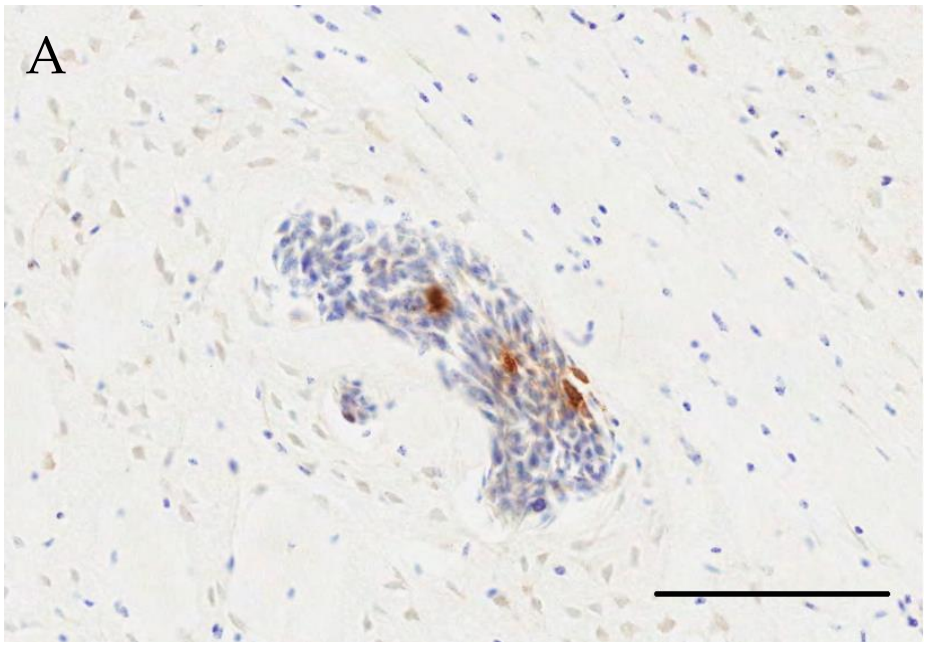

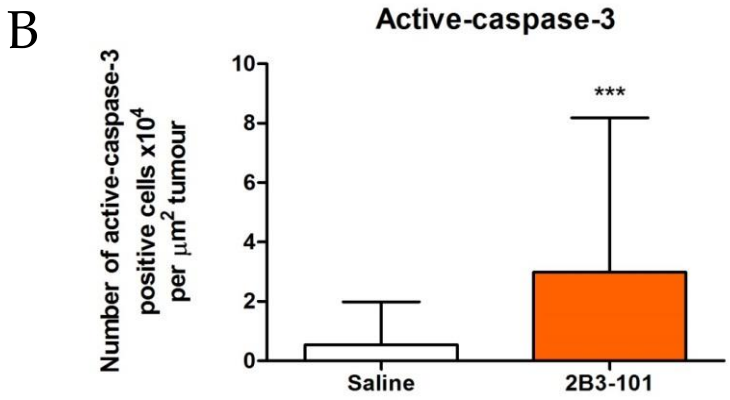

Figure 4.7: Detection of tumour cell apoptosis. (A) Example image of metastasis with brown active-caspase-3 staining. Scale bar = 100 μm. (B) The number of active-caspase 3 positive cells per tumour, normalised to area analysed, was significantly higher in 2B3-101 treated mice. Data shown are mean ±SD, Mann-Whitney U-test $P<0.0001$.

4.5 Discussion

In this chapter, the therapeutic effect of a chemotherapeutic agent, Caelyx (PEGylated liposomal doxorubicin) and a novel agent namely 2B3-101 (glutathione-tagged PEGylated liposomal doxorubicin), on a mouse model of brain metastasis has been described. A significant reduction in mean metastasis size was observed after treatment with Caelyx. Treatment with 2B3-101 in mice with brain metastases bearing an intact BBB induced a significant reduction in tumour burden. TNF co-administration did not enhance the therapeutic benefit of either of these treatment regimens. The contrast agent, VCAM-MPIO identified regions of metastasis, but was not successfully used as a surrogate marker of tumour burden.

Efficacy of Caelyx and 2B3-101 as chemotherapeutic agents *in vitro*

To demonstrate potential efficacy of Caelyx or 2B3-101 in the mouse model of brain metastasis, it was first necessary to demonstrate their cytotoxic efficacy in 4T1-GFP cells *in vitro*. Caelyx and 2B3-101 showed similar effects on 4T1-GFP cells, eliciting an inhibition of cell proliferation in a dose-dependent manner, with similar IC_{50} values.

While their efficacy was lower than doxorubicin, a reduction of cell proliferation of over 60% indicates the capacity to interfere with the cell cycle in this cell line. The liposomal formulation of both of these compounds would slow the *in vitro* efficacy through a delayed intracellular entry of the doxorubicin payload. However, with *in vivo* mouse models, the distribution half-life of Caelyx of 35 hours is substantially longer than

free doxorubicin (145,158), providing a greater likelihood of tumour cell entry and subsequent chemotherapeutic effect. The MTT assay measures cell metabolism as a surrogate for proliferation and does not directly indicate cell death. To add weight to these conclusions, experiments could be included to assess absolute cell number or in a clonogenic survival assay.

Model of brain metastasis

As anticipated, an increase in tumour burden was seen in the brains of control animals (saline injected) at the day 18 time point studied, compared to the day 14 time point; from 7020 ±988 $\mu m^2/mm^2$ to 8922 ±6789 $\mu m^2/mm^2$ (mean ±SD). Similarly, an increase in mean metastasis area was seen; from 2109 ±27.5 μm^2 to 2797 ±95.1 μm^2 (mean ±SEM; day 14 to day 18 post metastasis injection). A larger variability in tumour burden was noted at this later time point, possibly indicating variable acceleration in tumour growth. This also indicates that the model is of a dynamic and actively growing metastatic burden which is reflective of the rapid decline and poor prognosis of patients diagnosed with brain metastasis. The median patient survival time after diagnosis is 7 months (41), and response evaluation criteria in solid tumours (RECIST) defines progressive disease even after stereotactic radiosurgery as an increase of over 20% in diameter (159) as measured through follow-up MRI.

Efficacy of Caelyx as a chemotherapeutic agent in brain metastasis

Although tumour burden appeared to be substantially reduced (66% reduction) in mice treated with of Caelyx compared to control mice, the large standard deviation in the control group prevented a significant difference being reached. As discussed above, the greater variability in tumour burden in control animals at the time point studied here may reflect variation in the rate of acceleration of metastatic growth between animals. Power calculations based on these data indicated that group sizes of 13 in treatment and control groups would be required to reach a significant difference in tumour burden following treatment with Caelyx.

The significant reduction in tumour burden along with a reduction in mean metastasis area in mice treated with Caelyx compared to the control group suggests that the tumour colonies that were already seeded and in the growth phase were delayed in the growth pattern of a more infiltrative and perivascular style before development into intraparenchymal infiltration.

One explanation for the observed effects of Caelyx may be that owing to the dosing schedule spanning days 13 - 18, some tumours may be exhibiting a permeable BBB (see Figure 3.1 G and I; saline group). However, later work in the 2B3-101 study suggests that this is not the case at day 14. Alternatively, the double dosing schedule may have reached a sufficiently high level of free doxorubicin in the blood to achieve toxic levels in metastases. Whatever the reason, it appears that Caelyx treatment may have prevented the accelerated growth of already formed colonies that is observed subsequently in control mice.

Previous work has shown some efficacy of Caelyx in a rat model of glioblastoma, where an increase in overall survival was measured when the drug was administered 11 days after tumour implantation (158). However, significant BBB permeability was demonstrated at the tumour site in this model. The results presented here are the first study to use this drug formulation in a model of brain metastasis with an intact BBB.

Effect of TNF on efficacy of Caelyx

The efficacy of Caelyx was not enhanced by co-administration of TNF. The results, as presented here, do not support the hypothesis that administration of TNF into a mouse model of brain metastasis permeabilises the BBB to an extent to allow enhanced efficacy of Caelyx. However, there are a number of potential reasons for these results. Firstly, the histological method used in this study of area quantification may not be the most appropriate measure to study efficacy of doxorubicin. Whilst significant changes in metastasis size were found, an extended efficacy brought about by TNF-enhanced delivery may not be detectable as enhanced reductions in tumour proliferation may be of the order not measureable with the precision used here. Further, over the timescale studied here, it is possible that the metastatic colonies that have been effectively treated have not yet been cleared from the brain and, thus, the area measured in this study would still encompass the 'dead' colonies. However, the precision of the analysis method is certainly much better than that of alternative measures such as bioluminescence imaging which requires models of very large tumours (160).

Secondly, with the mechanisms of action proposed above, the time from drug injection to brain dissection may not have been sufficiently long. If the BBB permeabilisation had indeed enhanced drug delivery to sites of metastasis, the tumour cells now exposed to the chemotherapeutic agent may require longer than 4-5 days (as used here) for the drug to diffuse from the vasculature to the tumour cell nucleus and elicit a subsequent response in a measureable scale of volume as use here. Indeed, trials involving Caelyx on patients with breast cancer monitor the efficacy over weeks, with repeated dosing (161). Although the *in vitro* data presented above suggest a significant reduction in tumour cell viability within 36 h after exposure to Caelyx, the effective local concentrations are likely to be much lower in the *in vivo* model used here.

Thirdly, the size threshold of permeability may not be large enough for the agents used here. The previous chapter described how antibodies and horseradish peroxidase were facilitated crossing of the BBB. At a diameter of 3 nm (162), HRP is substantially smaller than the 80 nm diameter of Caelyx (163).

Efficacy of 2B3-101 as a chemotherapeutic agent in brain metastasis

A different treatment schedule was used in the 2B3-101 study in order to ensure treatment occurred prior to any possible BBB leakiness. Indeed, the patency of the BBB was confirmed at both at the time of 2B3-101 injection (day 7) and at the time of analysis (day 14) through contrast-enhanced MRI.

Injection of 2B3-101 seven days after metastasis induction elicited a reduction in tumour burden of 50%, but no change in mean metastasis

area. These data may indicate that the reduction in tumour burden is effected through action of the drug on intravascular or only partially perivascular tumour cells that are still in the early stages of tumour seeding and extravasation into the perivascular niche. Reduction in tumour cells at this stage would reduce total tumour volume, by forming fewer metastatic colonies, but not mean metastasis area as formed colonies that evade treatment may still grow as in untreated mice. However, further histological analysis demonstrated a significantly greater number of tumour cells expressing active-caspase 3, a marker of apoptosis, in 2B3-101 treated than in untreated mice.

This observation suggests that there is, in fact, some action of 2B3-101 on fully extravasated tumour cells, and this is in accord with the hypothesis that 2B3-101 effectively crosses the BBB. It is possible that owing to incomplete clearance of apoptotic cells, the reduction in tumour growth is not detected with the analysis approach used. Therefore repeating this study and analysing tumour burden at a later time point may clarify the mechanism of action of this novel therapeutic.

As discussed above, 2B3-101 is currently in Phase I/IIa study for patients with solid tumours with brain metastases or recurrent malignant glioma (153), and preclinical studies in a model of glioblastoma show a significant inhibition of tumour growth (154). Again, the patency of the BBB was not confirmed. The efficacy demonstrated here more solidly supports the concept of the enhanced drug delivery across an intact BBB through tagging of PEGylated liposomal doxorubicin with glutathione than the previously published studies.

Effect of TNF on efficacy of 2B3-101

As for Caelyx, the efficacy of and 2B3-101 was not enhanced by co-administration of TNF in the studies presented here. 2B3-101 elicited a 58% reduction in tumour burden, whilst a similar 45% reduction was elicited when mice were co-administered TNF. Further, the glutathione-tagged 2B3-101 compound is reported to be able to cross the intact BBB, so any enhanced delivery facilitated by permeabilising the BBB may not change the drug concentrations at sites of metastasis. Lastly, an enhanced reduction in tumour burden may not be measurable in the approach used here, for the reasons described above. Performing immunohistochemistry for more antigens could give a clearer picture of what has happened to the tumour cells after treatment. Assessment of proliferation through Ki67 staining and BrdU for apoptosis would facilitate this.

Use of VCAM-MPIO as a surrogate marker of therapeutic efficacy

Early stages of progression of metastatic burden in the mouse model used here has been detected through MRI using VCAM-MPIO as a contrast agent (131). This study presented here aimed to both reduce tumour burden and detect this *in vivo*. Various regions of hypointensities were found on T_2*-weighted images of mouse brains with a metastatic burden after injection of VCAM-MPIO. These regions correlated with sites of metastasis as shown by histology. No BBB breakdown was seen at these, or other, sites in the brain. There were no significant changes in volumes of hypointense regions after treatment with 2B3-101. Whilst a reduction in tumour burden was quantified in this treatment group, the target for this

contrast agent, VCAM-1, did not show a significantly different expression profile as detected by MRI. It appears, therefore, that the reduction in tumour volume was not great enough to have significantly reduced the vascular expression profile of VCAM-1. Although not significant, the volume of VCAM-MPIO hypointensity was in fact four-fold greater after treatment with 2B3-101. As this antigen is an indirect marker of brain metastasis, and is upregulated at sites of neuroinflammation, it is likely that this change may indicate that, while the tumour burden is lower, there are increased levels of neuroinflammation. This may be to a recruit of peripheral immune cells to facilitate removal of the apoptotic tumour cells. Quantifying the presence of peripheral immune cells may confirm whether the trend towards an increase in inflammatory marker seen here is an indication of a secondary effect of tumour cell death elicited by drug administration.

Effect of TNF alone

In the two studies involving Caelyx and 2B3-101, the co-administration of the drug with TNF necessitated a control group receiving administration of intravenous TNF. In both treatment regimens (injection of 3 μg at both day 13 and day 14 after tumour injection with histological analysis at day 18; and injection of 3 μg at day 7 after tumour injection with histological analysis at day 14), either a reduction in mean metastasis size or reduction tumour burden, respectively, was observed. This may be through the well documented vascular damage of TNF (164–166). However, vascular damage to an extent that would disrupt the blood

supply to these micrometastases is unlikely, as haemorrhage was not seen in the model presented here (see Figure 3.5).

Alternatively, stimulation of the immune system by systemic administration of TNF may trigger antitumourigenic effects of recruited macrophages. While it has been shown that a high level expression of TNF by cells in the microenvironment of a NSCLC with macrophages correlates with a favourable prognostic outcome (167), the extended local expression of TNF would likely produce different results to the bolus injection described here. Even through TNF is cytotoxic *in vitro* at very high doses (Figure 4.1), the unexpected effect of TNF casts doubt on the confidence in the conclusions of the effect seen from 2B3-101 and Caelyx.

4.6 Conclusions

This study has demonstrated for the first time, the efficacy of Caelyx in influencing early stage brain metastasis progression in a mouse model. Further, it has been shown that the novel compound, 2B3-101, can reduce tumour burden in a mouse model of brain metastasis with an impermeable BBB. However, co-administration of TNF did not enhance therapeutic efficacy in the study design used here.

Based on the data described, further experiments would be warranted to further develop the approach of TNF enhanced delivery of chemotherapeutic agents across the blood-brain barrier at sites of metastasis. Brain tissue from animals treated here could be analysed more closely for other markers of apoptosis, such as the TUNEL assay (terminal deoxynucleotidyl transferase dUTP nick end labelling). While apoptosis

was shown for 2B3-101 treated mouse brains, an in-depth stereological approach may provide interesting results. Repeated injection of TNF over the course of a number of drug half-lives may facilitate an extended window of permeabilisation. Additionally, performing the experiments on a range of time points after metastasis induction and on a range of end points may elucidate further the actions seen. Finally, analysis of the size threshold for crossing the permeabilised BBB at sites of metastasis could be investigated by measuring the extravasation of a range of sizes of dextran beads.

However, the exclusion of mice from some of the treatment groups owing to the display of hind limb paralysis may have influenced the outcome. Systemic tumour burden (117) was the likely cause for this, and this tumour burden along with brain tumour burden is probably related. Although these mice were randomised after injection with tumour cells, it casts doubt over the final conclusions.

Chapter 5 – Mechanism of action and potential translation of the strategy into the clinic.

5.1 Introduction

The work presented in the previous chapters has described a method of permeabilising the blood-brain barrier at sites of brain metastasis, and has demonstrated the delivery of imaging contrast agents and radiolabelled therapeutic antibody selectively to sites of metastasis. This approach was then extended under the hypothesis that the method could enhance the delivery of active therapeutic agents and effectively reduce tumour burden in the BALB/c mouse with haematogenously induced 4T1-GFP brain metastases. It was concluded that the anticipated enhancement of therapy efficacy induced by co-administration with TNF was not observed due to limitations in the growth pattern in the model. Consequently, further work is required to demonstrate the efficacy of the approach. At the same time a number of questions remain with regards to mechanism of permeability, applicability in man and potential toxicity concerns.

The original hypothesis of permeabilisation induced by TNF was developed by extending the work seen in the literature, where the administration of recombinant human TNF disrupted endothelial tight junctions in the vasculature of a systemic tumour thereby enhancing the

permeability of tumour vasculature to facilitate therapeutic virus particle delivery (124). It is known that the normal brain vasculature is resistant to the permeabilising effect of intravenous administration of TNF (129), so the acute selectivity that was observed in our model, must be due to a change in sensitivity to TNF in areas of brain metastases.

Work within the group has shown that the vasculature at sites of brain metastasis is 'activated', describing a change in expression profile owing to, and part of, inflammation (131). This has been exploited to detect brain metastases at a very early stage using *in vivo* contrast-enhanced MR imaging (156). Cellular adhesion molecules play important functional roles in the early stages of metastatic seeding in the brain and E-selectin, VCAM-1, ALCAM, ICAM-1, VLA-4 and integrin subunit β4 have been demonstrated to be upregulated specifically at sites of metastasis (157). These proteins have been shown to be involved in the tethering, rolling and arrest of circulating tumour cells along the vascular endothelium of the lung and liver (168,169). Moreover, recent work in our group suggests a role for a specific CAM subset in metastasis seeding to the brain (manuscript in preparation). Later in the progression of metastasis, endothelial upregulation of P-selectin may facilitate leukocyte recruitment (170).

Clearly, the cerebral vascular endothelium responds to the presence of metastases through a complex change in the expression profile of receptors and ligands involved in inflammatory pathways. This presents as a likely pathway through which the TNF permeabilisation occurs.

TNF and TNF receptors

Tumour necrosis factor is a cytokine with many functions and mediates a wide range of cellular responses. In normal physiology, TNF is involved in systemic inflammation and regulating the immune system (171). TNF was first studied and named based on the finding that a blood serum factor caused regression of tumours brought about by induction of a bacterial infection (164). It has attracted considerable interest in the past as an anticancer agent itself, however, trial results were not encouraging, with only 3 out of 57 patients with advanced malignant disease showing partial tumour regression (172). Clinical trials trialling the use of TNF as an addition to melphalan (DNA alkylating chemotherapeutic) in isolated limb perfusion for regionally advanced melanomas showed no improvement in overall response rate or overall survival (173) and no additional effect to melphalan alone (174). The rationale for use of TNF is based on the improved penetration of anti-cancer agents and the later selective destruction of the tumour-associated angiogenic vessels (175).

TNF is bound by a range of receptors within the TNF receptor superfamily. Following binding of TNF to the transmembrane receptor TNFR1, the receptor translocates to lipid rafts, triggers the formation of a signalling complex (176), and elicits a huge range of cellular effects such as apoptosis, survival, differentiation or proliferation (reviewed in (177)).

A wide array of *in vitro* studies has highlighted the effects of TNF on a range of cell types, influencing the cytoskeleton and cell shape: fibroblasts exposed to TNF were shown to have induced actin polymerisation through activation of Cdc42 (178); activation of TNF receptor 1 in macrophages

changed the cytoskeleton through decreased F-actin (179); and a monolayer of pulmonary endothelial cells exposed to TNF showed a reduced trans-endothelial electrical resistance (a marker of vascular permeability) and myosin light chain phosphorylation (180). The effect of TNF on the transendothelial permeability of *in vitro* monolayers is well documented (125,181), and it is known to be elicited through activation of TNFR1 (128,177).

A further consideration when considering translation of the permeabilisation strategy to the clinic is the dose-limiting side effects of TNF, which include hypotension and liver toxicity (172). Further understanding of the mechanism of this permeabilisation strategy could lead to the development of agents that can elicit the response described here, whilst minimising the adverse effects.

5.2 Hypotheses

In the subsequent work, the specific hypotheses to be tested are:

1. The permeabilisation of the blood-brain barrier induced by administration of TNF is selective to sites of metastasis owing to selective expression of specific TNF receptors on the associated vasculature.
2. Human brain metastasis is accurately reflected in the mouse model used in this thesis and, thus, this approach has potential for translation into the clinic.
3. The spatial selectivity then implied by TNF receptor upregulation and activation at sites of metastasis can be demonstrated on a cellular level.

5.3 Methods

Histological detection of TNF receptor 1 and 2

Female BALB/c mice were injected intracardially with 10,000 4T1-GFP cells. Animals were monitored for natural and provoked behaviour and weight for 13 days (see Chapter 2.2.2). Female SCID mice were injected intracardially with 10,000 MDA-231-Br-eGFP cells and monitored for 21 days as above. An additional cohort of SCID mice were injected intrastriatally with 5,000 MDA-231-Br-eGFP cells and monitored for 21 days (see Chapter 2.2.4). Mice were terminally anaesthetised, transcardially perfusion-fixed and brains removed. Brains were analysed immunhistochemically (see Chapter 2.3.1), using antibodies against TNFR1 and TNFR2. Co-localisation analysis was performed by triple immunofluorescence staining, using antibodies against Glut-1 to identify blood vessels or Iba-1 to identify microglia. Leukocytes were identified by morphological analysis of cresyl violet stained nuclei.

Human brain metastasis biopsy tissue sections were kindly provided by Prof. Olaf Ansorge, John Radcliffe Hospital, Oxford (under the Research Tissue Bank ethical approval for cancer research), and Mr Rasheed Zakaria and Mr Michael Jenkinson, The Walton Centre, Liverpool (under ethical approval of material transfer agreement 11/WN/o3/2). These formalin-fixed paraffin-embedded samples were dewaxed and analysed immunohistochemically (see Chapter 2.3.1) using antibodies against TNFR1 and TNFR2.

Selective permeabilisation of the blood-brain barrier by selective TNFR1 and TNFR2 agonist antibodies

Female BALB/c mice were injected intracardially with 10,000 4T1-GFP cells; animals were monitored for natural and provoked behaviour and weight for 13 days (see Chapter 2.2.2). Mice were injected intravenously with 3 μg of antibody htr-9 (TNFR1 selective agonist) or utr-1 (TNFR2 selective agonist) 2 hours prior to pre- and post-gadolinium MR imaging to assess BBB patency (see Chapter 2.2.5).

In vitro analysis of endothelial cell response to co-culture with tumour cells

Human cerebro-microvascular endothelial cells (hCMEC/d3) were kindly provided by Dr Pierre Couraud and colleagues at INSERM (Paris) under strict material transfer agreements. Cells were grown on rat collagen coated flasks and glass slides with a custom medium mixture containing foetal bovine serum, hydrocortisone, basic fibroblast growth factor, chemically defined lipid concentrate, HEPES buffer, penicillin/streptomycin mixture, L-ascorbic acid in endothelial basal medium-2. Full details are described in Chapter 2.1.1.

Cells were grown to confluence on 8-well glass slides and were then co-cultured with MDA-231-Br-eGFP cells on top. Cells were assessed by immunocytochemistry using antibodies against TNFR1 and TNFR2, DAPI to identify cell nuclei, and Phalloidin toxin to identify actin.

Liver function test in response to systemic administration of TNF

Naïve mice (n=3 per group) were injected intravenously with 3 μg rmTNF or saline as control. After 24 h, mice were terminally anaesthetised (see Chapter 2.2.1) and 500 μL of blood was collected from the heart using a heparinised syringe. Samples were centrifuged at 9500 g for 10 min. The plasma fraction was frozen and sent to Sequani Limited (UK) for liver function analysis.

5.4 Results

5.4.1 Histological detection of TNF receptor subtypes 1 and 2 in mouse brain

Expression of TNFR1 was immunohistochemically localized to cerebral vessels associated with metastases in BALB/c mice injected intracardially with 4T1-GFP cells (Figure 5.1 A and C, arrows). TNFR1 expression on the vasculature of metastases was confirmed through co-localisation of TNFR1 and Glut-1 by immunofluorescence (Figure 5.1 C). In contrast, TNFR2 expression, although also increased, was found primarily on intravascular leukocytes within the vicinity of metastases, but not on the vascular endothelium (Figure 5.1 B and D, arrows). TNFR2 expression was also detected on nonvascular structures with morphology similar to that of microglia. No TNFR1 or TNFR2 staining was found on normal appearing brain tissue (Figure 5.1 E and F).

A similar pattern of TNFR1 staining on the vascular endothelium (Figure 5.2 A) and TNFR2 staining on leukocytes (Figure 5.2 B) was seen in brains of SCID mice injected intracardially with MDA-231-Br cells. Further, after injection of MDA-231-Br-eGFP cells directly into the striatum, TNFR1 staining was again seen on the vascular endothelium (Figure 5.2 C) whilst TNFR2 was evident on microglia surrounding the tumour site (Figure 5.2 D).

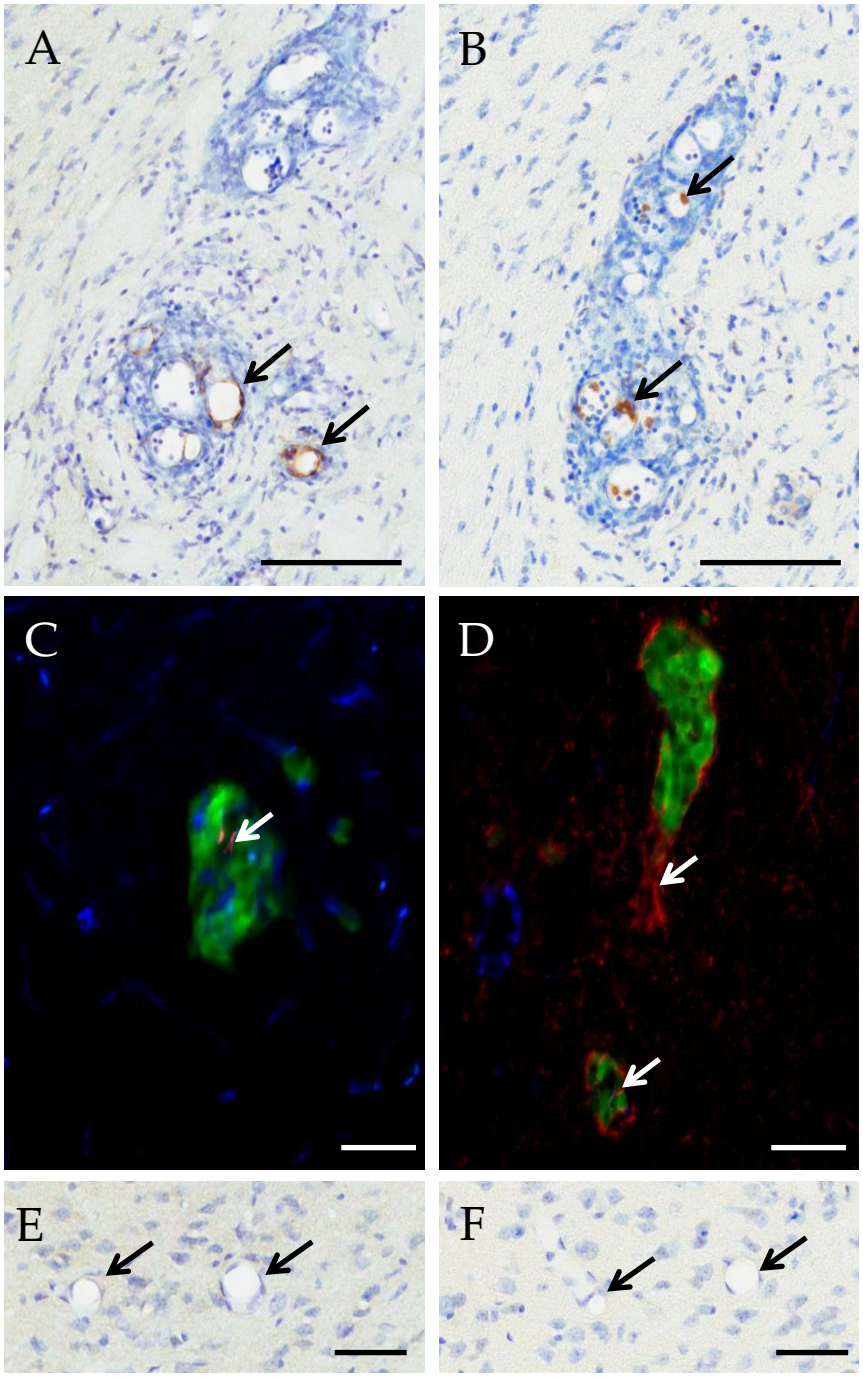

Figure 5.1. Histological detection of TNF receptors at sites of cerebral metastases in BALB/c mouse with intracardially induced 4T1-GFP tumour burden. (A and C) Tumour necrosis factor receptor 1 (TNFR1) (A: brown; C: red) is evident on blood vessels (C: blue) associated with metastases (arrows). (B and D) Tumour necrosis factor receptor 2 (TNFR2) (B: brown, D: red) is not visible on vascular endothelium (D: blue), but appears to colocalise with intravascular leukocytes (A) and infiltrating microglia (D)(arrows). (E and F) Neither receptor is present on non metastasis-associated vessels. Scale bars 100 μm (A – D), 50 μm (E and F).

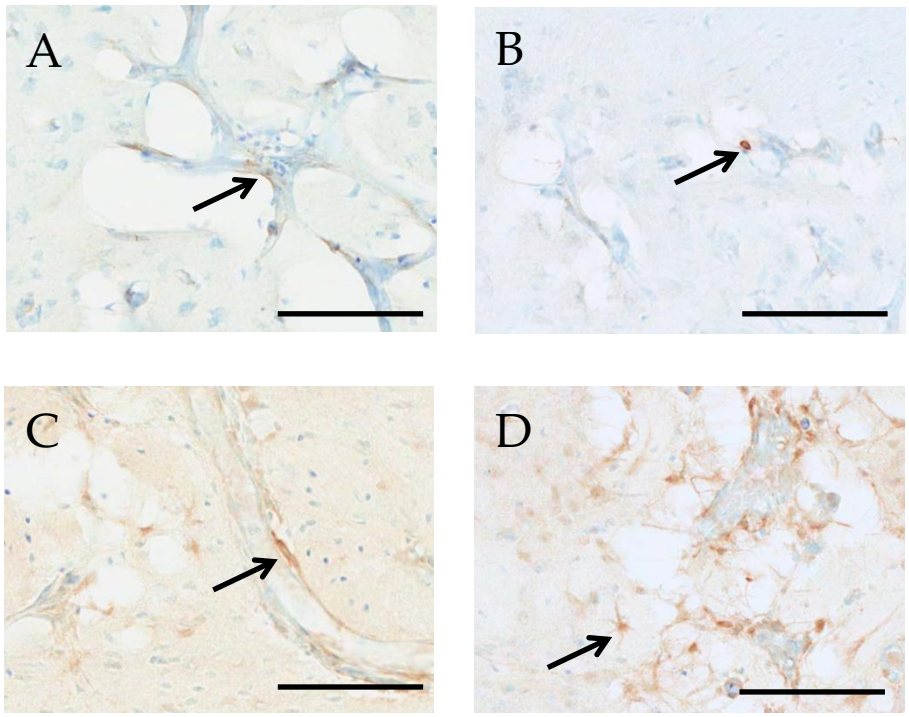

Figure 5.2. Histological detection of TNF receptors at sites of cerebral metastases in SCID mice with (A and B) intracardially induced and (C and D) intracerebrally induced MDA-231-Br-eGFP tumour burden. (A and C) TNFR1 staining (brown) is found on vascular endothelium and (B and D) TNFR2 staining (brown) on intravascular leukocytes and parenchymal microglia. Scale bars 100 μm.

5.4.2 Histological detection of TNF receptor subtypes 1 and 2 in human brain

Human brain samples from the John Radcliffe Hospital (Oxford) were used to assess expression of TNFR1 and TNFR2 in human metastasis tissue. A brain biopsy from acutely inflamed tissue was immunohistochemically stained as a positive control for TNFR1, and displayed TNFR1 (brown) staining on the blood vessel endothelium. In contrast, blood vessels in regions of biopsied brain tissue distant from a site of metastasis showed no TNFR1 staining (Figure 5.3 B). In a 5 of 6 brain metastasis biopsy samples from human patients, a pattern of TNFR1 staining was seen on metastasis-associated vasculature (Figure 5.3 C - E).

TNFR2 expression was seen on, wall associated leukocytes (Figure 5.4 A), infiltrating cells in the tumour mass (Figure 5.4 B - D) and intravascular neutrophils (Figure 5.4 E).

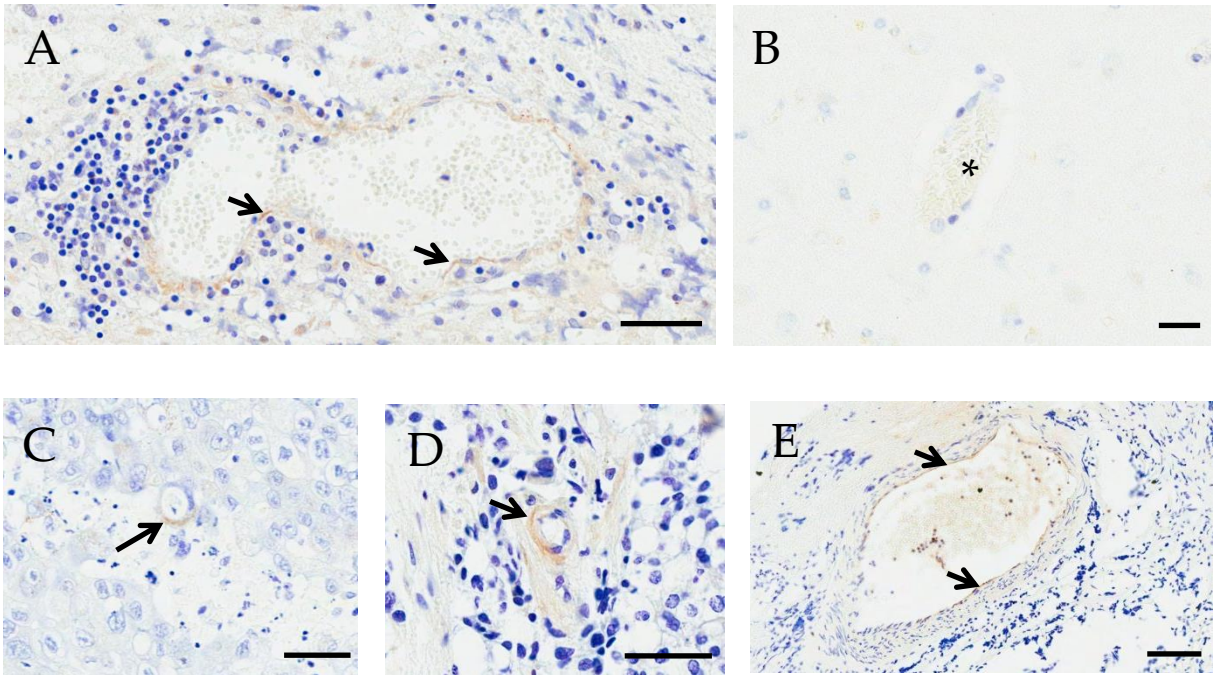

Figure 5.3. Histological detection of TNF receptors 1 in human brain biopsy tissue. (A) Positive control section showing TNFR1 expression (brown) on a brain vessel adjacent to acute inflammation. (B) Negative control section of human brain tissue 5 mm from boundary of metastasis. (C - E) TNFR1 expression (brown, arrows) on vessels within human brain metastases of unknown origin. Scale bars 50 μm.

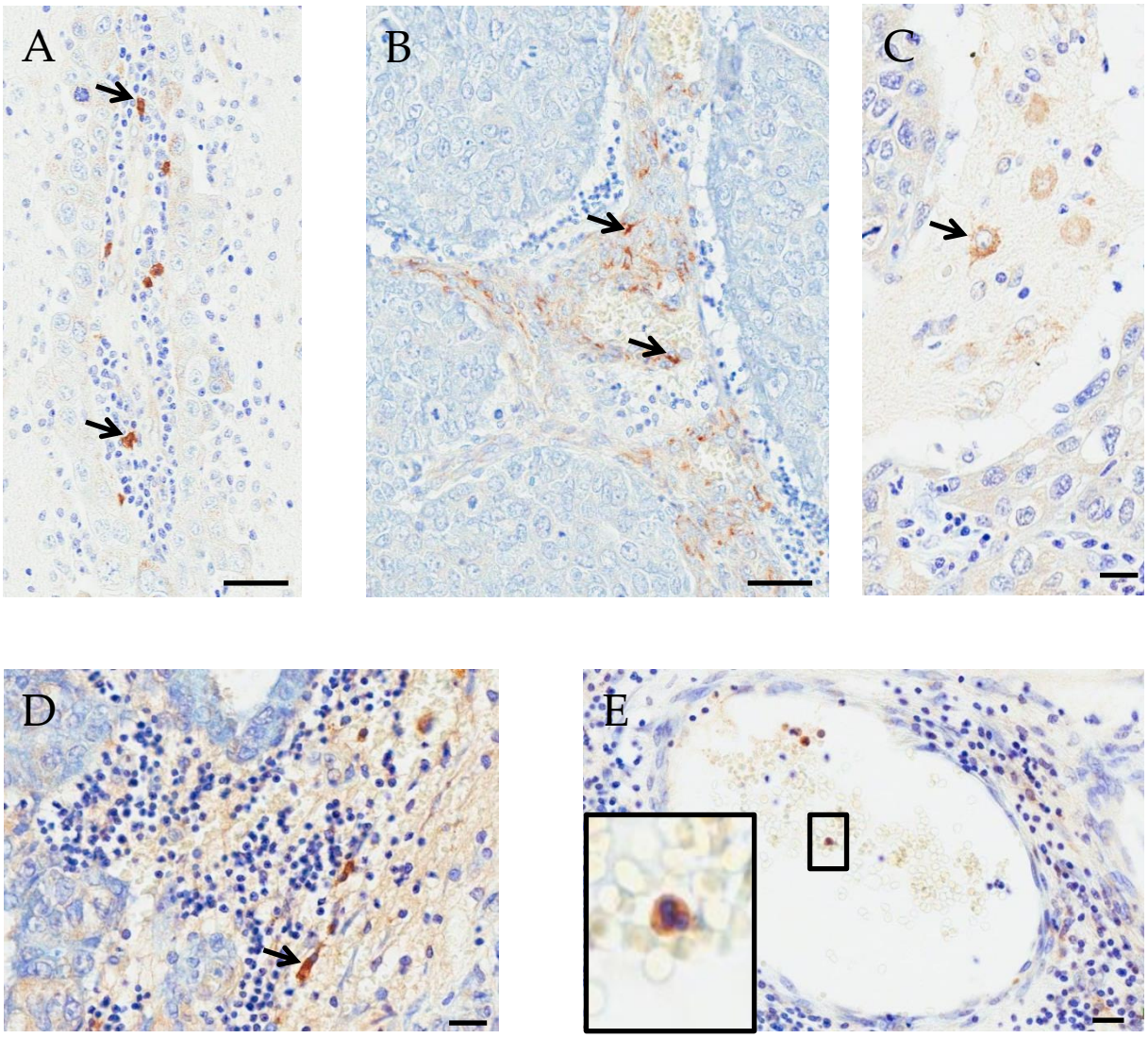

Figure 5.4. Histological detection of TNF receptor 2 at sites of cerebral metastases. (A - E) TNFR2 expression (brown, arrows) within human brain metastases of unknown origin. Staining appeared as recruited leukocytes (A), infiltrating cells in the tumour mass (B – D) and intravascular neutrophils (E). Scale bars 50 μm.

5.4.3 Spatial distribution of TNFR1 positive vessels

To assess the potential area of susceptibility of human brain metastases to the permeabilisation effects of TNF administration, a collection of 11 brain metastasis biopsies were acquired from The Walton Centre, Liverpool. The samples were collected from patients, with a range of primary tumours, where brain metastases had been confirmed by contrast-enhanced MRI. Samples from the biopsies were provided, through image-guidance, from the boundary of metastasis and brain, and normal brain was included to prevent cancer cells remaining.

Tissue sections were stained for TNFR1 and counterstained with cresyl violet. All samples showed vessels with brown staining as seen in samples shown in Figure 5.3 C – E, indicating expression of TNFR1. All TNFR1 positive vessels were identified in this cohort of biopsy samples and their positions were mapped within the space of the sample. From these coordinates, circles were generated of radius 50 μm with the origin at the centre of the TNFR1 positive vessel, and the total area of the sample covered by these circles was calculated. The radius of these circles was increased to 100, 250 and 500 μm (Figure 5.5), and the area of susceptibility as a percentage of the total sample area calculated (Figure 5.5 D). In 4 of the 11 samples, over 50% of the brain metastasis sample was within 500 μm of a TNFR1 positive vessel; in a further 4 samples, over 20-50% of the area was within 500 μm of a TNFR1 positive vessel.

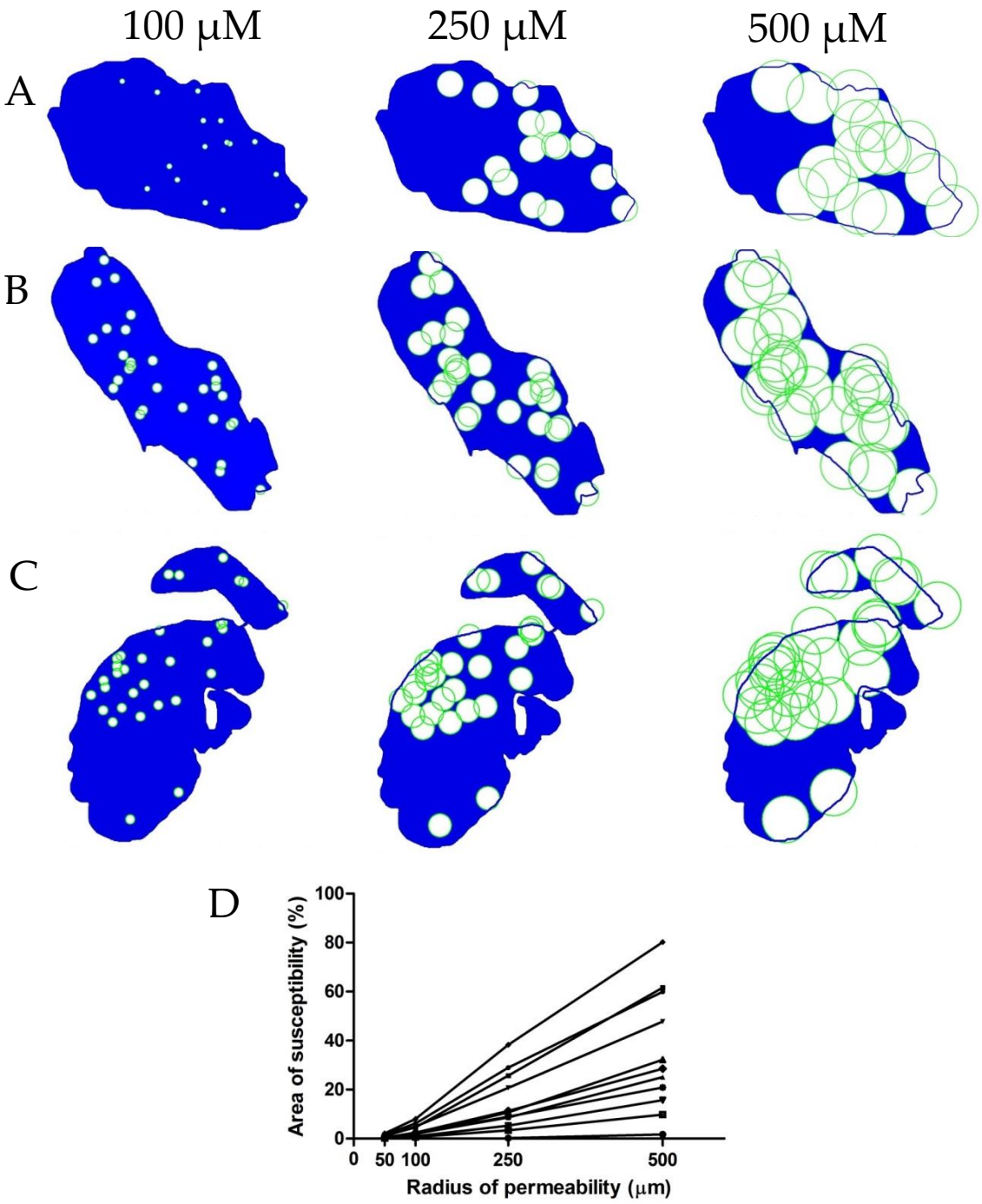

Figure 5.5. Spatial distribution of TNFR1 positive vessels and modelled area of susceptibility to permeabilisation strategy in human brain metastasis biopsy samples showing three representative examples . Eleven brain metastasis biopsy samples were immunohistochemically stained for TNFR1. (A-C) Each vessel displaying brown staining was identified and spatially mapped as a coordinate point on a digital slide (blue shape represents metastasis area). Circles of radius 50, 100, 250 and 500 µm were generated (white) around the points of TNFR1 positive vessels. (D) The percentage area of the brain metastasis covered by these circles was quantified and defined as area of susceptibility.

Adjacent sections were stained with haematoxylin and eosin and the boundary between brain and metastatic tissue was demarcated (Figure 5.6). Of 276 TNFR1 positive vessels observed over 11 samples, the proportion in metastatic tissue rather than normal appearing brain tissue was 57.6% indicating that permeabilisation effects could both be elicited directly on tumour-associated vasculature, and on the invasive boundary from where tumour recurrence originates after surgical resection.

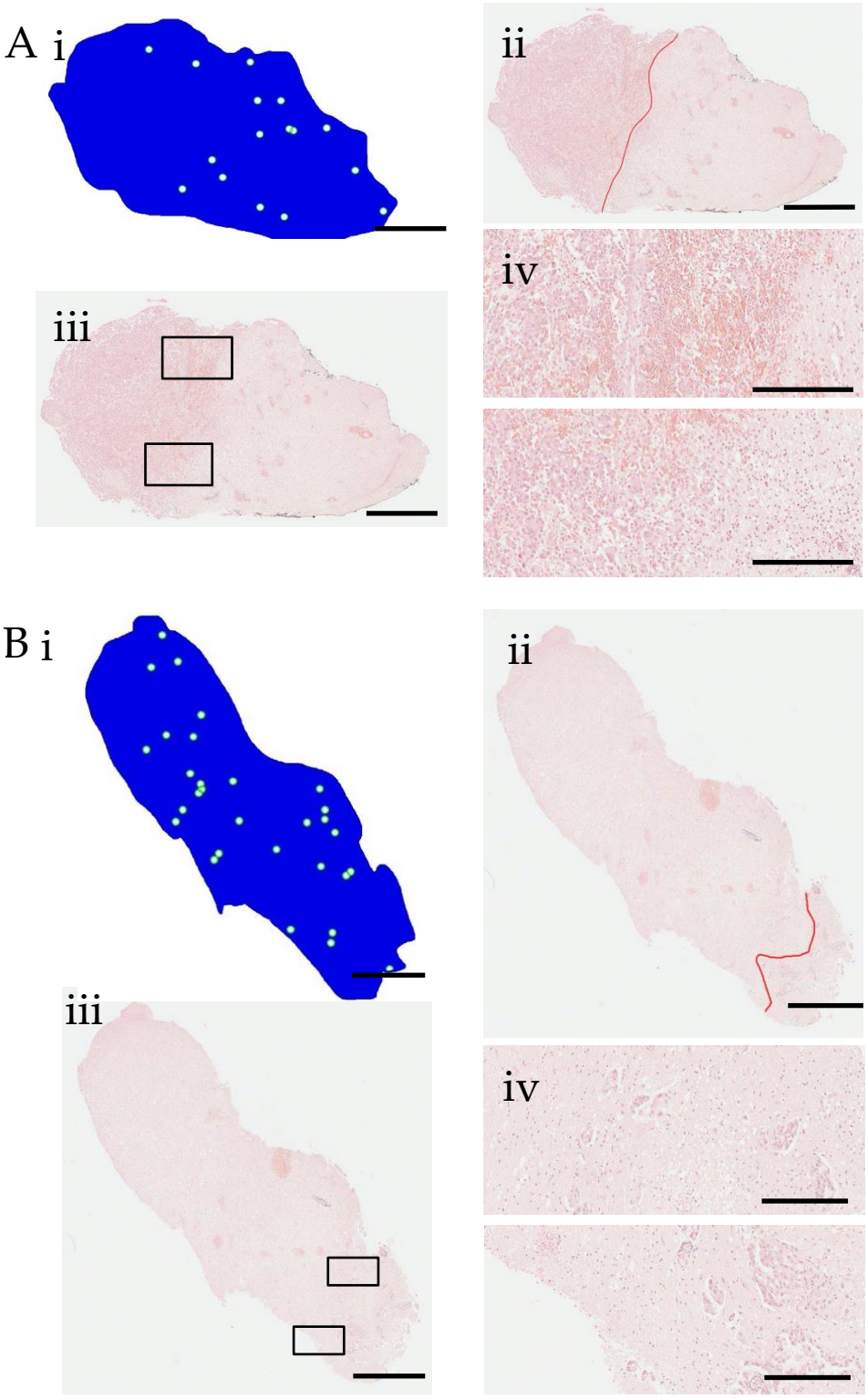

Figure 5.6. Two representative brain metastasis samples showing boundary of metastatic and parenchymal brain tissue. (i) Map of tissue section (blue) with location of TNFR1 positive vessels (green/white). (ii) Haematoxylin and eosin stained adjacent tissue section with red line indicating boundary between metastasis and brain. (iii) The same haematoxylin and eosin section with boxes indicating zoomed regions in (iv). Scale bars: 1 mm (i – iii); 250 μm (iv).

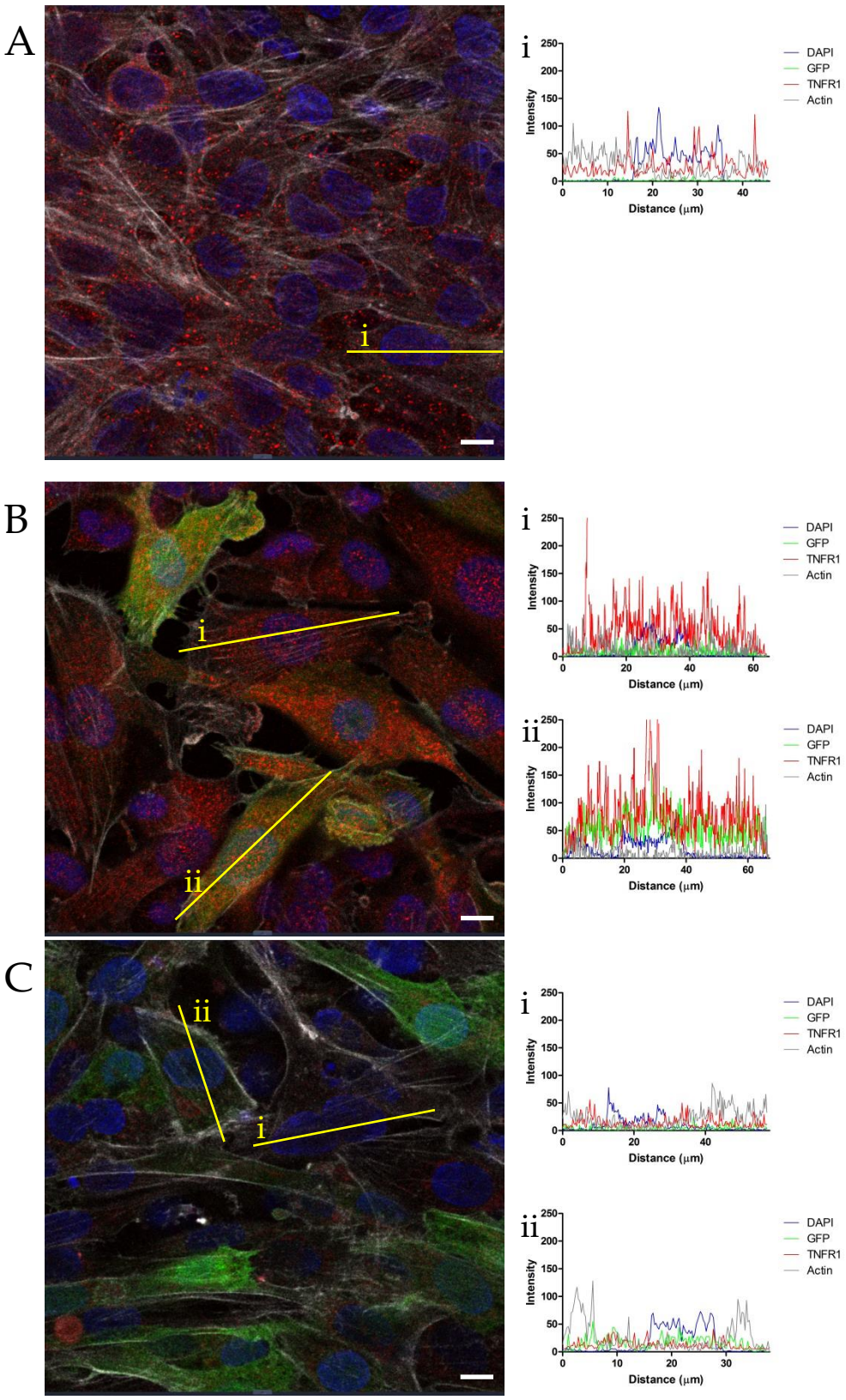

Fig 5.7: *In vitro* immunofluorescent staining of human cerebromicrovascular endothelial (hCMEC/d3) cells either alone (A), or co-cultured with MDA-231-Br-eGFP cells (B and C). Confocal images identifying presence of nuceli (DAPI, blue), tumour cells (GFP, green), TNFR1 (red) and actin cytoskeleton (white). (C) Negative controls; TNFR1 primary antibody omitted. Yellow lines intersecting endothelial cells (i) and tumour cells (ii) indicate 4-channel signal intensity graphs. Scale bars 10 μm.

To follow up on detection of TNFR1 expression on the vascular endothelium at sites of metastasis, preliminary experiments were designed to investigate TNFR1 mediation of the permeabilisation effect.

5.4.4.1 Immunofluorescent detection of TNFR1 *in vitro*

To generate a model for *in vitro* studies to probe the mechanisms involved in BBB permeabilisation induced by TNFR1 activation, a co-culture model system was developed. TNFR1 was detected in hCMEC/d3 cells *in vitro* through immunofluorescence (Figure 5.7 A) at low levels and in a punctate fashion. In cells co-cultured with MDA-231-Br-eGFP breast cancer cells, TNFR1 expression appeared to increase and displayed a more diffuse pattern (Figure 5.7 B i). The tumour cells themselves displayed immunoreactivity to TNFR1 (Figure 5.7 B ii). Visual assessment of actin staining was insufficient to observe any changes in actin cytoskeleton. More appropriate negative controls could have been used, involving cells known to not express the antigens such as fibroblasts.

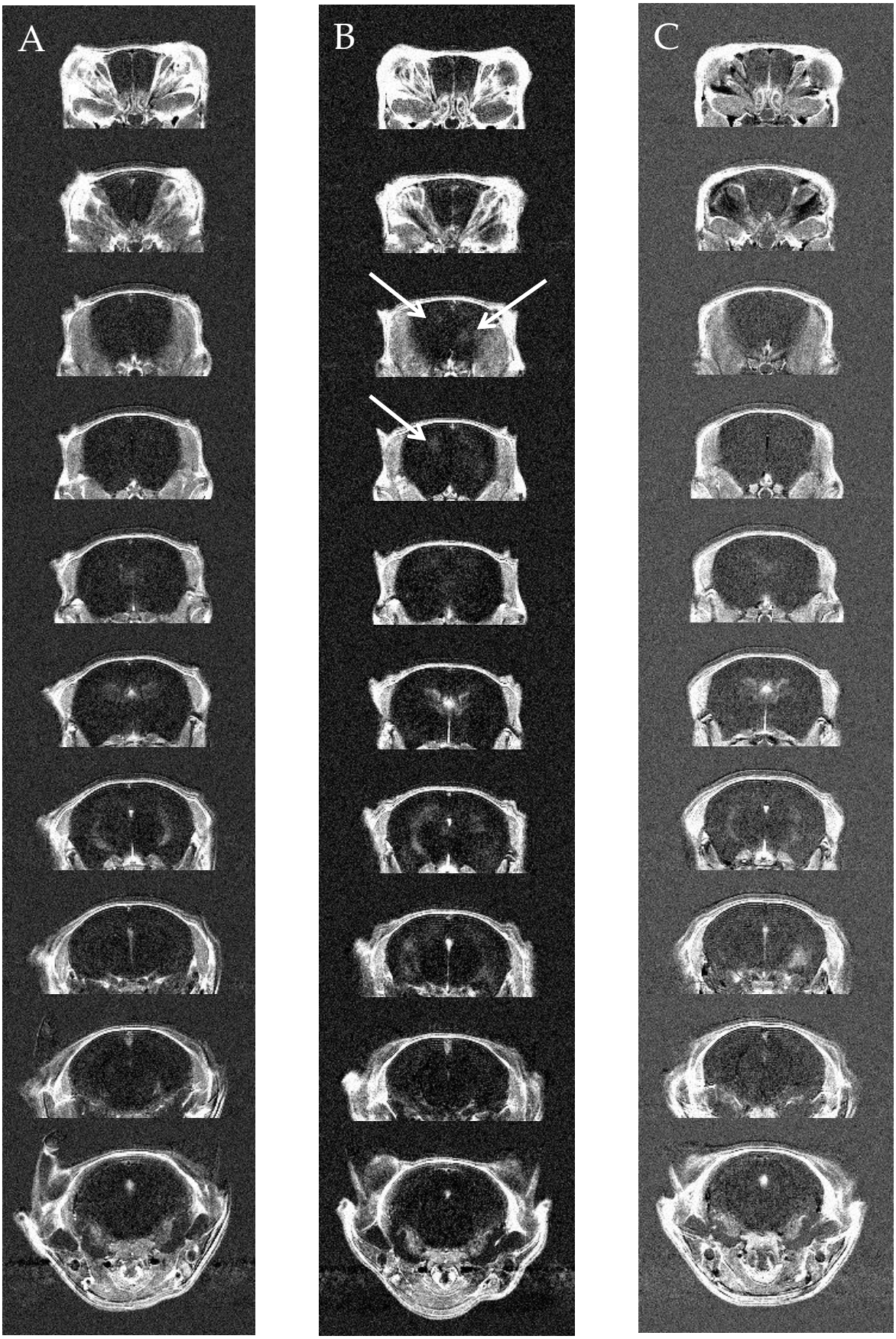

Fig 5.8: Subtraction image from T_1-weighted datasets (post-Gd minus pre-Gd) of mouse brains at day 13 post injection of tumour cells, two hours after intravenous injection of (A) saline, (B) 3 μg htr-9, (C) 3 μ g utr-1 (n=3 per group). Regions of hyperintensity (arrows) were observed in one mouse injected with htr-9, but in none of the mice injected with either saline or utr-1.

5.4.4.2 Selective permeabilisation of the blood-brain barrier by selective TNFR1 and TNFR2 agonist antibodies

To further test the hypothesis that the TNF induced permeabilisation is receptor specific, antibodies selective for either TNFR1 or TNFR2 were injected systemically into mice with brain metastases. BBB permeabilisation at sites of metastasis was not observed in mice injected with saline (Figure 5.8 A), but was detected in one out of three mice after injection with htr-9 (TNFR1 selective antibody; Figure 5.8 B arrows). BBB permeabilisation was not observed in any of the mice injected with utr-1 (TNFR2 selective antibody; Figure 5.8 C)

5.4.5 Toxicological study

To determine the potential toxicity of systemic TNF administration at the dose used here, the acute phase response was assessed in mice injected intravenously with TNF. A panel of liver function tests based on protein levels and enzyme activity was performed. Results indicated that there was no significant change in protein levels of glutamate dehydrogenase (GLDH), aspartate aminotransferase (AST), alanine aminotransferase (ALT) or in total protein levels as a consequence of intravenous TNF injection at either 24 or 74 h (Figure 5.9). A trend for a reduction in alkaline phosphatase (ALP) was seen at 24 h, which was resolved by 72 h.

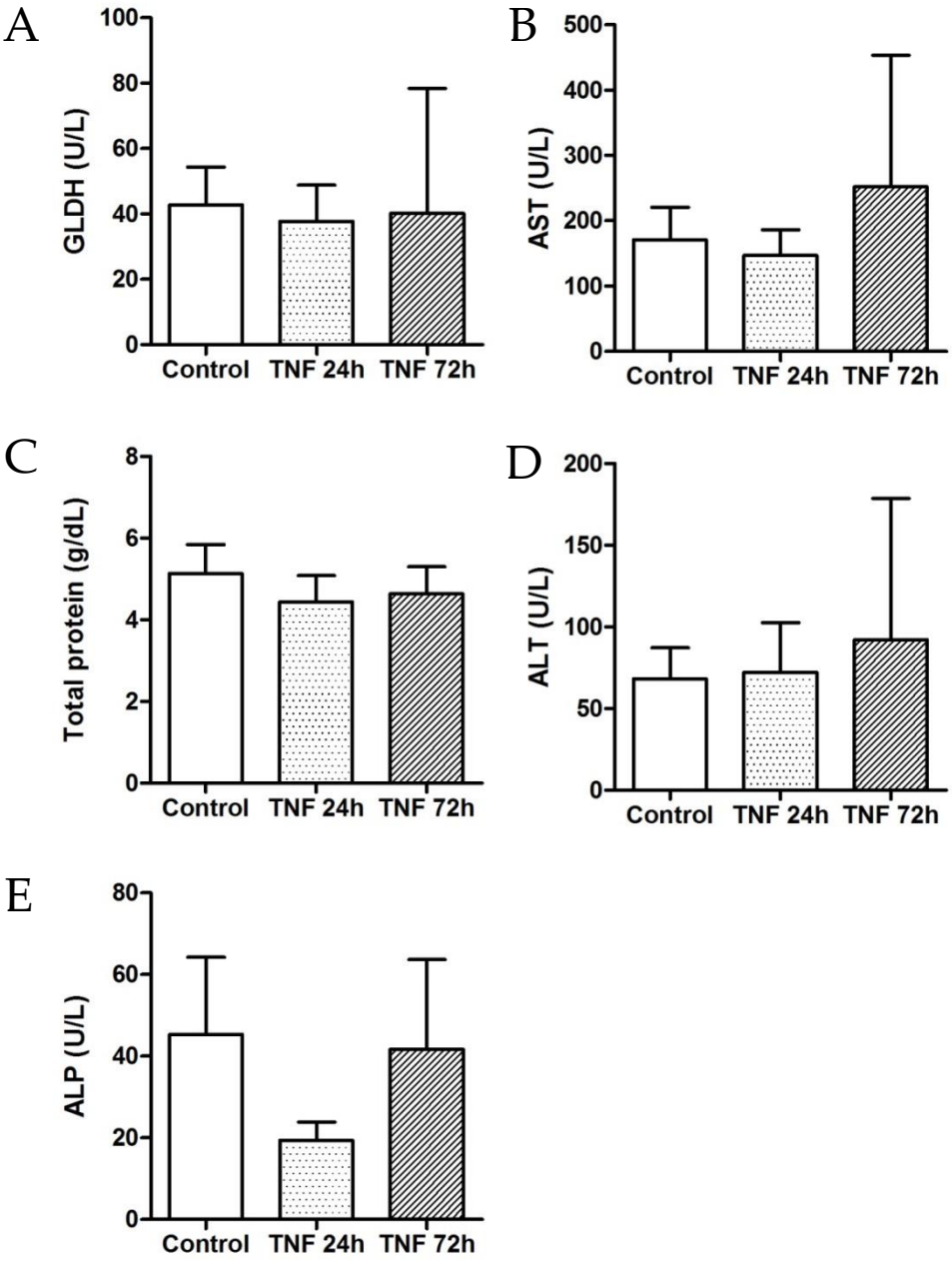

Fig 5.9: (A - E) Panel of liver function analyses of mouse plasma after systemic administration of 3 μg of TNF. No significant differences were found between any of groups for any of the liver function parameters measured, although a trend towards reduced ALP was evident 24h after TNF administration. Mean ±SD n = 3 per group. Two-tailed 1-way ANOVA showed no significant differences between groups. GLDH (glutamate dehydrogenase); AST (aspartate aminotransferase); ALT (alanine aminotransferase); ALP (alkaline phosphatase).

5.5 Discussion

The work presented in this chapter supports the hypothesis that administration of TNF induces permeabilisation of the BBB specifically at sites of metastasis, as a consequence of local TNFR1 upregulation. Results are also presented that indicate the potential for translation of this method into the human disease.

The data presented suggest that the demonstrated selective BBB permeabilisation in brain metastasis reflects the spatially restricted expression of both TNF receptors; TNFR1 on the vascular endothelium, and TNFR2 on recruited leukocytes and local microglia. Expression of these receptors was not evident in normal brain tissue, which indicates why the permeabilisation observed in Chapter 3 was spatially restricted to sites of metastasis. As discussed above, a range of transmembrane proteins are upregulated on the endothelium surrounding brain metastases (157). This phenomenon of spatially selective upregulation of endothelial proteins has been exploited to give spatial information of brain metastases at a very early stage, through *in vivo* imaging using contrast agent binding to VCAM-1 (131). The strategy used here exploits the spatially selective upregulation of a previously unidentified protein, TNFR1, to permeabilise the BBB as a method for enhanced drug delivery.

The same pattern of receptor expression was also found in two different models of brain metastasis using human breast cancer cells. These models employed two inoculation routes, intracardiac

administration of cells to promote vascular circulation and subsequent seeding of tumour cells into the brain; and direct implantation of tumour cells into the brain. As both models presented with similar TNF receptor upregulation profiles, it appears that it is the presence of tumour cells in the brain metastasis microenvironment that promotes vascular TNFR1 expression, rather than the process of extravasation itself.

Crucially, the TNF receptor expression profile seen in these mouse models was also observed in human brain metastasis biopsy samples. TNFR1 was found on the vascular endothelium, and TNFR2 on a range of immune cells including leukocytes and microglia. This finding indicates that the models of brain metastasis used throughout this thesis accurately reflect the human condition, whether using murine or human breast cancer cells. Moreover, this finding also indicates the potential for translation of the described permeabilisation strategy into the clinic. Issues involved with translation into the clinic will be discussed in Chapter 6.

In the results presented in Chapter 3, six hours after injection of TNF over 80% of metastases analysed in mouse brains (13 days after tumour cell injection; Figure 3.1 G) were permeable to contrast agents. In Chapter 4, the typical metastasis area (14 days after tumour cell injection; Figure 4.4 B) was less than 2500 μm^2, in contrast with the human brain metastasis samples of 487.3 mm^2 ±43.1 mm^2. In the human biopsy samples used here, where resectable metastases need to be of sufficient size to be detected through MRI (182), all presented with TNFR1 positive vessels. Accordingly, an appropriate measure of potential responsiveness was developed as frequency of metastasis permeability would not be useful.

Having identified the spatial location of each vessel that showed expression of TNFR1 through immunohistochemistry, the potential area of susceptibility to the permeabilisation technique was assessed. This measure provides information as to the potential area of targeting that should be expected. With metastases showing TNFR1 positive vessels more frequently, and distributed over more of the sample, the area of potential susceptibility increases. This indicates that the metastasis would thus have more drug delivered to it and would succumb to the cytotoxic effects of chemotherapy. If a large cohort of brain metastasis biopsy samples from a particular tumour origin displays a reliable level and distribution of TNFR1 expressing vessels, predictions can be made as to the likelihood of tumour regression as a consequence of this technique. Four of eleven samples showed that, owing to the frequency and spatial distribution of TNFR1 positive vessels, over half of the area would be accessible by chemotherapy, assuming a radius of access of 500 μm. Whilst data are required to define an accurate radius of permeabilisation, the possibility of delivering drugs to over 50% of the metastasis area could confer a significant improvement on brain metastasis treatment.

The part of the biopsy that was analysed is appropriate due to the conservative nature of the surgical resection. With an accurate map of the tumour volume and position within the brain available to the surgeon through pre- and peri-operative MRI, the location of the tumour boundary is known. As the BBB is inhomogenous particularly at the tumour boundary (121), where the tumour is infiltrative, the surgical resection encompassed a slightly larger volume. The area of interest of the BBB

permeabilisation strategy described here would primarily be the regions of metastasis that do not show a permeable BBB on MRI, and are thus outside the boundary that this defines. The extra tissue resected, and analysed here, constitutes this. As brain metastases can display an infiltrative morphology (183), delivering chemotherapy to the sites where cells are invading should slow metastasis growth. Half of the TNFR1 positive vessels in the eleven biopsy samples examined were directly adjacent to tumour cells, and half were in parenchymal brain tissue within the biopsy region, indicating that the influence of both critical regions would be targeted.

Pilot studies regarding specific TNFR1 agonism and toxicology

To further probe the mechanisms involved in BBB permeabilisation induced by TNFR1 activation, an *in vitro* model provides a platform for a particular range of experimental studies. The data presented here show that the well accepted human cerebral microvascular endothelial cell line (hCMEC/d3) (184) expresses TNFR1 in response to the presence of tumour cells. Whilst the fluorescent data are not quantitative and other *in vitro* techniques may provide a more precise measure of expression, the data indicate that the expression pattern is at a low level and punctate in cell monoculture, but increased and more diffuse across the cell when co-cultured with tumour cells. These data suggest that this model can serve as a platform to test TNFR1 agonists more quickly than using the *in vivo* model. Further experiments involving this approach are discussed in Chapter 6.

Toxicological studies suggested that at the dose used here of 3 μg of TNF per mouse induces no acute phase response in the liver which is a marker for systemic inflammation. This dose, considering a 20 g mouse with a body surface area of 46.4 cm^2 (185), can be expressed as 646.6 $\mu g/m^2$ (186) which is higher than that reported as the maximum tolerable dose in humans of 150 – 300 $\mu g/m^2$ (140,187–189). A 1 μg dose of TNF also elicited an increase in frequency of metastasis with BBB breakdown, which is a dose of 215.5 $\mu g/m^2$ which is within the MTD. However, the activity (190,191) and biological roles (192) of recombinant mouse TNF (used here) and recombinant human TNF (in the studies cited) are subtly different, as are the signalling cascades seen in humans and mice in response to TNF (193). As such, it may be better to investigate specific agonists of TNFR1 to limit side effects elicited by TNFR2, allowing work within the doses used here and those tolerable in humans.

5.6 Conclusion

The data presented here demonstrate that the ability to permeabilise the BBB specifically at sites of metastasis in a mouse model likely reflects the selective expression of TNFR1 on the vascular endothelium at sites of metastasis. Importantly, the expression of TNFR1 on the endothelium is conserved in human brain metastasis. The data presented suggest that, if the approach were to be applied to human brain metastases, the regions of tumour where the BBB is impermeable to intravenous agents would be successfully targeted, and to such an extent that it may be of clinical relevance.

Chapter 6 - General Discussion

The results presented in this thesis have described a strategy for permeabilising the BBB specifically at sites of brain metastasis in a mouse model. This approach facilitated the delivery of therapeutic and diagnostic agents to metastases that were previously inaccessible and, critically, to metastases that are smaller than currently detectable in the clinic. This strategy was extended in a model of brain metastasis with administration of active therapeutics (liposomally packaged doxorubicin) aiming to quantify change in tumour burden, but fell short of quantifying a significant reduction. Finally, an understanding of the receptor mediating the permeabilisation effect was developed, and the applicability of this strategy to the human condition was investigated. The findings of these studies suggest potential for the strategy to be effective in the areas most likely to evade therapy delivery.

6.1 Systemic administration of TNF enhances delivery of contrast agents to sites of brain metastasis.

Work published in 2011 demonstrated that in mice bearing subcutaneous lymphoma xenografts the accumulation of proteins from the bloodstream can be dramatically increased by intravenous injection of recombinant TNF (124). We hypothesised that intravenous TNF injection may facilitate delivery of, otherwise non-penetrating, chemotherapeutic agents to brain metastasis.

In two different mouse models of brain metastasis, systemic injection of TNF resulted in a significantly increased proportion of brain metastases displaying a permeable BBB compared to controls. A similar pattern was seen in mice injected with LT, the endogenous analogue of TNF. These proof-of-principle experiments gave justification to develop the analysis methodology, Hanker-Yates histological detection of HRP extravasation in *ex vivo* brain tissue slices, into an *in vivo* system. Histological experiments are inherently limited in observing the subject at a single time point. With the dynamic strategy of an impermeable BBB then being permeabilised, a system to observe changes over time would be beneficial. To this end, *in vivo* MRI experiments were designed to determine BBB permeability at different time points, both before and at an appropriate time after injection of TNF or LT. These data clearly demonstrated the permeability changes that systemic TNF or LT administration induces. Regions of hyperintensity induced by contrast agent extravasation indicate BBB permeability, and the presence and location of brain metastases was verified by *ex vivo* histology.

Whilst TNF and LT showed an increased delivery of contrast agents to sites of brain metastasis, the eventual aim of this project was to deliver an intravenous therapeutic compound to metastases. As the 4T1-GFP and MDA-231-Br-eGFP cell lines are derived from breast cancer biopsies (24,116), the most common agent used in treatment for patients with breast cancer, trastuzumab (133), was used to demonstrate the potential for delivery of a therapeutic compound. Previous reports of exclusion of trastuzumab from the brain (120,135,136) agreed with the results presented in Figure 3.4, where no radiolabelled trastuzumab was found through SPECT imaging within the brain. However, after treatment with TNF or LT, regions of SPECT signal enhancement were found within the brain, indicating an accumulation of trastuzumab. These regions co-localised with sites of brain metastasis as shown by histology. These findings provide further evidence for the potential of this drug delivery strategy in the treatment of brain metastasis at a very early stage. Additionally, the large molecular size of trastuzumab exceeds the maximum size tested in work presented in the literature (148 kDa trastuzumab compared to 3 kDa dextran beads (121)) indicating a further benefit of this strategy over alternative approaches. It is still important to note that this is accumulation of a contrast agent mimicking what a therapeutic agent would do, and does not show true drug delivery to an active site as there is no receptor present here.

The goal of the BBB permeabilisation strategy was to enhance the delivery of therapeutic compounds, but there is a serious potential risk of haemorrhage. This was investigated using a model of frank BBB

breakdown, by injecting CINC-1 directly into the brain which showed gross spread of MRI and histological contrast agents across the injected hemisphere, which were much more intense than the localised regions of hyperintensity seen in the brain metastasis model. Additionally, an orthotopic model of rat glioblastoma (183) showed extravasation and accumulation of erythrocytes surrounding the tumour, which shows that passage of blood components up to 5-8 μm in diameter can pass. As erythrocytes were not seen in metastases that were permeable to contrast agents, it suggests that the size threshold of the TNF induced BBB permeabilisation strategy presents an appropriate window for drug delivery whilst avoiding haemorrhage and gross BBB breakdown. This indicates a level of safety, as a typical concern raised throughout conversations with scientists at conferences was the risk of haemorrhage.

The maintenance of the permeabilisation effect at the sites of metastasis of up to 24 h (Figure 3.1 G) is substantially longer than that reported in the case of cereport injection (137). A longer window of opportunity for permeation of a circulating drug into the area of metastasis would undoubtedly confer an advantage to drug delivery. A further advantage over other mechanisms of BBB disruption for drug delivery, including injection of cereport or injection of mannitol, is the selectivity obtained through the use of TNF. The whole brain is affected in the alternative strategies, whereas with the strategy described here the normal healthy brain is spared. Consequently, it is anticipated that fewer adverse effects will arise.

Taken together, the proof-of-principle results presented in Chapter 3 suggest that the BBB permeabilisation strategy holds much promise and warranted further development.

6.2 Caelyx and 2B3-101 reduce brain metastasis burden

The proof-of-principle results from Chapter 3 prompted the development of experiments to probe the expected enhanced efficacy of therapeutic compounds. As both cell lines used in the previous chapter are erbB2 negative, efficacy of trastuzumab is not expected. Consequently, doxorubicin based chemotherapeutic agents were used. Caelyx and 2B3-101 were used in independent studies, and analysis of BBB patency, tumour burden and mean tumour size data indicated subtly different effects in their mechanisms of tumour burden reduction.

The exciting and novel results of the efficacy of Caelyx in reducing mean tumour size showed for the first time the potential use of this compound, already approved for use in advanced ovarian cancer (149), in treatment of early stage brain metastasis. Whilst administration of TNF in conjunction with Caelyx did not enhance efficacy, for the reasons described above (See Chapter 4.5), future experiments involving repeated dosing and extended experimental end points allow more time for Caelyx to induce apoptosis or allow more time for apoptosed cells to be cleared from the brain and be measured as a decrease in tumour burden. Using a dosing schedule where injections of Caelyx with TNF were administered so as to maintain a high concentration of Caelyx in the blood over a long time, e.g. at every 35 hour half-life of Caelyx.

Administration of the novel therapeutic compound 2B3-101 (glutathione-tagged PEGylated liposomal doxorubicin), at an earlier stage of brain metastasis than in the Caelyx study, elicited a reduction in tumour

burden yet no change in mean metastasis size. BBB patency had been confirmed in this model both at the time of drug administration, and at the time of sacrifice, suggesting that any reduction in tumour burden was elicited by the drug having crossed the BBB. This novel compound was designed to use the endothelial glutathione transporter to enhance delivery of the compound across the BBB (154). Glutathione is transported across the BBB by the glutathione transporter (151,152,194), and there is some evidence for glutathione-tagged liposomes to enhance drug delivery to the brain (195–197). The mechanism by which the enhanced delivery is facilitated is still unknown. Localisation of the liposomes to regions of vascular expression of glutathione receptor and subsequent endocytosis seems most likely as opposed to active transport of the huge liposome payload. To investigate this theory, mutation of the glutathione transporter to produce a functioning receptor to glutathione on the endothelial cell surface, but with ineffective transporter functions. However, there may be impeding downstream effects of defective glutathione transport on the model.

In control animals where TNF was injected not in conjunction with a cytotoxic agent, the surprising result of a reduced tumour burden was seen in both the early stage and slightly later stage metastases. As shown with *in vitro* data, TNF doesn't elicit 4T1-GFP cell death at concentrations that would be found in the blood circulation (assuming 3 μg injection of TNF dose in 2 mL blood volume ≈ 1.5 μg/mL ≈ 30 nM). As such, other mechanisms for this change in tumour burden must be considered. A

likely possibility may be a change in systemic inflammation, brought about by systemic administration of TNF, which may promote a microenvironment environment less permissive for tumour growth.

6.3 Permeabilisation occurs through TNF receptor 1

With promising results in the mouse models presented here, the clear development of the strategy is to assess whether it would be applicable in humans in the clinical setting. To get a level of understanding of this, the reason for brain metastases to be specifically susceptible to the actions of TNF as compared to the rest of the normal brain must be understood. The vasculature at sites of metastasis has been described to be 'activated' (157), meaning in a state of altered gene expression in reaction to, and as part of, the process of inflammation. As such, it was hypothesised that it was an altered expression of proteins on the endothelium at sites of metastasis that gave rise to the susceptibility to TNF at these sites.

As TNF has two main endogenous receptors (as part of a large superfamily (198)), studies were designed to see whether these receptors were present here, which would indicate a direct effect of TNF on the vasculature, rather than a more complicated system involving cascades of inflammatory mediators. TNFR2 was found to be expressed in a very distinct pattern, primarily on leukocytes that had been recruited (likely through VCAM-1 expression (199)) or on parenchymal microglia, but notably, exclusively at sites of metastasis, and not in regions of normal brain tissue. The functional roles of TNFR2 are described to be in cooperation with or independent of TNFR1, and influence cell proliferation and cell survival (200). However, the most interesting finding in these studies was the expression of TNFR1 on the vasculature at sites of metastasis, for three reasons. Firstly, expression exclusively at sites of

metastasis and not in normal brain accounts for the selectivity in BBB permeabilisation. Secondly, expression of the receptor on the endothelium would render the receptor exposed to the circulating TNF.

The bulk of literature describing downstream effects of TNFR1 activation suggests a clear mechanism for permeabilisation. As discussed in Chapter 5, TNFR1 activation can elicit a number of effects that affect the cytoskeleton and thus a key component of the BBB (178,179) (Figure 1.1). The use of TNF in a mouse model of systemic lymphoma induced a permeability of the vasculature to an injected dye and to oncolytic virus particles; a specific inhibitor to Rho kinase (a signalling molecule involved in actin filament phosphorylation and cytoskeletal rearrangement) inhibited this permeabilisation (124), indicating again the likely mechanism of TNF induced permeabilisation. TNF mediates tight junction regulation in the lung epithelium (85), and has been shown to alter permeability of endothelial monolayers *in vitro* through action on TNFR1 (128). Furthermore, a study has previously suggested that an alternative pharmacological strategy for BBB permeabilisation, through bradykinin B2 receptor activation (110,111), is in fact mediated by TNF (114).

Therefore, detection of TNFR1 provides confidence in the strategy, and a means of determining whether it would be applicable in the human disease. As such, TNFR1 and TNFR2 expression was investigated in human brain metastasis biopsy samples. The patterns of expression were strikingly similar to those seen in the mouse model, indicating the parallels between species and accuracy of the model. Furthermore, using predicted yet reasonable radii of permeability from TNFR1 expressing vessels, 4 of 11

biopsy samples could show permeabilisation over half of the biopsy area. Both the presence, and the number and spread of TNFR1 expressing vessels, especially in regions of metastasis at the bordering edge where BBB permeability is inhomogenous (121) and infiltration is most likely, suggests that this strategy has real potential for translation into the human condition.

Based on the preliminary data obtained from the *in vitro* model of endothelial cells in co-culture with tumour cells, experiments can be designed to precisely map the cytoskeleton after incubation with TNF. Current techniques involving quantifying length and number of actin cytoskeleton filaments may be sufficient to both give evidence for further understanding of the mechanism at play, and also to provide a cheap and reproducible platform for testing novel compounds.

6.4 Future Work

With this drug delivery strategy showing promising results and TNFR1 mediating the most likely mechanism, the remaining questions surrounding this approach must be discussed with a view towards extending the technique to the human condition.

6.4.1 Immediate future work

There are many interesting avenues down which research based on the work presented here can be developed. Critically, repeating and increasing statistical power and extending the work presented in Chapter 4 involving reduction of tumour burden by TNF enhanced delivery of Caelyx and 2B3-101 will give more confidence in the true usefulness of this approach. Primarily, careful changes to the treatment regimen and stage of mouse model to use will offer further insights into the type of metastasis (early stage, cooptive growth or later stage solid mass) that is affected most. Additionally, alternative chemotherapeutic agents could be used, such as Lapatinib, methotrexate or fluorouracil as they have different mechanisms and timeframes of action.

6.4.1.1 Size of permeability

Previous work has demonstrated an inherent permeability of the BBB at sites of late-stage metastasis to 3 kDa dextran beads (121). The techniques used in this body of work employed various tracers based on their utility in the particular detection methods, namely horseradish

peroxidase (44 kDa) for histology, Gd-DTPA (590 Da native, > 66 kDa when albumin bound) for MRI, and ^{111}In-Trastuzumab (145 kDa) for SPECT imaging. These tracers are substantially larger than the upper limit for passive diffusion across an intact BBB of 400-500 Da (along with high lipophilicity) (95), indicating that the size of permeability seen using this strategy is high enough for a vast array of therapeutics to enter the brain, from small molecule drugs to therapeutic monoclonal antibodies.

Accurate measurements of the size of BBB opening induced by focused ultrasound have been taken using dextrans in a range of molecular sizes (201). This strategy for opening the BBB facilitated the delivery of particles from 3 – 2000 kDa (2.3 – 54.4 nm hydrodynamic diameter) through increased pressure. This measurement technique could be extended to the TNF induced BBB permeabilisation strategy to ascertain the potential size of chemotherapeutics that could be delivered, along with further understanding of the dose/efficacy response that was investigated in Chapter 3.

Further, if the experiments presented in Chapter 4 are altered, as described, to show that TNF does indeed enhance delivery of Caelyx and 2B3-101, then the hydrodynamic diameter of these liposomal drug formulations of 80-100 nm (163,202) is larger than the top limit presented in the focussed ultrasound strategy study (201). This indicates a significant advantage to this technique, as not only are very early stage metastases targeted with no prior knowledge of their location, but a larger range of therapeutic compounds can be delivered.

To further understand the mechanisms involved, there are many *in vitro* experimental options involving for example: TNFR1/2 knocked-down cell lines, TNFR1/2 selective agonists, human TNF, *in vitro* measures of transendothelial permeability such as transendothelial electrical resistance, inhibitors of molecules involved in the signalling pathways.

6.4.2 Clinical translation

When systemic administration of TNF was first investigated in the field of cancer (reviewed in (175)) adverse effects slowed its progression into clinical use. Vasoplegia and "sceptic shock like syndrome" caused the maximum tolerable dose to be below a level where the sole use of TNF as an anti tumoural agent (through effects on killing angiogenic endothelial cells). Subsequently, efforts were made to target TNF to the intratumoural endothelial cells, through use of antibodies and peptides. By fusing TNF to an antibody against the extradomain B+ isoform of fibronectin (203,204), an isoform expressed highly in tumoural angiogenic vessels; or by fusing TNF to a peptide that binds to an isoform of aminopeptidase N (205), also expressed highly in tumoural angiogenic vessels, TNF was localised to the vessels where the effects of TNF were desired. Whilst data have not yet shown the expression of markers of angiogenesis in the mouse model of brain metastasis used in the work presented here, there is great potential for mimicking this approach but using an antibody directed against VCAM-1 (131), or any other of the endothelial markers that have been shown to be upregulated at the sites of metastasis (157) in combination with a chemotherapeutic. This may then allow markedly lower doses of

TNF to be administered, whilst maintaining efficacy of permeabilisation of the BBB at sites of metastasis to enhance drug delivery and minimising adverse effects of systemic inflammation. Indeed, work has demonstrated the antitumour activity of combination treatment of doxorubicin with fibronectin-targeted TNF in a model of sarcoma (206). Extension of this strategy in a model of brain metastasis may be of significant interest.

In another approach to improving the therapeutic index of TNF, a recombinant human TNF mutant was generated that exhibited an increase in cytotoxicity *in vitro* whilst showing an LD_{50} fifty times higher than the wild-type form *in vivo* (207). The authors of that study then combined this mutant TNF with the antibody targeting paradigm described above, by targeting $\alpha V\beta_3$ integrin that is expressed on angiogenic vessels, to increase delivery of doxorubicin to a hepatoma or sarcoma xenograft models through increased vessel permeability (208), thereby enhancing the antitumour response.

TNFR2, and not TNFR1, overexpression has been shown to sensitise mice to the toxicity of an otherwise sub-lethal dose of TNF (209). These findings indicate that many of the dose-limiting adverse effects of TNF reflect binding to TNFR2, likely as a consequence of increased NFκB and NO production. Therefore, development of TNFR1 selective agonists such as htr-9 used here, or a TNFR1 selective mutein (210) may maximise affinity for TNFR1 whilst eliminating activity at TNFR2.

6.4.3 Clinical trial considerations

As intravenous administration of TNF has been extensively studied in the past, early phase clinical trials can be entered into with some level of expectation of the risks of adverse effects involved.

The clinical populations that would be most appropriate for the trials of this strategy are a serious consideration if preclinical studies are still required. As delivery of trastuzumab as already been demonstrated, and HER2+ve breast cancer patients are at a higher risk of brain metastases (211), this population may be relevant. Treatment of metastatic breast cancer with trastuzumab has been shown to improve overall survival (133,212,213), but resistances to this drug occurs often in the metastatic setting (214). It is not known if it is trastuzumab-resistant breast cancer cells that are more likely to form brain metastases. Alternatively, as SCLC and nonSCLC accounts for 39%, and melanoma accounts for 11%, of incidences of brain metastasis (39), clinical trial cohorts of these patient populations would equally be appropriate. In all of these cohorts, two approaches to the outcome measure could be taken. First, in patients with brain metastases confirmed by MRI, the efficacy a treatment plan involving TNF with a drug could be measured by change in volume of the metastasis by post-therapy follow-up MRI. Response measures should follow RECIST guidelines (215). Second, in patients where there is a known high risk of developing brain metastases, such as those described above, but for whom MRI is not an option, monitoring of neurological symptoms, and survival time may be appropriate.

Furthermore, as the administration of TNF facilitated the delivery of Gd-DTPA sites of brain metastasis and allowed detection of previously 'invisible' metastases, this strategy has potential to be used for the early detection of brain metastasis. At-risk patients could be imaged using gadolinium-enhanced MRI both before and after administration of TNF. Comparison of differences in T_1-weighted images, as shown in Figure 3.3, may uncover the presence of small metastases, improve detection of tumour margins in previously detected metastases. The ability to better conclude the metastatic state of the brain will undoubtedly inform treatment planning.

6.5 Strengths and limitations

As with all novel academic research, studies are performed with the most well informed approach possible and within the limitations of reasonable study design, time and expense. Accordingly, there are inherent limitations in the strength of all conclusions. Translation of the conclusions formulated from data generated in mice into what the situation might be in humans has been demonstrated to be correct and incorrect in a raft of disease states and therapeutic approaches. As such, the conclusions raised here must be assessed critically and cynically. I feel that this has been described fully in the relevant chapters, but one limitation should be re-addressed. With the exception of two subjects in the data points in Figure 4.3 owing to their reaching a humane end point, the statistical validity of the data should be questioned. While planning of this study was performed with an understanding of tumour burden, expected response and similar studies to base the number of subjects on, this unexpected outcome of this novel and complicated work should suggest a repeat of the study with a more strongly powered design.

6.6 Concluding remark

With an estimated 27,000 cases of brain metastasis diagnosed in the UK per year (35), and therapeutic options limited to surgery, WBRT and SRS, with minimal gain, the potential added benefit of treating this disease with chemotherapy could have huge implications in the management of patients.

References

1. Hanahan D, Weinberg RA. The hallmarks of cancer. Cell. 2000 Jan 7;100(1):57–70.

2. Hanahan D, Weinberg RA. Hallmarks of cancer: the next generation. Cell. 2011 Mar 4;144(5):646–74.

3. Witsch E, Sela M, Yarden Y. Roles for Growth Factors in Cancer Progression. Physiology. 2010 Apr 1;25(2):85–101.

4. Lemmon MA, Schlessinger J. Cell Signaling by Receptor Tyrosine Kinases. Cell. 2010 Jun 25;141(7):1117–34.

5. Hynes NE, MacDonald G. ErbB receptors and signaling pathways in cancer. Curr Opin Cell Biol. 2009;21(2):177–84.

6. Burkhart DL, Sage J. Cellular mechanisms of tumour suppression by the retinoblastoma gene. Nat Rev Cancer. 2008 Sep;8(9):671–82.

7. Deshpande A, Sicinski P, Hinds PW. Cyclins and cdks in development and cancer: a perspective. Oncogene. 2005;24(17):2909–15.

8. Sherr CJ, McCormick F. The RB and p53 pathways in cancer. Cancer Cell. 2002;2(2):103–12.

9. Murphree AL, Benedict WF. Retinoblastoma: clues to human oncogenesis. Science. 1984 Mar 9;223(4640):1028–33.

10. Adams JM, Cory S. The Bcl-2 apoptotic switch in cancer development and therapy. Oncogene. 2007;26(9):1324–37.

11. Blasco MA. Telomeres and human disease: Ageing, cancer and beyond. Nat Rev Genet. 2005;6(8):611–22.

12. Shay JW, Wright WE. Hayflick, his limit, and cellular ageing. Nat Rev Mol Cell Biol. 2000;1(1):72–6.

13. Baeriswyl V, Christofori G. The angiogenic switch in carcinogenesis. Semin Cancer Biol. 2009;19(5):329–37.

14. Bergers G, Benjamin LE. Tumorigenesis and the angiogenic switch. Nat Rev Cancer. 2003;3(6):401–10.

15. Carmeliet P. VEGF as a key mediator of angiogenesis in cancer. Oncology. 2005;69(SUPPL. 3):4–10.

16. Nagy JA, Chang S-H, Shih S-C, Dvorak AM, Dvorak HF. Heterogeneity of the tumor vasculature. Semin Thromb Hemost. 2010;36(3):321–31.

17. Baluk P, Hashizume H, McDonald DM. Cellular abnormalities of blood vessels as targets in cancer. Curr Opin Genet Dev. 2005;15(1):102–11.

18. Jia J, Zhang W, Liu J-Y, Chen G, Liu H, Zhong H-Y, et al. Epithelial mesenchymal transition is required for acquisition of anoikis resistance and metastatic potential in adenoid cystic carcinoma. PloS One. 2012;7(12):e51549.

19. Frisch SM, Schaller M, Cieply B. Mechanisms that link the oncogenic epithelial-mesenchymal transition to suppression of anoikis. J Cell Sci. 2013 Jan 1;126(Pt 1):21–9.

20. Bierie B, Moses HL. Tumour microenvironment: TGFbeta: the molecular Jekyll and Hyde of cancer. Nat Rev Cancer. 2006 Jul;6(7):506–20.

21. Ikushima H, Miyazono K. TGFbeta signalling: a complex web in cancer progression. Nat Rev Cancer. 2010 Jun;10(6):415–24.

22. Paget S. The distribution of secondary growths in cancer of the breast. The Lancet. 1889 Mar;133(3421):571–3.

23. Minn AJ, Kang Y, Serganova I, Gupta GP, Giri DD, Doubrovin M, et al. Distinct organ-specific metastatic potential of individual breast cancer cells and primary tumors. J Clin Invest. 2005 Jan;115(1):44–55.

24. Yoneda T, Williams PJ, Hiraga T, Niewolna M, Nishimura R. A Bone-Seeking Clone Exhibits Different Biological Properties from the MDA-MB-231 Parental Human Breast Cancer Cells and a Brain-

Seeking Clone In Vivo and In Vitro. J Bone Miner Res. 2001;16(8):1486–95.

25. Nguyen DX, Massagué J. Genetic determinants of cancer metastasis. Nat Rev Genet. 2007 May;8(5):341–52.

26. Nicolson GL. Organ specificity of tumor metastasis: role of preferential adhesion, invasion and growth of malignant cells at specific secondary sites. Cancer Metastasis Rev. 1988 Jun;7(2):143–88.

27. Calabrese C, Poppleton H, Kocak M, Hogg TL, Fuller C, Hamner B, et al. A perivascular niche for brain tumor stem cells. Cancer Cell. 2007 Jan;11(1):69–82.

28. Ghajar CM, Peinado H, Mori H, Matei IR, Evason KJ, Brazier H, et al. The perivascular niche regulates breast tumour dormancy. Nat Cell Biol. 2013 Jul;15(7):807–17.

29. Ewing J. Neoplastic diseases; a treatise on tumors. Philadelphia, W.B.Saunders Company; 1919.

30. Hwang TL, Close TP, Grego JM, Brannon WL, Gonzales F. Predilection of brain metastasis in gray and white matter junction and vascular border zones. Cancer. 1996 Apr 15;77(8):1551–5.

31. Krumina G. Metastatic disease of the brain: parenchyma. Eur Radiol. 2005 Mar;15(3):608–16.

32. Gavrilovic IT, Posner JB. Brain metastases: Epidemiology and pathophysiology. J Neurooncol. 2005;75(1):5–14.

33. Pestalozzi BC, Zahrieh D, Price KN, Holmberg SB, Lindtner J, Collins J, et al. Identifying breast cancer patients at risk for Central Nervous System (CNS) metastases in trials of the International Breast Cancer Study Group (IBCSG). Ann Oncol. 2006 Jun 1;17(6):935–44.

34. Soffietti R, Ruda R, Mutani R. Management of brain metastases. J Neurol. 2002;249(10):1357–69.

35. Brem S, Panattil JG. An era of rapid advancement: diagnosis and treatment of metastatic brain cancer. Neurosurgery. 2005 Nov;57(5 Suppl):S5–9; discusssion S1–4.

36. Soffietti R, Rudà R, Trevisan E. Brain metastases: current management and new developments. Curr Opin Oncol. 2008 Nov;20(6):676–84.

37. Chang EL, Wefel JS, Maor MH, Hassenbusch SJ 3rd, Mahajan A, Lang FF, et al. A pilot study of neurocognitive function in patients with one to three new brain metastases initially treated with stereotactic radiosurgery alone. Neurosurgery. 2007 Feb;60(2):277–83; discussion 283–4.

38. Meyers CA, Smith JA, Bezjak A, Mehta MP, Liebmann J, Illidge T, et al. Neurocognitive function and progression in patients with brain metastases treated with whole-brain radiation and motexafin gadolinium: results of a randomized phase III trial. J Clin Oncol Off J Am Soc Clin Oncol. 2004 Jan 1;22(1):157–65.

39. Nussbaum ES, Djalilian HR, Cho KH, Hall WA. Brain metastases. Histology, multiplicity, surgery, and survival. Cancer. 1996 Oct 15;78(8):1781–8.

40. Ferlay J, Shin H-R, Bray F, Forman D, Mathers C, Parkin DM. Estimates of worldwide burden of cancer in 2008: GLOBOCAN 2008. Int J Cancer J Int Cancer. 2010 Dec 15;127(12):2893–917.

41. Sperduto PW, Chao ST, Sneed PK, Luo X, Suh J, Roberge D, et al. Diagnosis-Specific Prognostic Factors, Indexes, and Treatment Outcomes for Patients With Newly Diagnosed Brain Metastases: A Multi-Institutional Analysis of 4,259 Patients. Int J Radiat Oncol. 2010 Jul 1;77(3):655–61.

42. Hammond EM, Giaccia AJ. The role of p53 in hypoxia-induced apoptosis. Biochem Biophys Res Commun. 2005 Jun 10;331(3):718–25.

43. Brat DJ, Van Meir EG. Vaso-occlusive and prothrombotic mechanisms associated with tumor hypoxia, necrosis, and accelerated growth in glioblastoma. Lab Invest. 2004 Mar 1;84(4):397–405.

44. Jenkinson MD, Haylock B, Shenoy A, Husband D, Javadpour M. Management of cerebral metastasis: Evidence-based approach for surgery, stereotactic radiosurgery and radiotherapy. Eur J Cancer. 2011 Mar;47(5):649–55.

45. NICE. CG121 Lung cancer: NICE guideline [Internet]. 2011 [cited 2014 Jun 16]. Available from: http://publications.nice.org.uk/lung-cancer-cg121/guidance#palliative-interventions-and-supportive-and-palliative-care

46. Ryken TC, McDermott M, Robinson PD, Ammirati M, Andrews DW, Asher AL, et al. The role of steroids in the management of brain metastases: a systematic review and evidence-based clinical practice guideline. J Neurooncol. 2010 Jan;96(1):103–14.

47. NICE. CG81 Advanced breast cancer: NICE guideline [Internet]. 2009 [cited 2014 Jun 16]. Available from: http://publications.nice.org.uk/advanced-breast-cancer-cg81/guidance#systemic-disease-modifying-therapy

48. Boogerd W. Neuro-Oncologic Complications of Breast Cancer. In: MD DS, MD PYW, editors. Cancer Neurology in Clinical Practice [Internet]. Humana Press; 2003 [cited 2014 Jul 20]. p. 309–25. Available from: http://link.springer.com/chapter/10.1007/978-1-59259-317-0_21

49. Cancer Research UK. Breast cancer survival statistics [Internet]. 2014 [cited 2014 Jul 20]. Available from: http://www.cancerresearchuk.org/cancer-info/cancerstats/types/breast/survival/breast-cancer-survival-statistics

50. Trudeau ME, Crump M, Charpentier D, Yelle L, Bordeleau L, Matthews S, et al. Temozolomide in metastatic breast cancer (MBC): a phase II trial of the National Cancer Institute of Canada - Clinical Trials Group (NCIC-CTG). Ann Oncol Off J Eur Soc Med Oncol ESMO. 2006 Jun;17(6):952–6.

51. Omuro AM, Raizer JJ, Demopoulos A, Malkin MG, Abrey LE. Vinorelbine combined with a protracted course of temozolomide for

recurrent brain metastases: a phase I trial. J Neurooncol. 2006 Jul;78(3):277–80.

52. Bachelot T, Romieu G, Campone M, Diéras V, Cropet C, Dalenc F, et al. Lapatinib plus capecitabine in patients with previously untreated brain metastases from HER2-positive metastatic breast cancer (LANDSCAPE): a single-group phase 2 study. Lancet Oncol. 2013 Jan;14(1):64–71.

53. Verger E, Gil M, Yaya R, Viñolas N, Villà S, Pujol T, et al. Temozolomide and concomitant whole brain radiotherapy in patients with brain metastases: A phase II randomized trial. Int J Radiat Oncol. 2005 Jan;61(1):185–91.

54. Kouvaris JR, Miliadou A, Kouloulias VE, Kolokouris D, Balafouta MJ, Papacharalampous XN, et al. Phase II study of temozolomide and concomitant whole-brain radiotherapy in patients with brain metastases from solid tumors. Onkologie. 2007 Jul;30(7):361–6.

55. Chua D, Krzakowski M, Chouaid C, Pallotta MG, Martinez JI, Gottfried M, et al. Whole-brain radiation therapy plus concomitant temozolomide for the treatment of brain metastases from non-small-cell lung cancer: a randomized, open-label phase II study. Clin Lung Cancer. 2010 May;11(3):176–81.

56. Robinet G, Thomas P, Breton JL, Léna H, Gouva S, Dabouis G, et al. Results of a phase III study of early versus delayed whole brain radiotherapy with concurrent cisplatin and vinorelbine combination in inoperable brain metastasis of non-small-cell lung cancer: Groupe Français de Pneumo-Cancérologie (GFPC) Protocol 95-1. Ann Oncol Off J Eur Soc Med Oncol ESMO. 2001 Jan;12(1):59–67.

57. Drappatz J, Wen PY. Chemotherapy and targeted molecular therapies for brain metastases. Expert Rev Neurother. 2006 Oct;6(10):1465–79.

58. Cappuzzo F, Ardizzoni A, Soto-Parra H, Gridelli C, Maione P, Tiseo M, et al. Epidermal growth factor receptor targeted therapy by ZD 1839 (Iressa) in patients with brain metastases from non-small cell

lung cancer (NSCLC). Lung Cancer Amst Neth. 2003 Aug;41(2):227–31.

59. Mehta MP, Rodrigus P, Terhaard CHJ, Rao A, Suh J, Roa W, et al. Survival and neurologic outcomes in a randomized trial of motexafin gadolinium and whole-brain radiation therapy in brain metastases. J Clin Oncol Off J Am Soc Clin Oncol. 2003 Jul 1;21(13):2529–36.

60. Turner EH, Matthews AM, Linardatos E, Tell RA, Rosenthal R. Selective publication of antidepressant trials and its influence on apparent efficacy. N Engl J Med. 2008 Jan 17;358(3):252–60.

61. Bouffet E, Doumi N, Thiesse P, Mottolese C, Jouvet A, Lacroze M, et al. Brain metastases in children with solid tumors. Cancer. 1997 Jan 15;79(2):403–10.

62. Boogerd W, Vos VW, Hart AA, Baris G. Brain metastases in breast cancer; natural history, prognostic factors and outcome. J Neurooncol. 1993 Feb;15(2):165–74.

63. Paterson AH, Agarwal M, Lees A, Hanson J, Szafran O. Brain metastases in breast cancer patients receiving adjuvant chemotherapy. Cancer. 1982 Feb 15;49(4):651–4.

64. Lauterbur PC. Image Formation by Induced Local Interactions: Examples Employing Nuclear Magnetic Resonance. Nature. 1973 Mar 16;242(5394):190–1.

65. Garroway AN, Grannell PK, Mansfield P. Image formation in NMR by a selective irradiative process. J Phys C Solid State Phys. 1974 Dec 21;7(24):L457.

66. Rabi II, Zacharias JR, Millman S, Kusch P. A New Method of Measuring Nuclear Magnetic Moment. Phys Rev. 1938 Feb 15;53(4):318–318.

67. Nomoto Y, Miyamoto T, Yamaguchi Y. Brain Metastasis of Small Cell Lung Carcinoma: Comparison of Gd-DTPA Enhanced Magnetic Resonance Imaging and Enhanced Computerized Tomography. Jpn J Clin Oncol. 1994 Oct 1;24(5):258–62.

68. Sheehan JP, Yen C-P, Nguyen J, Rainey JA, Dassoulas K, Schlesinger DJ. Timing and risk factors for new brain metastasis formation in patients initially treated only with Gamma Knife surgery. Clinical article. J Neurosurg. 2011 Mar;114(3):763–8.

69. Schlageter KE, Molnar P, Lapin GD, Groothuis DR. Microvessel Organization and Structure in Experimental Brain Tumors: Microvessel Populations with Distinctive Structural and Functional Properties. Microvasc Res. 1999 Nov;58(3):312–28.

70. Chi J-T, Chang HY, Haraldsen G, Jahnsen FL, Troyanskaya OG, Chang DS, et al. Endothelial cell diversity revealed by global expression profiling. Proc Natl Acad Sci. 2003 Sep 16;100(19):10623–8.

71. Abe M, Sato Y. cDNA microarray analysis of the gene expression profile of VEGF-activated human umbilical vien endothelial cells. Angiogenesis. 2001 Dec 1;4(4):289–98.

72. Jackson WF. Ion Channels and Vascular Tone. Hypertension. 2000 Jan 1;35(1):173–8.

73. Golias C, Tsoutsi E, Matziridis A, Makridis P, Batistatou A, Charalabopoulos K. Review. Leukocyte and endothelial cell adhesion molecules in inflammation focusing on inflammatory heart disease. Vivo Athens Greece. 2007 Oct;21(5):757–69.

74. Peppiatt CM, Howarth C, Mobbs P, Attwell D. Bidirectional control of CNS capillary diameter by pericytes. Nature. 2006 Oct 12;443(7112):700–4.

75. O'Brien ER, Kersemans V, Tredwell M, Checa B, Serres S, Soto MS, et al. Glial activation in the early stages of brain metastasis: TSPO as a diagnostic biomarker. J Nucl Med Off Publ Soc Nucl Med. 2014 Feb;55(2):275–80.

76. Johansson BB. Blood-Brain Barrier: Role of Brain Endothelial Surface Charge and Glycocalyx. In: M.D YF, M.D MT, M.D AK, editors. Ischemic Blood Flow in the Brain [Internet]. Springer Japan; 2001 [cited 2015 Feb 21]. p. 33–8. Available from: http://link.springer.com/chapter/10.1007/978-4-431-67899-1_5

77. Krause G, Winkler L, Mueller SL, Haseloff RF, Piontek J, Blasig IE. Structure and function of claudins. Biochim Biophys Acta. 2008 Mar;1778(3):631–45.

78. Van Itallie CM, Anderson JM. Claudins and epithelial paracellular transport. Annu Rev Physiol. 2006;68:403–29.

79. Aijaz S, Balda MS, Matter K. Tight junctions: molecular architecture and function. Int Rev Cytol. 2006;248:261–98.

80. Cereijido M, Shoshani L, Contreras RG. Molecular Physiology and Pathophysiology of Tight Junctions I. Biogenesis of tight junctions and epithelial polarity. Am J Physiol - Gastrointest Liver Physiol. 2000 Sep 1;279(3):G477–82.

81. Matter K, Balda MS. Signalling to and from tight junctions. Nat Rev Mol Cell Biol. 2003 Mar;4(3):225–37.

82. Turowski P, Martinelli R, Crawford R, Wateridge D, Papageorgiou A-P, Lampugnani MG, et al. Phosphorylation of vascular endothelial cadherin controls lymphocyte emigration. J Cell Sci. 2008 Jan 1;121(Pt 1):29–37.

83. Van Wetering S, van den Berk N, van Buul JD, Mul FPJ, Lommerse I, Mous R, et al. VCAM-1-mediated Rac signaling controls endothelial cell-cell contacts and leukocyte transmigration. Am J Physiol Cell Physiol. 2003 Aug;285(2):C343–52.

84. Hartsock A, Nelson WJ. Adherens and Tight Junctions: Structure, Function and Connections to the Actin Cytoskeleton. Biochim Biophys Acta. 2008 Mar;1778(3):660–9.

85. Shen L. Tight junctions on the move: molecular mechanisms for epithelial barrier regulation. Ann N Y Acad Sci. 2012 Jul;1258:9–18.

86. Sandig M, Voura EB, Kalnins VI, Siu CH. Role of cadherins in the transendothelial migration of melanoma cells in culture. Cell Motil Cytoskeleton. 1997;38(4):351–64.

87. Brown H, Rogerson S, Taylor T, Tembo M, Mwenechanya J, Molyneux M, et al. Blood-brain barrier function in cerebral malaria in Malawian children. Am J Trop Med Hyg. 2001 Apr;64(3-4):207–13.

88. Brown H, Turner G, Rogerson S, Tembo M, Mwenechanya J, Molyneux M, et al. Cytokine expression in the brain in human cerebral malaria. J Infect Dis. 1999 Nov;180(5):1742–6.

89. Minagar A, Alexander JS. Blood-brain barrier disruption in multiple sclerosis. Mult Scler Houndmills Basingstoke Engl. 2003 Dec;9(6):540–9.

90. Bolton SJ, Anthony DC, Perry VH. Loss of the tight junction proteins occludin and zonula occludens-1 from cerebral vascular endothelium during neutrophil-induced blood–brain barrier breakdown in vivo. Neuroscience. 1998 Jun 18;86(4):1245–57.

91. Carbonell WS, Ansorge O, Sibson N, Muschel R. The Vascular Basement Membrane as "Soil" in Brain Metastasis. PLoS ONE. 2009 Jun 10;4(6):e5857.

92. Juliano RL, Ling V. A surface glycoprotein modulating drug permeability in Chinese hamster ovary cell mutants. Biochim Biophys Acta. 1976 Nov 11;455(1):152–62.

93. Borst P, Evers R, Kool M, Wijnholds J. A family of drug transporters: the multidrug resistance-associated proteins. J Natl Cancer Inst. 2000 Aug 16;92(16):1295–302.

94. Dolghih E, Jacobson MP. Predicting efflux ratios and blood-brain barrier penetration from chemical structure: combining passive permeability with active efflux by P-glycoprotein. ACS Chem Neurosci. 2013 Feb 20;4(2):361–7.

95. Pardridge WM. The Blood-Brain Barrier: Bottleneck in Brain Drug Development. NeuroRx. 2005 Jan;2(1):3–14.

96. Judy KD, Olivi A, Buahin KG, Domb A, Epstein JI, Colvin OM, et al. Effectiveness of controlled release of a cyclophosphamide derivative with polymers against rat gliomas. J Neurosurg. 1995 Mar;82(3):481–6.

97. Westphal M, Hilt DC, Bortey E, Delavault P, Olivares R, Warnke PC, et al. A phase 3 trial of local chemotherapy with biodegradable carmustine (BCNU) wafers (Gliadel wafers) in patients with primary malignant glioma. Neuro-Oncol. 2003 Apr;5(2):79–88.

98. Bobo RH, Laske DW, Akbasak A, Morrison PF, Dedrick RL, Oldfield EH. Convection-enhanced delivery of macromolecules in the brain. Proc Natl Acad Sci U S A. 1994 Mar 15;91(6):2076–80.

99. Bertrand N, Wu J, Xu X, Kamaly N, Farokhzad OC. Cancer nanotechnology: the impact of passive and active targeting in the era of modern cancer biology. Adv Drug Deliv Rev. 2014 Feb;66:2–25.

100. Alexandrakis G, Brown EB, Tong RT, McKee TD, Campbell RB, Boucher Y, et al. Two-photon fluorescence correlation microscopy reveals the two-phase nature of transport in tumors. Nat Med. 2004 Feb;10(2):203–7.

101. Haluska M, Anthony M. Osmotic Blood-Brain Barrier Modification for the Treatment of Malignant Brain Tumors. Clin J Oncol Nurs. 2004 Jun 1;8(3):263–7.

102. Doolittle ND, Miner ME, Hall WA, Siegal T, Jerome E, Osztie E, et al. Safety and efficacy of a multicenter study using intraarterial chemotherapy in conjunction with osmotic opening of the blood-brain barrier for the treatment of patients with malignant brain tumors. Cancer. 2000 Feb 1;88(3):637–47.

103. Gumerlock MK, Belshe BD, Madsen R, Watts C. Osmotic blood-brain barrier disruption and chemotherapy in the treatment of high grade malignant glioma: patient series and literature review. J Neurooncol. 1992 Jan;12(1):33–46.

104. Neuwelt EA, Howieson J, Frenkel EP, Specht HD, Weigel R, Buchan CG, et al. Therapeutic efficacy of multiagent chemotherapy with drug delivery enhancement by blood-brain barrier modification in glioblastoma. Neurosurgery. 1986 Oct;19(4):573–82.

105. Hildebrand J. Radiotherapy and chemotherapy of malignant brain gliomas. Drugs Exp Clin Res. 1986;12(1-3):167–75.

106. Siegal T, Rubinstein R, Bokstein F, Schwartz A, Lossos A, Shalom E, et al. In vivo assessment of the window of barrier opening after osmotic blood—brain barrier disruption in humans. J Neurosurg. 2000 Apr 1;92(4):599–605.

107. Neuwelt EA, Frenkel EP, Gumerlock MK, Braziel R, Dana B, Hill SA. Developments in the diagnosis and treatment of primary CNS lymphoma. A prospective series. Cancer. 1986 Oct 15;58(8):1609–20.

108. Kinoshita M, McDannold N, Jolesz FA, Hynynen K. Noninvasive localized delivery of Herceptin to the mouse brain by MRI-guided focused ultrasound-induced blood–brain barrier disruption. Proc Natl Acad Sci. 2006 Aug 1;103(31):11719–23.

109. Park E-J, Zhang Y-Z, Vykhodtseva N, McDannold N. Ultrasound-mediated blood-brain/blood-tumor barrier disruption improves outcomes with trastuzumab in a breast cancer brain metastasis model. J Controlled Release [Internet]. [cited 2012 Oct 10];(0). Available from: http://www.sciencedirect.com/science/article/pii/S0168365912006931

110. Borlongan CV, Emerich DF. Facilitation of drug entry into the CNS via transient permeation of blood brain barrier: laboratory and preliminary clinical evidence from bradykinin receptor agonist, Cereport. Brain Res Bull. 2003 May 15;60(3):297–306.

111. Matsukado K, Inamura T, Nakano S, Fukui M, Bartus RT, Black KL. Enhanced tumor uptake of carboplatin and survival in glioma-bearing rats by intracarotid infusion of bradykinin analog, RMP-7. Neurosurgery. 1996 Jul;39(1):125–33; discussion 133–4.

112. Prados MD, Schold SC JR SC, Fine HA, Jaeckle K, Hochberg F, Mechtler L, et al. A randomized, double-blind, placebo-controlled, phase 2 study of RMP-7 in combination with carboplatin administered intravenously for the treatment of recurrent malignant glioma. Neuro-Oncol. 2003 Apr;5(2):96–103.

113. Sanovich E, Bartus RT, Friden PM, Dean RL, Le HQ, Brightman MW. Pathway across blood-brain barrier opened by the bradykinin agonist, RMP-7. Brain Res. 1995 Dec 24;705(1-2):125–35.

114. Qin L-J, Gu Y-T, Zhang H, Xue Y-X. Bradykinin-induced blood–tumor barrier opening is mediated by tumor necrosis factor-α. Neurosci Lett. 2009 Jan 30;450(2):172–5.

115. Hoffmann A, Bredno J, Wendland M, Derugin N, Ohara P, Wintermark M. High and Low Molecular Weight Fluorescein Isothiocyanate (FITC)–Dextrans to Assess Blood-Brain Barrier Disruption: Technical Considerations. Transl Stroke Res. 2011 Mar;2(1):106–11.

116. Aslakson CJ, Miller FR. Selective Events in the Metastatic Process Defined by Analysis of the Sequential Dissemination of Subpopulations of a Mouse Mammary Tumor. Cancer Res. 1992 Mar 15;52(6):1399–405.

117. Balathasan L, Beech JS, Muschel RJ. Ultrasonography-guided intracardiac injection: an improvement for quantitative brain colonization assays. Am J Pathol. 2013 Jul;183(1):26–34.

118. Cornelissen B, McLarty K, Kersemans V, Scollard DA, Reilly RM. Properties of [111In]-labeled HIV-1 tat peptide radioimmunoconjugates in tumor-bearing mice following intravenous or intratumoral injection. Nucl Med Biol. 2008 Jan;35(1):101–10.

119. Carbonell WS, Ansorge O, Sibson N, Muschel R. The Vascular Basement Membrane as "Soil" in Brain Metastasis. PLoS ONE [Internet]. 2009 Jun 10 [cited 2014 May 7];4(6). Available from: http://www.ncbi.nlm.nih.gov/pmc/articles/PMC2689678/

120. Lampson LA. Monoclonal antibodies in neuro-oncology: Getting past the blood-brain barrier. mAbs. 2011 Apr;3(2):153–60.

121. Lockman PR, Mittapalli RK, Taskar KS, Rudraraju V, Gril B, Bohn KA, et al. Heterogeneous Blood-Tumor Barrier Permeability Determines Drug Efficacy in Experimental Brain Metastases of Breast Cancer. Clin Cancer Res Off J Am Assoc Cancer Res. 2010 Dec 1;16(23):5664–78.

122. Eichler AF, Chung E, Kodack DP, Loeffler JS, Fukumura D, Jain RK. The biology of brain metastases[mdash]translation to new therapies. Nat Rev Clin Oncol. 2011 Jun;8(6):344–56.

123. Treat LH, McDannold N, Vykhodtseva N, Zhang Y, Tam K, Hynynen K. Targeted delivery of doxorubicin to the rat brain at therapeutic levels using MRI-guided focused ultrasound. Int J Cancer. 2007 Aug 15;121(4):901–7.

124. Seki T, Carroll F, Illingworth S, Green N, Cawood R, Bachtarzi H, et al. Tumour necrosis factor-alpha increases extravasation of virus particles into tumour tissue by activating the Rho A/Rho kinase pathway. J Controlled Release. 2011 Dec 20;156(3):381–9.

125. Friedl J, Puhlmann M, Bartlett DL, Libutti SK, Turner EN, Gnant MFX, et al. Induction of permeability across endothelial cell monolayers by tumor necrosis factor (TNF) occurs via a tissue factor–dependent mechanism: relationship between the procoagulant and permeability effects of TNF. Blood. 2002 Aug 15;100(4):1334–9.

126. Tumor necrosis factor/cachectin increases permeability of endothelial cell monolayers by a mechanism involving regulatory G proteins. J Exp Med. 1989 Jun 1;169(6):1977–91.

127. Ferro T, Neumann P, Gertzberg N, Clements R, Johnson A. Protein kinase C-alpha mediates endothelial barrier dysfunction induced by TNF-alpha. Am J Physiol Lung Cell Mol Physiol. 2000 Jun;278(6):L1107–17.

128. Ferrero E, Zocchi MR, Magni E, Panzeri MC, Curnis F, Rugarli C, et al. Roles of tumor necrosis factor p55 and p75 receptors in TNF-alpha-induced vascular permeability. Am J Physiol Cell Physiol. 2001 Oct;281(4):C1173–9.

129. Schnell L, Fearn S, Schwab ME, Perry VH, Anthony DC. Cytokine-induced acute inflammation in the brain and spinal cord. J Neuropathol Exp Neurol. 1999 Mar;58(3):245–54.

130. Sibson NR, Blamire AM, Perry VH, Gauldie J, Styles P, Anthony DC. TNF-alpha reduces cerebral blood volume and disrupts tissue

homeostasis via an endothelin- and TNFR2-dependent pathway. Brain J Neurol. 2002 Nov;125(Pt 11):2446–59.

131. Serres S, Soto MS, Hamilton A, McAteer MA, Carbonell WS, Robson MD, et al. Molecular MRI enables early and sensitive detection of brain metastases. Proc Natl Acad Sci U S A. 2012 Apr 24;109(17):6674–9.

132. Katakami N, Inaba Y, Sugata S, Tsurusaki M, Itoh T, Machida T, et al. Magnetic resonance evaluation of brain metastases from systemic malignances with two doses of gadobutrol 1.0 m compared with gadoteridol: a multicenter, phase ii/iii study in patients with known or suspected brain metastases. Invest Radiol. 2011 Jul;46(7):411–8.

133. Vogel CL, Cobleigh MA, Tripathy D, Gutheil JC, Harris LN, Fehrenbacher L, et al. Efficacy and safety of trastuzumab as a single agent in first-line treatment of HER2-overexpressing metastatic breast cancer. J Clin Oncol Off J Am Soc Clin Oncol. 2002 Feb 1;20(3):719–26.

134. Valabrega G, Montemurro F, Aglietta M. Trastuzumab: mechanism of action, resistance and future perspectives in HER2-overexpressing breast cancer. Ann Oncol Off J Eur Soc Med Oncol ESMO. 2007 Jun;18(6):977–84.

135. Stemmler H-J, Schmitt M, Willems A, Bernhard H, Harbeck N, Heinemann V. Ratio of trastuzumab levels in serum and cerebrospinal fluid is altered in HER2-positive breast cancer patients with brain metastases and impairment of blood-brain barrier. Anti-Cancer Drugs January 2007. 2007;18(1):23–8.

136. Pestalozzi BC, Brignoli S. Trastuzumab in CSF. J Clin Oncol Off J Am Soc Clin Oncol. 2000 Jun;18(11):2349–51.

137. Bartus RT, Elliott PJ, Dean RL, Hayward NJ, Nagle TL, Huff MR, et al. Controlled Modulation of BBB Permeability Using the Bradykinin Agonist, RMP-7. Exp Neurol. 1996 Nov;142(1):14–28.

138. Borlongan CV, Emerich DF, Hoffer BJ, Bartus RT. Bradykinin receptor agonist facilitates low-dose Cyclosporine-A protection against 6-hydroxydopamine neurotoxicity. Brain Res. 2002 Nov 29;956(2):211–20.

139. Bonvalot S, Laplanche A, Lejeune F, Stoeckle E, Péchoux CL, Vanel D, et al. Limb salvage with isolated perfusion for soft tissue sarcoma: could less TNF-α be better? Ann Oncol. 2005 Jul 1;16(7):1061–8.

140. Abbruzzese JL, Levin B, Ajani JA, Faintuch JS, Saks S, Patt YZ, et al. Phase I Trial of Recombinant Human γ-Interferon and Recombinant Human Tumor Necrosis Factor in Patients with Advanced Gastrointestinal Cancer. Cancer Res. 1989 Jul 15;49(14):4057–61.

141. Talmadge JE, Tribble HR, Pennington RW, Phillips H, Wiltrout RH. Immunomodulatory and immunotherapeutic properties of recombinant gamma-interferon and recombinant tumor necrosis factor in mice. Cancer Res. 1987 May 15;47(10):2563–70.

142. Imaizumi T, Itaya H, Fujita K, Kudoh D, Kudoh S, Mori K, et al. Expression of Tumor Necrosis Factor-α in Cultured Human Endothelial Cells Stimulated With Lipopolysaccharide or Interleukin-1α. Arterioscler Thromb Vasc Biol. 2000 Feb 1;20(2):410–5.

143. Hurvitz S, Hu Y, O'Brien N, Finn RS. Current approaches and future directions in the treatment of HER2-positive breast cancer. Cancer Treat Rev [Internet]. 2013 May [cited 2014 May 7];39(3). Available from: http://www.ncbi.nlm.nih.gov/pmc/articles/PMC3835685/

144. Koukourakis MI, Koukouraki S, Fezoulidis I, Kelekis N, Kyrias G, Archimandritis S, et al. High intratumoural accumulation of stealth liposomal doxorubicin (Caelyx) in glioblastomas and in metastatic brain tumours. Br J Cancer. 2000 Nov;83(10):1281–6.

145. Charrois GJR, Allen TM. Multiple Injections of Pegylated Liposomal Doxorubicin: Pharmacokinetics and Therapeutic Activity. J Pharmacol Exp Ther. 2003 Sep 1;306(3):1058–67.

146. Fornari FA, Randolph JK, Yalowich JC, Ritke MK, Gewirtz DA. Interference by doxorubicin with DNA unwinding in MCF-7 breast tumor cells. Mol Pharmacol. 1994 Apr;45(4):649–56.

147. Johnson&Johnson. Johnson&Johnson Annual Report [Internet]. 2012 [cited 2014 Jun 24]. Available from: http://2012annualreport.jnj.com/ie/2012_Johnson_Johnson_Proxy_Statement.pdf

148. Gabizon A, Martin F. Polyethylene glycol-coated (pegylated) liposomal doxorubicin. Rationale for use in solid tumours. Drugs. 1997;54 Suppl 4:15–21.

149. NICE. Final Appraisal Determination: Guidance on the use of pegylated liposomal doxorubicin hydrochloride (Caelyx®) for advanced ovarian cancer [Internet]. NICE. 2010 [cited 2014 Jun 24]. Available from: http://www.nice.org.uk/

150. Gabizon A, Shmeeda H, Barenholz Y. Pharmacokinetics of pegylated liposomal Doxorubicin: review of animal and human studies. Clin Pharmacokinet. 2003;42(5):419–36.

151. Kannan R, Kuhlenkamp JF, Jeandidier E, Trinh H, Ookhtens M, Kaplowitz N. Evidence for carrier-mediated transport of glutathione across the blood-brain barrier in the rat. J Clin Invest. 1990 Jun;85(6):2009–13.

152. Kannan R, Chakrabarti R, Tang D, Kim KJ, Kaplowitz N. GSH transport in human cerebrovascular endothelial cells and human astrocytes: evidence for luminal localization of Na+-dependent GSH transport in HCEC. Brain Res. 2000 Jan 10;852(2):374–82.

153. ClinicalTrials.gov. An Open-label, Phase I/IIa, Dose Escalating Study of 2B3-101 in Patients With Solid Tumors and Brain Metastases or Recurrent Malignant Glioma. - Full Text View - ClinicalTrials.gov [Internet]. 2013 [cited 2014 Jun 24]. Available from: http://clinicaltrials.gov/ct2/show/NCT01386580

154. Gaillard PJ, Appeldoorn CCM, Dorland R, van Kregten J, Manca F, Vugts DJ, et al. Pharmacokinetics, Brain Delivery, and Efficacy in Brain Tumor-Bearing Mice of Glutathione Pegylated Liposomal Doxorubicin (2B3-101). PLoS ONE. 2014 Jan 8;9(1):e82331.

155. Anthony DC, Sibson NR, McAteer MA, Davis B, Choudhury RP. Detection of Brain Pathology by Magnetic Resonance Imaging of Iron Oxide Micro-particles. The Blood-Brain and Other Neural Barriers [Internet]. Humana Press; 2011 [cited 2014 May 7]. p. 213–27. Available from: http://link.springer.com/protocol/10.1007/978-1-60761-938-3_9

156. McAteer MA, Sibson NR, von zur Muhlen C, Schneider JE, Lowe AS, Warrick N, et al. In vivo magnetic resonance imaging of acute brain inflammation using microparticles of iron oxide. Nat Med. 2007 Oct;13(10):1253–8.

157. Soto MS, Serres S, Anthony DC, Sibson NR. Functional role of endothelial adhesion molecules in the early stages of brain metastasis. Neuro-Oncol. 2014 Apr;16(4):540–51.

158. Siegal T, Horowitz A, Gabizon A. Doxorubicin encapsulated in sterically stabilized liposomes for the treatment of a brain tumor model: biodistribution and therapeutic efficacy. J Neurosurg. 1995 Dec 1;83(6):1029–37.

159. Follwell MJ, Khu KJ, Cheng L, Xu W, Mikulis DJ, Millar B-A, et al. Volume specific response criteria for brain metastases following salvage stereotactic radiosurgery and associated predictors of response. Acta Oncol Stockh Swed. 2012 May;51(5):629–35.

160. Kemper EM, Leenders W, Küsters B, Lyons S, Buckle T, Heerschap A, et al. Development of luciferase tagged brain tumour models in mice for chemotherapy intervention studies. Eur J Cancer. 2006 Dec;42(18):3294–303.

161. O'Brien MER, Wigler N, Inbar M, Rosso R, Grischke E, Santoro A, et al. Reduced cardiotoxicity and comparable efficacy in a phase III trial of pegylated liposomal doxorubicin HCl (CAELYX/Doxil) versus conventional doxorubicin for first-line treatment of metastatic breast cancer. Ann Oncol Off J Eur Soc Med Oncol ESMO. 2004 Mar;15(3):440–9.

162. Hirano A, Becker NH, Zimmerman HM. The use of peroxidase as a tracer in studies of alterations in the blood-brain barrier. J Neurol Sci. 1970 Mar;10(3):205–13.

163. Li L, ten Hagen TLM, Hossann M, Süss R, van Rhoon GC, Eggermont AMM, et al. Mild hyperthermia triggered doxorubicin release from optimized stealth thermosensitive liposomes improves intratumoral drug delivery and efficacy. J Controlled Release. 2013 Jun 10;168(2):142–50.

164. O'Malley WE, Achinstein B, Shear MJ. Action of Bacterial Polysaccharide on Tumors. II. Damage of Sarcoma 37 by Serum of Mice Treated With Serratia Marcescens Polysaccharide, and Induced Tolerance. J Natl Cancer Inst. 1962 Dec 1;29(6):1169–75.

165. Rüegg C, Yilmaz A, Bieler G, Bamat J, Chaubert P, Lejeune FJ. Evidence for the involvement of endotheliai cell integrin $\alpha V\beta 3$ in the disruption of the tumor vascuiature induced by TNF and IFN-γ. Nat Med. 1998 Apr;4(4):408–14.

166. Balkwill F. Tumor necrosis factor or tumor promoting factor? Cytokine Growth Factor Rev. 2002 Apr;13(2):135–41.

167. Ohri CM, Shikotra A, Green RH, Waller DA, Bradding P. Macrophages within NSCLC tumour islets are predominantly of a cytotoxic M1 phenotype associated with extended survival. Eur Respir J. 2009 Jan;33(1):118–26.

168. Brodt P, Fallavollita L, Bresalier RS, Meterissian S, Norton CR, Wolitzky BA. Liver endothelial E-selectin mediates carcinoma cell adhesion and promotes liver metastasis. Int J Cancer J Int Cancer. 1997 May 16;71(4):612–9.

169. Jantscheff P, Schlesinger M, Fritzsche J, Taylor LA, Graeser R, Kirfel G, et al. Lysophosphatidylcholine pretreatment reduces VLA-4 and P-Selectin-mediated b16.f10 melanoma cell adhesion in vitro and inhibits metastasis-like lung invasion in vivo. Mol Cancer Ther. 2011 Jan;10(1):186–97.

170. Liang S, Hoskins M, Khanna P, Kunz RF, Dong C. Effects of the Tumor-Leukocyte Microenvironment on Melanoma-Neutrophil Adhesion to the Endothelium in a Shear Flow. Cell Mol Bioeng. 2008 Sep 1;1(2-3):189–200.

171. Locksley RM, Killeen N, Lenardo MJ. The TNF and TNF receptor superfamilies: integrating mammalian biology. Cell. 2001 Feb 23;104(4):487–501.

172. Gamm H, Lindemann A, Mertelsmann R, Herrmann F. Phase I trial of recombinant human tumour necrosis factor alpha in patients with advanced malignancy. Eur J Cancer Oxf Engl 1990. 1991;27(7):856–63.

173. Fraker DL. A phase III trial of isolated limb perfusion for extremity melanoma comparing melphalan alone versus melhpalan plus tumor necrosis factor (TNF) plus interferon-gamma (IFN). SSO 55th Annual Cancer Symposium. 2002.

174. Noorda EM, Vrouenraets BC, Nieweg OE, van Geel BN, Eggermont AMM, Kroon BBR. Isolated limb perfusion for unresectable melanoma of the extremities. Arch Surg Chic Ill 1960. 2004 Nov;139(11):1237–42.

175. Lejeune FJ, Liénard D, Matter M, Rüegg C. Efficiency of recombinant human TNF in human cancer therapy. Cancer Immun Electron Resour J Acad Cancer Immunol. 2006;6:6.

176. Legler DF, Micheau O, Doucey M-A, Tschopp J, Bron C. Recruitment of TNF receptor 1 to lipid rafts is essential for TNFalpha-mediated NF-kappaB activation. Immunity. 2003 May;18(5):655–64.

177. Aggarwal BB. Signalling pathways of the TNF superfamily: a double-edged sword. Nat Rev Immunol. 2003 Sep;3(9):745–56.

178. Puls A, Eliopoulos AG, Nobes CD, Bridges T, Young LS, Hall A. Activation of the small GTPase Cdc42 by the inflammatory cytokines TNF(alpha) and IL-1, and by the Epstein-Barr virus transforming protein LMP1. J Cell Sci. 1999 Sep;112 (Pt 17):2983–92.

179. Peppelenbosch M, Boone E, Jones GE, van Deventer SJ, Haegeman G, Fiers W, et al. Multiple signal transduction pathways regulate TNF-induced actin reorganization in macrophages: inhibition of Cdc42-mediated filopodium formation by TNF. J Immunol Baltim Md 1950. 1999 Jan 15;162(2):837–45.

180. Petrache I, Verin AD, Crow MT, Birukova A, Liu F, Garcia JG. Differential effect of MLC kinase in TNF-alpha-induced endothelial cell apoptosis and barrier dysfunction. Am J Physiol Lung Cell Mol Physiol. 2001 Jun;280(6):L1168–78.

181. Kerkar S, Williams M, Blocksom JM, Wilson RF, Tyburski JG, Steffes CP. TNF-alpha and IL-1beta increase pericyte/endothelial cell co-culture permeability. J Surg Res. 2006 May;132(1):40–5.

182. Zakaria R, Das K, Radon M, Bhojak M, Rudland PR, Sluming V, et al. Diffusion-weighted MRI characteristics of the cerebral metastasis to brain boundary predicts patient outcomes. BMC Med Imaging. 2014 Aug 3;14:26.

183. Serres S, Martin CJ, Sarmiento Soto M, Bristow C, O'Brien ER, Connell JJ, et al. Structural and functional effects of metastases in rat brain determined by multimodal MRI. Int J Cancer. 2014 Feb 1;134(4):885–96.

184. Weksler B, Romero IA, Couraud P-O. The hCMEC/D3 cell line as a model of the human blood brain barrier. Fluids Barriers CNS. 2013 Mar 26;10(1):16.

185. Gad SC. Animal Models in Toxicology, Second Edition. CRC Press; 2006. 964 p.

186. Pinkel D. The use of body surface area as a criterion of drug dosage in cancer chemotherapy. Cancer Res. 1958 Aug;18(7):853–6.

187. Furman WL, Strother D, McClain K, Bell B, Leventhal B, Pratt CB. Phase I clinical trial of recombinant human tumor necrosis factor in children with refractory solid tumors: a Pediatric Oncology Group study. J Clin Oncol. 1993 Nov 1;11(11):2205–10.

188. Demetri GD, Spriggs DR, Sherman ML, Arthur KA, Imamura K, Kufe DW. A phase I trial of recombinant human tumor necrosis factor and interferon-gamma: effects of combination cytokine administration in vivo. J Clin Oncol. 1989 Oct 1;7(10):1545–53.

189. Mittelman A, Puccio C, Gafney E, Coombe N, Singh B, Wood D, et al. A phase I pharmacokinetic study of recombinant human tumor necrosis factor administered by a 5-day continuous infusion. Invest New Drugs. 1992 Aug 1;10(3):183–90.

190. Kramer SM, Aggarwal BB, Eessalu TE, McCabe SM, Ferraiolo BL, Figari IS, et al. Characterization of the in Vitro and in Vivo Species Preference of Human and Murine Tumor Necrosis Factor-α. Cancer Res. 1988 Feb 15;48(4):920–5.

191. Brouckaert P, Libert C, Everaerdt B, Fiers W. Selective species specificity of tumor necrosis factor for toxicity in the mouse. Lymphokine Cytokine Res. 1992 Aug;11(4):193–6.

192. Functional characterization of the human tumor necrosis factor receptor p75 in a transfected rat/mouse T cell hybridoma. J Exp Med. 1992 Oct 1;176(4):1015–24.

193. Reed JC, Doctor K, Rojas A, Zapata JM, Stehlik C, Fiorentino L, et al. Comparative Analysis of Apoptosis and Inflammation Genes of Mice and Humans. Genome Res. 2003 Jun;13(6b):1376–88.

194. Zlokovic BV, Mackic JB, McComb JG, Weiss MH, Kaplowitz N, Kannan R. Evidence for transcapillary transport of reduced glutathione in vascular perfused guinea-pig brain. Biochem Biophys Res Commun. 1994 May 30;201(1):402–8.

195. Birngruber T, Raml R, Gladdines W, Gatschelhofer C, Gander E, Ghosh A, et al. Enhanced doxorubicin delivery to the brain administered through glutathione PEGylated liposomal doxorubicin (2B3-101) as compared with generic Caelyx,(®)/Doxil(®)--a cerebral open flow microperfusion pilot study. J Pharm Sci. 2014 Jul;103(7):1945–8.

196. Gaillard PJ, Appeldoorn CCM, Rip J, Dorland R, van der Pol SMA, Kooij G, et al. Enhanced brain delivery of liposomal methylprednisolone improved therapeutic efficacy in a model of neuroinflammation. J Control Release Off J Control Release Soc. 2012 Dec 28;164(3):364–9.

197. Lindqvist A, Rip J, Gaillard PJ, Björkman S, Hammarlund-Udenaes M. Enhanced brain delivery of the opioid peptide DAMGO in glutathione pegylated liposomes: a microdialysis study. Mol Pharm. 2013 May 6;10(5):1533–41.

198. Bossen C, Ingold K, Tardivel A, Bodmer J-L, Gaide O, Hertig S, et al. Interactions of Tumor Necrosis Factor (TNF) and TNF Receptor Family Members in the Mouse and Human. J Biol Chem. 2006 May 19;281(20):13964–71.

199. Ley K, Laudanna C, Cybulsky MI, Nourshargh S. Getting to the site of inflammation: the leukocyte adhesion cascade updated. Nat Rev Immunol. 2007 Sep;7(9):678–89.

200. Wallach D, Varfolomeev EE, Malinin NL, Goltsev YV, Kovalenko AV, Boldin MP. Tumor necrosis factor receptor and Fas signaling mechanisms. Annu Rev Immunol. 1999;17:331–67.

201. Chen H, Konofagou EE. The size of blood-brain barrier opening induced by focused ultrasound is dictated by the acoustic pressure. J Cereb Blood Flow Metab Off J Int Soc Cereb Blood Flow Metab. 2014 Jul;34(7):1197–204.

202. PRODUCT INFORMATION - Caelyx_PI.pdf [Internet]. [cited 2014 Jun 26]. Available from: https://www.janssen.com.au/files/Products/Caelyx_PI.pdf?6e31d0a1b3db3ac731fe7e792d7407ed

203. Carnemolla B, Neri D, Castellani P, Leprini A, Neri G, Pini A, et al. Phage antibodies with pan-species recognition of the oncofoetal angiogenesis marker fibronectin ED-B domain. Int J Cancer J Int Cancer. 1996 Nov 4;68(3):397–405.

204. Nilsson F, Kosmehl H, Zardi L, Neri D. Targeted delivery of tissue factor to the ED-B domain of fibronectin, a marker of angiogenesis, mediates the infarction of solid tumors in mice. Cancer Res. 2001 Jan 15;61(2):711–6.

205. Corti A, Ponzoni M. Tumor vascular targeting with tumor necrosis factor alpha and chemotherapeutic drugs. Ann N Y Acad Sci. 2004 Dec;1028:104–12.

206. Hemmerle T, Probst P, Giovannoni L, Green AJ, Meyer T, Neri D. The antibody-based targeted delivery of TNF in combination with doxorubicin eradicates sarcomas in mice and confers protective immunity. Br J Cancer. 2013 Sep 3;109(5):1206–13.

207. Yan Z, Zhao N, Wang Z, Li B, Bao C, Shi J, et al. A mutated human tumor necrosis factor-alpha improves the therapeutic index in vitro and in vivo. Cytotherapy. 2006;8(4):415–23.

208. Jiang C, Niu J, Li M, Teng Y, Wang H, Zhang Y. Tumor Vasculature-Targeted Recombinant Mutated Human TNF-α Enhanced the Antitumor Activity of Doxorubicin by Increasing Tumor Vessel Permeability in Mouse Xenograft Models. PLoS ONE. 2014 Jan 22;9(1):e87036.

209. Douni E, Kollias G. A critical role of the p75 tumor necrosis factor receptor (p75TNF-R) in organ inflammation independent of TNF, lymphotoxin alpha, or the p55TNF-R. J Exp Med. 1998 Oct 5;188(7):1343–52.

210. Loetscher H, Stueber D, Banner D, Mackay F, Lesslauer W. Human tumor necrosis factor alpha (TNF alpha) mutants with exclusive specificity for the 55-kDa or 75-kDa TNF receptors. J Biol Chem. 1993 Dec 15;268(35):26350–7.

211. Musolino A, Ciccolallo L, Panebianco M, Fontana E, Zanoni D, Bozzetti C, et al. Multifactorial central nervous system recurrence susceptibility in patients with HER2-positive breast cancer: epidemiological and clinical data from a population-based cancer registry study. Cancer. 2011 May 1;117(9):1837–46.

212. Slamon DJ, Leyland-Jones B, Shak S, Fuchs H, Paton V, Bajamonde A, et al. Use of chemotherapy plus a monoclonal antibody against HER2 for metastatic breast cancer that overexpresses HER2. N Engl J Med. 2001 Mar 15;344(11):783–92.

213. Eiermann W, International Herceptin Study Group. Trastuzumab combined with chemotherapy for the treatment of HER2-positive metastatic breast cancer: pivotal trial data. Ann Oncol Off J Eur Soc Med Oncol ESMO. 2001;12 Suppl 1:S57–62.

214. Romond EH, Perez EA, Bryant J, Suman VJ, Geyer CE, Davidson NE, et al. Trastuzumab plus adjuvant chemotherapy for operable HER2-positive breast cancer. N Engl J Med. 2005 Oct 20;353(16):1673–84.

215. Eisenhauer EA, Therasse P, Bogaerts J, Schwartz LH, Sargent D, Ford R, et al. New response evaluation criteria in solid tumours: revised RECIST guideline (version 1.1). Eur J Cancer Oxf Engl 1990. 2009 Jan;45(2):228–47.

Publications, presentations, prizes, grants and collaborations relevant to this thesis

Publications

Selective permeabilization of the blood-brain barrier at sites of metastasis.
Connell JJ, Chatain G, Cornelissen B, Vallis KA, Hamilton A, Seymour L, Anthony DC, Sibson NR.
J Natl Cancer Inst. 2013 Nov 6;105(21):1634-43. doi: 10.1093/jnci/djt276.

Structural and functional effects of metastases in rat brain determined by multimodal MRI.
Serres S, Martin CJ, Sarmiento Soto M, Bristow C, O'Brien ER, Connell JJ, Khrapitchev AA, Sibson NR.
Int J Cancer. 2014 Feb 15;134(4):885-96. doi: 10.1002/ijc.28406.

Presentations

Selective permeabilisation of the blood-brain barrier at sites of metastasis (or variants thereof)

National Cancer Research Institute, Liverpool 2011
Keystone Symposia on Inflammation during Carcinogenesis, Dublin, 2012
European Society for Radiotherapy and Oncology - Novel Targeting Drugs and Radiotherapy, Toulouse, 2012
Oxford Cancer Research Centre Symposium, Oxford, 2012
Oxford Cancer Imaging Centre Conference, Oxford, 2012 & 2013
British Neuroscience Association Festival of Neuroscience, London, 2013
XXVIth International Symposium on Cerebral Blood Flow, Metabolism and Function, Shanghai, 2013
European Organisation for Research and Treatment of Cancer 3rd Annual Brain Metastases Research and Emerging Therapy Conference, Marseille, 2013
2nd CRUK/MRC Gray Institute Symposium, Oxford, 2013
MedImmune 3rd UK & Ireland Early Career BBB Symposium, Cambridge, 2013
First Preclinical Nuclear Imaging Symposium, London, 2013

Prizes

European Organisation for Research and Treatment of Cancer 3rd Annual Brain Metastases Research and Emerging Therapy Conference, Marseille, 2013 (Poster prize, €250)
2nd CRUK/MRC Gray Institute Symposium, Oxford, 2013 (Poster prize, £50)
First Preclinical Nuclear Imaging Symposium, London, 2013 (Poster prize, Society for Radiopharmaceutical Sciences 1 year membership)

Grants

MRC Capacity Building Studentship Doctoral Training Grant Studentship (£25,000 p.a.)
MRC i*n vivo* Strategic Skills Award (£14,976)
MRC Doctoral Training Programme Supplementary Funding (£1000)
Guarantors of Brain travel award (£800)
Wolfson College travel award (£400)

Collaborations

Dr Peter Gaillard & Dr David Maussang, toBBB, Leiden
Dr Mike Kershaw, Peter MacCallum Cancer Centre, Melbourne
Dr Rasheed Zakaria and Mr Michael Jenkinson, The Walton Centre NHS Foundation Trust, Liverpool
Prof Olaf Ansorge, University of Oxford
Dr Pierre Couraud, Institut National de la Santé et de la Recherché Médicale, Paris
Dr John Fletcher & Tina Angerer, University of Gothenburg